

On Load-Sharing in the Lumbosacral Spine during Neutral Standing and Forward Flexion
Postures: A Combined Finite Element and Musculoskeletal Study

by

Tao Liu

A thesis submitted in partial fulfillment of the requirements for the degree of

Doctor of Philosophy

in

Structural Engineering

Department of Civil and Environmental Engineering
University of Alberta

© Tao Liu, 2018

Abstract

Understanding load-sharing in the spine during *in-vivo* conditions is critical for better spinal implant design and testing. Previous studies of load-sharing that considered detailed spinal geometry applied compressive Follower Load (FL), with or without moment, to simulate muscle forces. Other studies used musculoskeletal models included muscle forces, but model the discs by simple beams or spherical joints and omitted the articular facet joints. Therefore, it is imperative to develop a model that is able to predict the load-sharing and stress/strain distribution in passive structures while accounting for muscle forces. The current study developed and validated a computational tool that combines a musculoskeletal model (MSK) and a Finite Element (FE) model of lumbosacral spine to predict spinal loads and load-sharing in neutral standing and forward flexion postures. The model also investigated the effects of lumbo-pelvic rhythm and intra-abdominal pressure (IAP) during flexion on spinal load-sharing.

First, the MSK of the upper body available in AnyBody modeling environment was improved and validated. This model predicted muscle forces in the postures studied using inverse statics and considered the IAP variation due to the posture changes from upright to forward flexion. The muscle, gravitational forces and disc moment at the thoracolumbar junction T12-L1 were applied to the FE model as external loads to predict spinal load and load-sharing. The FE model was also validated using *in-vivo* data. Forward flexion was simulated in the MSK model by employing the spine rhythm measured in a previous *in-vivo* study. The FE model predicted intradiscal pressure (IDP) in the muscles, strains in the annular fibers, contact forces in the facet joints, and forces in the ligaments. The load-sharing of a spinal component at a given level is defined as the percentage of the total force/moment at that level resisted by that spinal component. The results revealed that spinal loads, which increased substantially from the upright to the flexed posture,

were mainly supported by the discs in the upright posture, whereas the ligaments' contribution in resisting shear and moment was more significant in the flexed posture.

Previous *in-vivo* studies suggest that the ratio of total lumbar rotation over pelvic rotation (lumbo-pelvic rhythm) during trunk sagittal movement is essential to evaluate spinal loads and discriminate between low back pain and asymptomatic population. Also, MSK models require the lumbo-pelvic rhythm to predict muscle forces, joint reaction forces and moment. This study also investigated the effects of three lumbo-pelvic rhythms defined based on *in-vivo* measurements on the spinal response during moderate forward flexion (60°). The developed tool was used to compute the disc force and moment, IDP, annular fibers strain, and load-sharing. The results revealed that a rhythm with high pelvic rotation and low lumbar flexion involves more global muscles and increases the role of the disc in resisting spinal loads, while its counterpart, with low pelvic rotation, recruits more local muscles and engages the ligaments to lower the disc loads. On the other hand, a normal rhythm that has balanced pelvic and lumbar rotations yields almost equal disc and ligament load-sharing and results in more balanced synergy between global and local muscles.

In addition, most of the MSK and FE models employed to study the spine behavior omit the IAP, a parameter that plays an important role in reducing the spine loading. Hence, the predictions of these models in terms of spinal loads are not realistic. The effects of IAP variation in forward flexion on spinal loads and load-sharing were also investigated using this novel tool. Two IAP settings (ON/OFF) were considered in the MSK model and the trunk muscle forces and reaction forces at the junction T12-L1 were compared. The effects of IAP on spinal loads and load-sharing were determined as well. The findings confirmed the unloading role of IAP, especially at large flexion angles. Inclusion of IAP reduced the global muscle forces, disc loads as well as

IDP. The drop in disc loads was compensated by an increase in ligament forces. The annular fibers strain and IDP were more sensitive to IAP at upper levels of the spine.

The findings of this work are beneficial to clinical applications and disc implants design, and are expected to improve knowledge of spinal response in upright posture and forward flexion.

Preface

This thesis is an original work done by Tao Liu. All the analyses and conclusions in chapters 3-5 are original work, as well as the literature review in chapter 2. The work is financially supported by the Chinese Scholarship Council (CSC).

Chapter 3 has been published as Liu, T., Khalaf, K., Naserkhaki, S., El-Rich, M., “Load-sharing in the lumbosacral spine in neutral standing & flexed postures - A combined finite element and inverse static study”, <http://doi: 10.1016/j.jbiomech.2017.10. 033> in Journal of Biomechanics. I was responsible for the analysis and writing of the manuscript. Dr. Khalaf provided supports for musculoskeletal analysis and reviewed the manuscript. Dr. Naserkhaki was involved in the modeling preparation and discussion. Dr. El-Rich was my PhD supervisor. He contributed to the methodology developing, finite element analysis and manuscript composition.

Chapter 4 of the thesis has been published as Liu, T., Khalaf, K., Samer, A., El-Rich, M., “Effects of Lumbo-Pelvic Rhythm on Trunk Muscle Forces and Disc Loads during Forward Flexion: A Combined Musculoskeletal and Finite Element Simulation Study”, *J. Biomech.* (2018), <https://doi.org/10.1016/j.jbiomech.2018.10.009>. I was responsible for the analysis and manuscript composition. Dr. Khalaf provided supports for analysis and reviewed the manuscript. Dr. Adeeb provided supports for finite element analysis and reviewed the manuscript. Dr. El-Rich (my PhD supervisor) contributed to the manuscript composition and idea formation.

Chapter 5 of the thesis has been submitted to Journal of Biomechanics as Liu, T., Khalaf, K., Samer, A., El-Rich, M., “Numerical Investigation of Intra-abdominal Pressure Effects on Spinal Loads and Load-sharing in Flexion” (BM-D-18-01123). I am responsible for the analysis and manuscript composition. Dr. Khalaf provided supports for the model and reviewed the manuscript. Dr. Adeeb provided supports for finite element analysis. Dr. El-Rich was the supervisory author and was involved in the idea formation and manuscript composition.

Acknowledgements

First, I would like to take this opportunity to express my sincere gratitude to my family. To my father and mother, for their unconditional and continuous supports, understandings and love that they have given me throughout my life, and in particular during my PhD at University of Alberta; thank you.

Secondly, my deepest thanks go to my advisors Dr. El-Rich and Dr. Adeeb, for ample supports and insightful suggestions they provided me throughout my PhD program. It is your generosity, knowledge and wisdom that inspired and cultivated my analytical and critical thinking skills. These valuable skills that you bestowed upon me has allowed me to refine, analyze and solve a scientific question independently, which I have no doubt will continue to guide my future study and life. It was enjoyable time working and learning from you in such a friendly and intellectually stimulating environment at University of Alberta. Without your kind and encouraging feedback, it would not have been possible for me to be introduced to the astonishing and fascinating realm of spinal biomechanics.

I would also like to thank Dr. Kinda Khalaf, Dr. Neil Duncan, Dr. Hossein Rouhani and Dr. Walied Mousa as well as Dr. Douglas Tomlinson for their assistance and encouragement in my PhD program, and valuable time in reviewing the thesis. I owe my special thanks to Chinese scholarship Council (CSC) which provided me with financial support throughout my PhD and Khalifa University which provided software assistance in my research.

I wish to thank my beloved girlfriend, Alice, for her continuous encouragements, help and supports throughout my PhD work. Last but not the least; I thank each and every one who has helped to complete this fruitful research project.

Table of Contents

| | |
|--|-----------|
| Chapter 1 (Introduction) | 1 |
| 1.1 Overview | 2 |
| 1.2 Objectives and hypotheses | 4 |
| 1.3 Contributions of the research | 5 |
| 1.4 Scope and limitations | 5 |
| 1.5 Thesis outline | 6 |
| References | 8 |
| | |
| Chapter 2 (Literature Review) | 12 |
| 2.1 Overview | 13 |
| 2.2 Lumbosacral spine anatomy | 13 |
| 2.3 Biomechanics of lumbar spine | 15 |
| 2.3.1 Lumbar spine kinematics | 15 |
| 2.3.2 <i>In vivo</i> measurements of spinal loads | 15 |
| 2.3.3 Load sharing in lumbosacral spine | 16 |
| 2.4 Musculoskeletal models | 17 |
| 2.5 Finite element models | 18 |
| 2.6 Combined MSK and FE models | 18 |
| 2.7 Summary | 19 |
| References | 20 |
| | |
| Chapter 3 (Load-Sharing in the Lumbosacral Spine in Neutral Standing & Flexed Postures- A combined Finite Element and Inverse static Study) | 27 |
| Abstract | 28 |
| 3.1 Introduction | 29 |
| 3.2 Methods | 30 |
| 3.2.1 MSK model | 30 |
| 3.2.2 FE model | 32 |
| 3.2.3 Model testing and validation..... | 34 |
| 3.2.4 Loading transfer from the MSK model to the FE model | 37 |
| 3.2.5 Mathematical background of load sharing | 40 |
| 3.3 Results of the FE model | 42 |
| 3.3.1 IDP | 42 |
| 3.3.2 Spinal loads | 42 |
| 3.3.3 Disc force and moment | 43 |
| 3.3.4 Strain in annular fibers | 44 |
| 3.3.5 Load-sharing | 44 |
| 3.4 Discussions | 45 |
| 3.4.1 Models validation | 46 |
| 3.4.2 Spinal load and load-sharing | 46 |
| 3.4.3 Methodological issues and limitations | 47 |
| 3.4.4 Conclusions | 47 |
| References | 49 |

| | |
|--|-----------|
| Chapter 4 (Effects of Lumbo-Pelvic Rhythm on Trunk Muscle Forces and Disc Loads during Forward Flexion: A Combined Musculoskeletal and Finite Element Simulation Study) | 53 |
| Abstract | 54 |
| 4.1 Introduction | 55 |
| 4.2 Methods | 56 |
| 4.2.1 Musculoskeletal model | 56 |
| 4.2.2 Passive FE model | 57 |
| 4.2.3 Load transfer from the MSK model to the FE model | 57 |
| 4.2.4 Validation | 58 |
| 4.2.5 Simulated tasks | 59 |
| 4.3 Results | 59 |
| 4.3.1 Posture and Center of Mass | 59 |
| 4.3.2 Trunk muscle force | 60 |
| 4.3.3 Disc strain | 61 |
| 4.3.4 IDP | 62 |
| 4.3.5 Disc force and moment | 63 |
| 4.3.6 Load-sharing | 64 |
| 4.4 Discussions | 64 |
| 4.4.1 Muscle forces and disc loads | 65 |
| 4.4.2 IDP and annular fiber strain | 66 |
| 4.4.3 Disc and ligament load-sharing | 67 |
| 4.4.4 Methodological issues and limitations | 67 |
| References | 69 |
| | |
| Chapter 5 (Numerical Investigation of Intra-Abdominal Pressure Effects on Spinal Loads and Load-sharing in Flexion) | 72 |
| Abstract | 73 |
| 5.1 Introduction | 74 |
| 5.2 Materials and methods | 76 |
| 5.2.1 Musculoskeletal model | 76 |
| 5.2.2 Finite Element model | 79 |
| 5.2.3 Simulated tasks | 79 |
| 5.3 Results | 80 |
| 5.3.1 Muscle force | 80 |
| 5.3.2 Annular fibers strain | 81 |
| 5.3.3 IDP | 82 |
| 5.3.4 Disc force and moment | 83 |
| 5.3.5 Ligament force | 84 |
| 5.3.6 Spinal load-sharing | 84 |
| 5.4 Discussions | 85 |
| 5.4.1 Model assumptions and limitations | 86 |
| 5.4.2 Conclusions | 87 |
| References | 88 |

| | |
|--|------------|
| Chapter 6 (Summary and Conclusions) | 91 |
| 6.1 Summary | 92 |
| 6.2 Conclusions | 92 |
| 6.2.1 Spinal load and load-sharing in standing and forward flexion postures using a new computational tool (Objective1, Chapter 3) | 92 |
| 6.2.2 Effects of lumbo-pelvic rhythm on spinal load and load-sharing (Objective2, Chapter 4) | 93 |
| 6.2.3 Role of intra-abdominal pressure in flexed posture (Objective3, Chapter 5) | 93 |
| 6.3 Recommendations for the future research | 94 |
| Bibliography | 95 |
| Appendix A (The loading reference points and their influence radius for FE model).... | 110 |

List of Tables

| | |
|--|----|
| Table 2.1. Common loading scenarios used in FE models of the lumbar ligamentous spine | 18 |
| Table 3.1. Material properties of the FE model..... | 33 |
| Table 3.2. Material properties of the ligaments..... | 35 |
| Table 4.1. The lumbo-pelvic rhythms applied to the model..... | 59 |
| Table 5.1. Muscle physiological cross-sectional area (PCSA, cm ²) for each side of the spine at different insertion level and the muscle stress for each individual muscle group (in parentheses, N/cm ²)..... | 77 |

List of Figures

| | |
|---|----|
| Fig. 2.1. Anatomy of human lumbar spine (Adapted from http://www.universityorthopedics.com/educational_resources/anatomy_library2.html# and https://www.spineuniverse.com/Anatomy/ligaments). | 13 |
| Fig. 2.2. Musculature of the trunk (Adapted from https://anatomical.us/muscles-in-the-lumbar-region/muscles-in-the-lumbar-region-anatomy-of-lumbar-spine-and-muscles-muscle-anatomy-anatomy-body/). | 14 |
| Fig. 2.3. The spinal stability system consists of CNS, spinal column and spinal muscles (Panjabi, 1992). | 15 |
| Fig. 3.1. Load Transfer from the MSK model to the FE model. U_{FR} : Translation in the direction of the reaction force at T12-L1; R_M : Reaction moment at joint T12-L1; LF : Ligament forces; FJF : Facet joint forces; MF : Muscle forces; Gr : Gravitational force for each spinal level. | 31 |
| Fig. 3.2. Nonlinear flexural stiffness of the discs predicted by FE models of functional spinal units and used in the modified MSK model versus the original stiffness of the joints used in the default MSK model. | 32 |
| Fig. 3.3. Comparison between the compressive force predicted by the MSK model and the one calculated using the IDP value measured at L4-5. | 36 |
| Fig. 3.4. Comparison of total global (G) muscle forces and total local (L) muscle forces predicted by the current MSK model and the KD model of Arjmand et al. (2010). | 36 |
| Fig. 3.5. Comparison of moment-rotation curves of the current FE model, the default and the modified MSK models as well as other <i>in-vitro</i> and numerical studies. | 37 |
| Fig. 3.6. Sagittal and top view of the FE model with the continuum distributing coupling constraints used to apply muscle forces. | 38 |
| Fig. 3.7. Flowchart of the loading scenario applied to the FE model. | 39 |
| Fig. 3.8. Comparison of intersegmental horizontal (+ve: anterior) and total vertical (+ve: inferior) displacements predicted by the FE model and MSK model in standing and forward flexion postures. | 40 |
| Fig. 3.9. IDP at each spinal level predicted by the FE model. Magnitude at level L4-5 is compared to <i>in-vivo</i> value reported by Wilke et al. (2001). NS: neutral stand; FLX: forward flexion. | 42 |
| Fig. 3.10. Total internal force and moment at each spinal level predicted by the FE model for neutral standing (NS) and forward flexion (FLX). | 43 |
| Fig. 3.11. Internal disc forces and moment (shear force: +ve in anterior direction, sagittal moment: +ve in flexion). | 43 |
| Fig. 3.12. Tensile stain distributions in the annular fibres at L1-S1 levels (NS: neutral standing; FLX: forward flexion). | 44 |
| Fig. 3.13. Spinal load sharing in neutral standing (NS) and forward flexion posture (FLX) (LM: Ligaments; FJF: Facet joints; DISC: Discs). | 45 |
| Fig. 4.1. Trunk muscle architecture in Anybody and individual muscle groups. Global muscles (1 rectus abdominis (RA), 12 internal oblique (IO), 12 external oblique (EO), 16 iliocostalis lumborum pars thoracic (ICPT), 24 longissimus thoracis pars thoracic (LGPT)) and Local muscles (8 iliocostalis lumborum pars lumborum | |

| | |
|--|----|
| (ICPL), 10 longissimus thoracis pars lumborum (LGPL), 22 psoas major (PM), 38 multifidus (MF) and 10 quadratus lumborum muscle fascicles (QL)) (Arshad et al., 2016). | 56 |
| Fig. 4.2. The process of transferring forces from the MSK model to FE model. (U_{FR} : Translation in the direction of the reaction force at T12-L1; R_M : Reaction moment at joint T12-L1; LF: Ligament forces; FJF: Facet joint forces; MF: Muscle forces; Gr: Gravitational force for each vertebra). | 58 |
| Fig. 4.3. Variation of posture and Center of Mass (CoM) of the upper body at 60° flexion with lumbo-pelvic rhythms. | 59 |
| Fig. 4.4. (a) Variation of total local (L) and total global (G) muscle forces with lumbo-pelvic rhythms during 60° trunk forward flexion. (b) Variation of individual muscle group forces with lumbo-pelvic rhythms at 60° trunk forward flexion. | 60 |
| Fig. 4.5. Variation of annular fibers strain with lumbo-pelvic rhythms at 60° trunk forward flexion. | 62 |
| Fig. 4.6. Variation of IDP with lumbo-pelvic rhythms at 60° trunk forward flexion. | 62 |
| Fig. 4.7. Variation of disc internal forces (a) and moments (b) as well as load-sharing (c) with lumbo-pelvic rhythms at 60° trunk forward flexion (anterior shear force +ve, sagittal moment: +ve in flexion, LM: ligament force, DISC: disc force, Facet joints have zero forces for three lumbo-pelvic rhythms). | 63 |
| Fig. 5.1. Musculature of the MSK model; <u>Global Muscles</u> : RA-Rectus Abdominis, IO-Internal Oblique, EO-External Oblique, ICPT-Iliocostalis Lumborum Pars Thoracic, LGPT- Longissimus Thoracis Pars Thoracic; <u>Local Muscles</u> : ICPL-Iliocostalis Lumborum Pars Lumborum, LGPL-Longissimus Thoracis Pars Lumborum, PM-Psoas Major, MF- Multifidus, QL-Quadratus Lumborum. | 75 |
| Fig. 5.2. Description of the IAP modelling (a) and mechanism of IAP generation (b) in AnyBody. | 78 |
| Fig. 5.3. Comparison of the predicted global and local muscle forces under activation or deactivation of the IAP during forward flexion. | 80 |
| Fig. 5.4. Local and global muscle forces at 60° forward flexion for both activated IAP and deactivated IAP models. | 81 |
| Fig. 5.5. Visualization variations (with respect to FLX+IAP model) of disc strain of all levels (L1-S1) from FE model at 60° forward flexion with (FLX+IAP) and without (FLX-IAP) IAP. | 82 |
| Fig. 5.6. IDP values at all spinal levels predicted at 60° forward flexion angle for both IAP settings. | 83 |
| Fig. 5.7. Disc compressive and shear forces (+ve in anterior direction) and disc moments (+ve in flexion) at 60° forward flexion predicted by the FE model. | 83 |
| Fig. 5.8. Effects of IAP on ligaments (a) and spinal load sharing of the passive structures (disc, facet joints (FJF), ligaments) (b) evaluated at 60° forward flexion (FJF has zero forces). | 84 |

Chapter 1

Introduction

1.1 Overview

With immense prevalence rates, low back pain (LBP) (70-80%) is considered among the fastest rising 21st century epidemics, plaguing the lives of millions of individuals and imposing huge health and socioeconomic challenges worldwide. World Health Organization statistics reveal that LBP is the leading cause of disability in the world, interfering with an individual's quality of life and as well as the quantity and quality of work performance [World Health Organization. Fact Report. 2016: (www.who.int)]. In industrialized countries, LBP has been cited as the second most frequent chronic condition that warrants visiting a doctor, the fifth most common reason for hospitalization, and the third most frequent cause for invasive spinal surgeries [McKinsey Global Report: The Global Obesity Threat. 2015: (www.Mckinsy.com)]. The worldwide lifetime prevalence of LBP is reported to be as high as 84%, and the prevalence of chronic LBP is about 27%, with 11–15% of the population being disabled [World Health Organization. Fact Report. 2016: (www.who.int)].

Although LBP has multifactorial etiology and the underlying pathology remains elusive, it is well accepted that disc degeneration (Boden et al., 1990), mechanical loads (Pope and Novotny, 1993) and muscle weakness (Heydari et al., 2010) are regarded as the most influential factors contributing to LBP. “Mechanical” LBP, by definition, excludes pain resulting from neoplasia, fracture or inflammatory arthropathy, as well as referred pain (anatomical sites outside the spine). Large percentage of mechanical LBP is caused by occupational activities involving manual material handling (MMH) tasks such as lifting (Garg et al., 2014; Hoozemans et al., 1998, 2004; Jäger et al., 2007; Knapik and Marras, 2009).

From a biomechanical perspective, the mechanical environment of the discs and spinal loads are well recognized to play a causative role in LBP (Shirazi-Adl, 2006). During the last few decades, researchers have used a number of techniques to estimate spinal loads by measuring *in-vivo* changes in the intradiscal pressure (IDP) (Nachemson, 1981; Wilke et al., 2001), body height, or forces and moments transmitted via instrumented vertebral implants (Dreischarf et al., 2013). In parallel, computational models of the spine have been extensively used as a viable time and cost effective tool to investigate spinal loading. Finite Element (FE) model studies, in particular, have contributed substantially to the understanding of functional biomechanics of intervertebral discs (Naserkhaki et al., 2016a, 2016b; Rohlmann et al., 2006; Shirazi-Adl, 2006), both in reducing

dependence on animal and cadaver experiments as well as complementing biomechanical and clinical studies (Schmidt et al., 2013). Understanding the mechanical function of the spine requires a solid knowledge of the interaction between the various spinal components and their role in sharing the load during daily activities. Previous experimental studies that investigated load-sharing have tested cadaveric lumbar spines under flexion (Adams et al., 1980), extension (Adams et al., 1988), lateral bending (Schultz et al., 1979) and axial rotation (Adams and Hutton, 1981), after sequential removal of the spinal structures (using superposition). Some FE studies used similar approach to investigate the influence of ligaments, facet joints, and nucleotomy (Ivicsics et al., 2014; Noailly et al., 2007). This approach, however, is not suitable to explain load-sharing in the intact/healthy spine, as it does not account for material and geometry nonlinearities of the various structures, nor for the sequence in which the nonlinear structures are removed (Funabashi et al., 2015). Other numerical studies have used models of the spinal unit L4-5 (Gudavalli and Triano, 1999) or multibody models (Abouhossein et al., 2011) to predict the load-sharing in extension/flexion. Strains of ligaments were also investigated in spinal units (Mustafy et al., 2014) and in the entire lumbar structure (Gudavalli and Triano, 1999). More recently, Naserkhaki et al. (2016a, 2016b) calculated load-sharing of intact lumbosacral spine in flexion and extension using forces of ligaments and facet joints predicted by a FE model, together with disc forces and moments calculated using equilibrium conditions. Nevertheless, the load scenarios used in the abovementioned models were limited to a Follower Load (FL) of constant magnitude alone or combined with moment, which oversimplifies the realistic load supported by the spine during daily activities. For realistic spinal loading assessment, load-sharing must be evaluated mimicking *in-vivo* conditions, and must include muscles, in addition to the passive structures of the spine (Liu et al., 2018).

The aim of this study is to develop a novel computational tool that combines musculoskeletal (MSK) model of the upper body and FE model of the ligamentous lumbosacral spine to investigate spinal load-sharing in upright standing and forward flexion postures. In addition, effects of two physiological parameters: the lumbo-pelvic rhythm and intra-abdominal pressure (IAP) on spinal load-sharing are studied. The MSK model predicts the reaction force and moment at the junction T12-L1, and the muscle forces for each posture. These forces and moments in addition to the gravitational forces will be applied to the FE model to predict

ligament forces, disc forces and moments, IDP, and annular fibers strain, necessary for load-sharing calculation (Naserkhaki et al., 2016a, 2016b; Liu et al., 2018).

1.2 Objectives and hypotheses

The overall objective of the current study is to develop a new computational tool that combines MSK and FE models to predict the spinal load-sharing in upright standing and forward flexion postures. The objectives are as following:

Objective 1: Develop a new computational tool that combines a MSK model of the upper body and a FE model of ligamentous lumbosacral spine to predict muscle forces, spinal loads and load-sharing in upright and forward flexion postures. (Chapter 3)

Hypothesis:

- a. Determination of spinal loads in upright and forward flexion using numerical models must include the muscle forces in addition to the gravitational forces rather than using simplified loads such as bending moments alone or combined with compressive FL.
- b. Determination of spinal load-sharing in upright and forward flexion must consider all passive structures and satisfy the equilibrium conditions at all spinal levels.

Objective 2: Quantify the effects of the lumbo-pelvic rhythm during forward flexion on the lumbosacral spine biomechanics. (Chapter 4)

Hypothesis:

- a. *In-vivo* findings revealed that people adopt various lumbo-pelvic rhythms when bending forward. Thus, the spinal load and load-sharing in forward flexion are affected by the lumbo-pelvic rhythm.

Objective 3: Investigate the influence of the IAP on spinal load and load-sharing in forward flexion. (Chapter 5)

Hypothesis:

- a. The spine biomechanics community agrees that IAP has beneficial unloading effects on the lumbar spine. Thus, estimation of muscle force, spinal loads and spinal load-sharing in forward flexion must include IAP.

1.3 Contributions of the research

Accurate determination of spinal load and spinal load-sharing, which explains contribution of the various passive components of the spine to resist external load such as gravitational load, is of prime importance to understand the spine biomechanics in general and more particularly spinal diseases caused by loads such as mechanical LBP. It also advances the development of spinal implants and improves their outcomes. Numerous MSK models are employed to predict the muscle forces and joint reaction forces and moments using inverse static/dynamic analysis. These models simplify the MSK system to a multi-joint structure and resolve the redundant system by optimization. This simplification makes the MSK models converge fast but limit their predictions to muscle forces and reaction forces in the joints. Some advanced MSK models can also predict the ligament and facet joint contact forces. On the other hand, FE models of the spine are used to calculate strain and stress in the spinal passive components under various loading scenarios. Most of the recent FE models are detailed, sophisticated and consider the real 3D geometry of the spinal structures. Due to lack of muscles, these FE models are subjected to simplified loads, such as bending moments applied in the anatomical planes combined or not with compressive FL. In the current research, a novel computational tool is created to investigate spinal loads and load-sharing in upright and forward flexion postures. This tool consists of a MSK model of the upper body combined with a FE model of the ligamentous lumbosacral spine. Both models use the same geometry of the spine. The MSK model predicts muscle forces of the upper body including the spine and reaction forces at the thoracic-lumbar junction T12-L1 joint, and those will be in turn applied to the FE model in addition to the gravitational forces. This approach is novel as it applies realistic load that mimics *in-vivo* conditions to the FE model of the spine in order to predict spinal load and load-sharing. The developed tool can predict person-specific spinal load and load-sharing as well as stress and strain profile as the MSK model and FE model can be personalized.

1.4 Scope and limitations

The MSK model does not consider abdominal muscle co-activation, known to increase the stability of the lumbar spine especially in standing posture (El-Rich et al., 2004) and forward flexion posture (Arjmand and Shirazi et al., 2006). None of the MSK and FE models includes ligaments pretension. The MSK model predicts total muscle force that includes passive and active components. This total force is applied as external load to the FE model. It is, however,

recommended to determine the passive component and include it in the load-sharing calculation, particularly in flexion as the passive resistance of the trunk musculature played an important role in the spine equilibrium and stability as the trunk flexion increased (Arjmand and Shirazi-Adl, 2006). Due to lack of geometry of the unloaded spine, the FE model used the geometry of the MSK model's spine, which is loaded with gravitational forces as initial geometry. The spine rhythm measured *in-vivo* by Granata and Sanford (2000) and used by Arjmand and Shirazi (2006) was considered by the MSK model and kept constant during entire flexion for simplification. The current MSK model predicted the IAP based on the change of the abdominal cavity volume during forward flexion rather than using prescribed experimental IAP values like other models (Stokes et al., 2011 and Cholewicki et al., 1999). The transversus muscle, considered as significant contributor to raise the IAP (Cresswell et al., 1992; Cresswell, 1993) was also included in the IAP modelling. Setting the IAP (artificial muscle activity) to zero did not vanish the force in the Oblique muscles as these muscles are attached to the buckle and disks and contribute to their equilibrium.

1.5 Thesis outline

The thesis can be divided into two main parts: the process of developing the model (Chapter 3) and the applications of the model (Chapter 4 and Chapter 5).

Chapter 1 presents a brief introduction to the motivation of the research. The overall objectives are defined, and the research hypotheses, contributions, and limitations are then described.

Chapter 2 elaborates on the anatomy of the lumbosacral spine, the development of the MSK model and FE model as well as limitations. State-of-the-art models attempting to predict both muscle forces and disc stress/strain are reviewed as well.

Chapter 3 describes the modifications of the MSK model available in Anybody software as well as geometry acquisition of the FE model. It also includes the way of transferring muscle forces, gravitational forces and the reaction forces at the thoracolumbar junction T12-L1 to the FE model.

Chapter 4 describes how the lumbo-plevic rhythm is changed in the MSK mode,, and then the corresponding loading conditions are applied to the FE model to predict spinal loads and load-sharing.

Chapter 5 explains how the IAP is modelled in the MSK model and the way of changing the setting of IAP to ON or OFF. The effects of IAP on muscle forces, spinal load and load-sharing are then quantified.

Chapter 6 summarizes findings, conclusions and recommendations of the current research.

References

- Abouhossein, A., Weisse, B., Ferguson, S.J., 2011. A multibody modelling approach to determine load sharing between passive elements of the lumbar spine. *Comput. Methods Biomech. Biomed. Engin.* 14, 527–537. <https://doi.org/10.1080/10255842.2010.485568>
- Adams, M.A., Dolan, P., Hutton, W.C., 1988. The lumbar spine in backward bending. *Spine* 13, 1019–1026.
- Adams, M.A., Hutton, W.C., 1981. The relevance of torsion to the mechanical derangement of the lumbar spine. *Spine* 6, 241–248.
- Adams, M.A., Hutton, W.C., Stott, J.R., 1980. The resistance to flexion of the lumbar intervertebral joint. *Spine* 5, 245–253.
- Arjmand, N., Shirazi-Adl, A., 2006. Model and in vivo studies on human trunk load partitioning and stability in isometric forward flexions. *J. Biomech.* 39, 510–521. <https://doi.org/10.1016/j.jbiomech.2004.11.030>
- Boden, S.D., Davis, D.O., Dina, T.S., Patronas, N.J., Wiesel, S.W., 1990. Abnormal magnetic-resonance scans of the lumbar spine in asymptomatic subjects. A prospective investigation. *J. Bone Joint Surg. Am.* 72, 403–408.
- Cholewicki, J., Juluru, K., McGill, S.M., 1999. Intra-abdominal pressure mechanism for stabilizing the lumbar spine. *J. Biomech.* 32, 13–17.
- Cresswell, A.G., 1993. Responses of intra-abdominal pressure and abdominal muscle activity during dynamic trunk loading in man. *Eur. J. Appl. Physiol.* 66, 315–320.
- Cresswell, A.G., Grundström, H., Thorstensson, A., 1992. Observations on intra-abdominal pressure and patterns of abdominal intra-muscular activity in man. *Acta Physiol. Scand.* 144, 409–418. <https://doi.org/10.1111/j.1748-1716.1992.tb09314.x>
- Dreischarf, M., Rohlmann, A., Zhu, R., Schmidt, H., Zander, T., 2013. Is it possible to estimate the compressive force in the lumbar spine from intradiscal pressure measurements? A finite element evaluation. *Med. Eng. Phys.* 35, 1385–1390. <https://doi.org/10.1016/j.medengphy.2013.03.007>
- El-Rich, M., Shirazi-Adl, A., Arjmand, N., 2004. Muscle activity, internal loads, and stability of the human spine in standing postures: combined model and in vivo studies. *Spine* 29, 2633. <https://doi.org/10.1097/01.brs.0000146463.05288.0e>

- Funabashi, M., El-Rich, M., Prasad, N., Kawchuk, G.N., 2015. Quantification of loading in biomechanical testing: the influence of dissection sequence. *J. Biomech.* 48, 3522–3526. doi:10.1016/j.jbiomech.2015.06.020
- Garg, A., Waters, T., Kapellusch, J., Karwowski, W., 2014. Psychophysical basis for maximum pushing and pulling forces: A review and recommendations. *Int. J. Ind. Ergon.* 44, 281–291. <https://doi.org/10.1016/j.ergon.2012.09.005>
- Granata, K.P., Sanford, A.H., 2000. Lumbar-pelvic coordination is influenced by lifting task parameters. *Spine* 25, 1413–1418.
- Gudavalli, M.R., Triano, J.J., 1999. An analytical model of lumbar motion segment in flexion. *J. Manipulative Physiol. Ther.* 22, 201–208.
- Heydari, A., Nargol, A.V.F., Jones, A.P.C., Humphrey, A.R., Greenough, C.G., 2010. EMG analysis of lumbar paraspinal muscles as a predictor of the risk of low-back pain. *Eur. Spine J. Off. Publ. Eur. Spine Soc. Eur. Spinal Deform. Soc. Eur. Sect. Cerv. Spine Res. Soc.* 19, 1145–1152. <https://doi.org/10.1007/s00586-010-1277-1>
- Hoozemans, M.J., van der Beek, A.J., Frings-Dresen, M.H., van Dijk, F.J., van der Woude, L.H., 1998. Pushing and pulling in relation to musculoskeletal disorders: a review of risk factors. *Ergonomics* 41, 757–781. <https://doi.org/10.1080/001401398186621>
- Hoozemans, M.J.M., Kuijter, P.P.F.M., Kingma, I., van Dieën, J.H., de Vries, W.H.K., van der Woude, L.H.V., Veeger, D.J.H.E.J., van der Beek, A.J., Frings-Dresen, M.H.W., 2004. Mechanical loading of the low back and shoulders during pushing and pulling activities. *Ergonomics* 47, 1–18. <https://doi.org/10.1080/00140130310001593577>
- Ivicsics, M.F., Bishop, N.E., Püschel, K., Morlock, M.M., Huber, G., 2014. Increase in facet joint loading after nucleotomy in the human lumbar spine. *J. Biomech.* 47, 1712–1717. <https://doi.org/10.1016/j.jbiomech.2014.02.021>
- Jäger, M., Sawatzki, K., Glitsch, U., Ellegast, R., Ottersbach, H.J., Schaub, K., Franz, G., Luttmann, A., 2007. Load on the lumbar spine of flight attendants during pushing and pulling trolleys aboard aircraft. *Int. J. Ind. Ergon., Musculoskeletal Load of Push–Pull Tasks* 37, 863–876. <https://doi.org/10.1016/j.ergon.2007.07.010>
- Knapik, G.G., Marras, W.S., 2009. Spine loading at different lumbar levels during pushing and pulling. *Ergonomics* 52, 60–70. <https://doi.org/10.1080/00140130802480828>

- Liu, T., Khalaf, K., Naserkhaki, S., El-Rich, M., 2018. Load-sharing in the lumbosacral spine in neutral standing & flexed postures - A combined finite element and inverse static study. *J. Biomech.* 70, 43–50. <https://doi.org/10.1016/j.jbiomech.2017.10.033>
- Mustafy, T., El-Rich, M., Mesfar, W., Moglo, K., 2014. Investigation of impact loading rate effects on the ligamentous cervical spinal load-partitioning using finite element model of functional spinal unit C2–C3. *J. Biomech.* 47, 2891–2903. <https://doi.org/10.1016/j.jbiomech.2014.07.016>
- Nachemson, A.L., 1981. Disc pressure measurements. *Spine* 6, 93–97.
- Naserkhaki, S., Jaremko, J.L., Adeeb, S., El-Rich, M., 2016a. On the load-sharing along the ligamentous lumbosacral spine in flexed and extended postures: Finite element study. *J. Biomech.* 49, 974–982. <https://doi.org/10.1016/j.jbiomech.2015.09.050>
- Naserkhaki, S., Jaremko, J.L., El-Rich, M., 2016b. Effects of inter-individual lumbar spine geometry variation on load-sharing: Geometrically personalized Finite Element study. *J. Biomech.* 49, 2909–2917. <https://doi.org/10.1016/j.jbiomech.2016.06.032>
- Noailly, J., Wilke, H.-J., Planell, J.A., Lacroix, D., 2007. How does the geometry affect the internal biomechanics of a lumbar spine bi-segment finite element model? Consequences on the validation process. *J. Biomech.* 40, 2414–2425. <https://doi.org/10.1016/j.jbiomech.2006.11.021>
- Pope, M.H., Novotny, J.E., 1993. Spinal biomechanics. *J. Biomech. Eng.* 115, 569–574.
- Rohlmann, A., Zander, T., Schmidt, H., Wilke, H.J., Bergmann, G., 2006. Analysis of the influence of disc degeneration on the mechanical behaviour of a lumbar motion segment using the finite element method. *J. Biomech.* 39, 2484–2490. <https://doi.org/10.1016/j.jbiomech.2005.07.026>
- Schmidt, H., Galbusera, F., Rohlmann, A., Shirazi-Adl, A., 2013. What have we learned from finite element model studies of lumbar intervertebral discs in the past four decades? *J. Biomech.* 46, 2342–2355. <https://doi.org/10.1016/j.jbiomech.2013.07.014>
- Schultz, A.B., Warwick, D.N., Berkson, M.H., Nachemson, A.L., 1979. Mechanical properties of human lumbar spine motion segments. *J Biomech Eng* 101, 46–52.
- Shirazi-Adl, A., 2006. Analysis of large compression loads on lumbar spine in flexion and in torsion using a novel wrapping element. *J. Biomech.* 39, 267–275. <https://doi.org/10.1016/j.jbiomech.2004.11.022>

- Stokes, I.A.F., Gardner-Morse, M.G., Henry, S.M., 2011. Abdominal muscle activation increases lumbar spinal stability: Analysis of contributions of different muscle groups. *Clin. Biomech.* 26, 797–803. <https://doi.org/10.1016/j.clinbiomech.2011.04.006>
- Wilke, H., Neef, P., Hinz, B., Seidel, H., Claes, L., 2001. Intradiscal pressure together with anthropometric data-a data set for the validation of models. *Clin. Biomech.* Bristol Avon 16 Suppl 1, S111-126.

Chapter 2

Literature Review

2.1 Overview

This chapter reviews the anatomy of the lumbosacral spine and its functions during our daily activities. Recognizing the important role of the spine in resisting external loads, numerous experimental and computational studies have been attempted to quantify and predict the spinal loads in various postures and under different loading conditions.

2.2 Lumbosacral spine anatomy

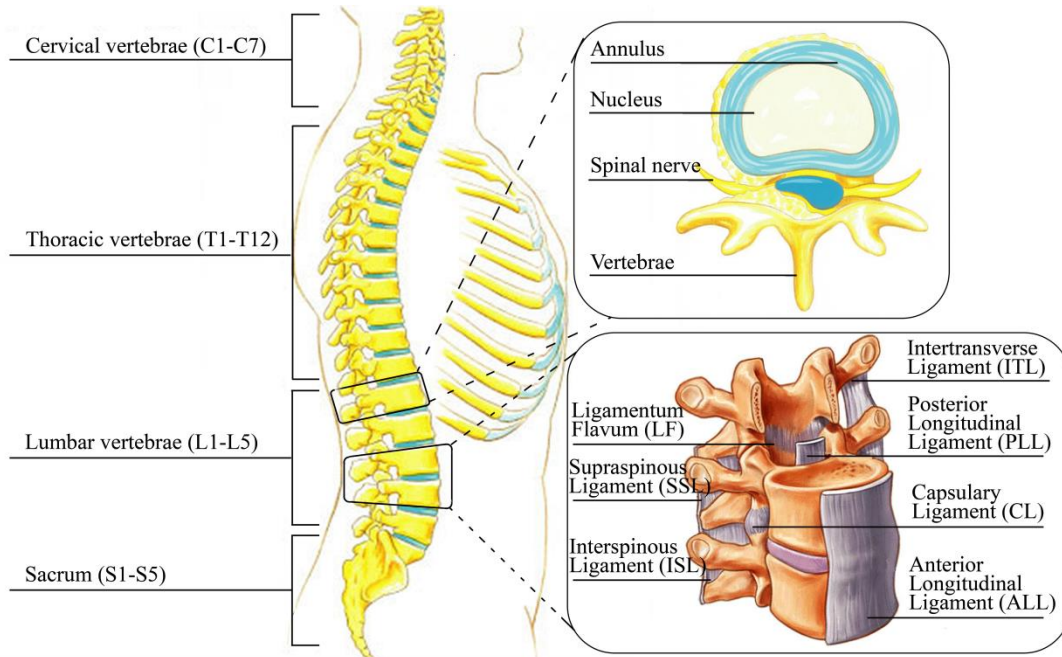


Fig. 2.1. Anatomy of human lumbar spine (Adapted from

http://www.universityorthopedics.com/educational_resources/anatomy_library2.html# and <https://www.spineuniverse.com/anatomy/ligaments>).

The human spine is composed of cervical spine (C1-C7), thoracic spine (T1-T12) and lumbar spine (L1-L5) together with sacrum (S1-S5). The ligamentous lumbosacral spine lacks muscles and consists of 5 lumbar vertebrae from L1 to L5, the sacrum (including 5 fused vertebrae, S1-S5, and the coccyx), 5 discs, and 7 surrounding ligaments as shown in Fig. 2.1. Each vertebra is divided into the vertebral body, endplates, and posterior elements that include the articular facets, spinous and transvers processes. Each disc is divided into annular matrix reinforced by crosswise collagen fibers and nucleus pulposus with a proportion according to the histological findings (44%_nucleus, 56%_annulus) (El-Rich et al., 2009; Schmidt et al., 2006). The ligaments are the Anterior (ALL) and Posterior (PLL) Longitudinal Ligaments, Capsular Ligament (CL),

Intertransverse Ligament (ITL), Ligament Flavum (LF), Supraspinous Ligaments (SSL), and Interspinous Ligaments (ISL) (Breau et al., 1991).

The trunk muscles attached to the vertebrae can be divided into anterior and posterior muscles. The anterior muscles include chest muscles (Pectoralis Major, Intercostal Muscles and other muscles) which are recruited during respiration and abdominal muscles which ensure stability of the spine during trunk movement. The abdominal muscles are part of the abdominal wall and can also be classified into five groups based on their directions and positions-External Oblique (EO), Internal Oblique (IO), Transversus Abdominis (TA), Rectus Abdominis (RA) and Pyramidalis. (<https://courses.lumenlearning.com/boundless-ap/chapter/trunk-muscles/>).

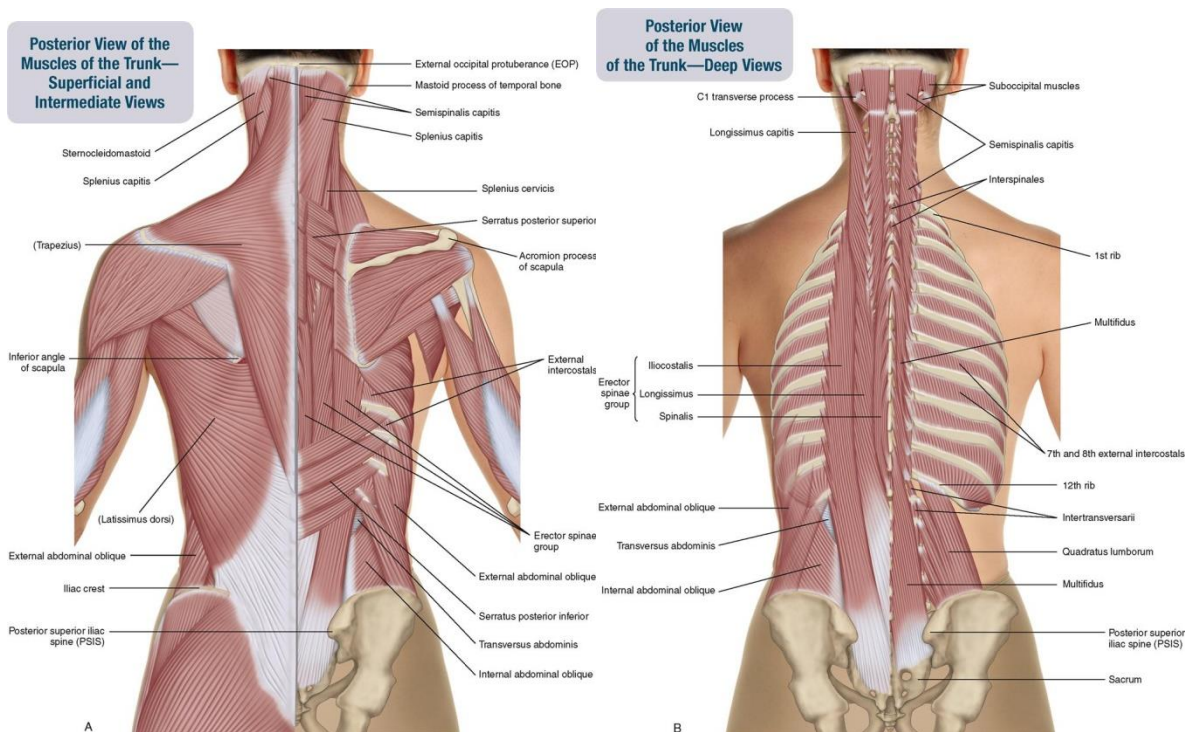


Fig. 2.2. Musculature of the trunk (Adapted from <https://anatomical.us/muscles-in-the-lumbar-region/muscles-in-the-lumbar-region-anatomy-of-lumbar-spine-and-muscles-muscle-anatomy-anatomy-body/>).

The posterior muscles are composed of superficial posterior muscles responsible for movement of the shoulder, intermediate muscles assisting rib cage movement and respiration, and intrinsic back muscles facilitating motion of the head and neck as well as maintaining posture and balance of the trunk. The intrinsic posterior muscles can also be divided into three layers-superficial layer, intermediate layer and deep layer. The details of each muscle can be seen in Fig. 2.2.

2.3 Biomechanics of lumbar spine

2.3.1 Lumbar spine kinematics

The spine is one of the most important parts of the body as it supports the body weight, transfers load from upper level to lower level and protects spinal cord. Generally, the human spine can exert five types of motion under the control of the central nervous system (CNS)- flexion/extension, axial rotation, lateral bending and axial compression. Among these movements, the lumbar spine has relatively significant range of motion (ROM) as compared to cervical spine and thorax. Another function of the spine is to maintain the stability of whole body. All movements and functions of the lumbar spine are controlled by the CNS and muscle forces (Panjabi, 1992). The relationship between muscles, CNS and spine is illustrated in Figure 2.3.

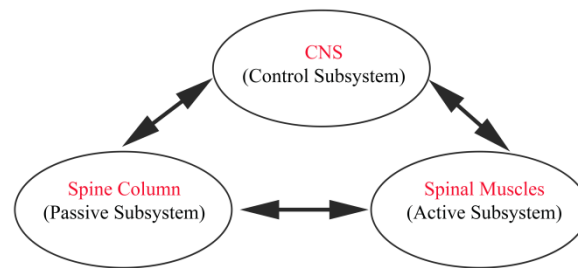


Fig. 2.3. The spinal stability system consists of CNS, spinal column and spinal muscles (Panjabi, 1992).

2.3.2 *In vivo* measurements of spinal loads

Excessive loads in the spine are regarded as one of the major causative factors in the etiology of back disorders and pain (Dreischarf et al., 2016; Hoogendoorn et al., 2000; Manchikanti, 2000; Thiese et al., 2014). Accurate estimation of spinal loads is essential to injury prevention and rehabilitation programs as well as preclinical testing of spinal implants. *In vivo* measurement of intra-disc pressure (IDP) was first conducted by Nachemson and Morris (1964) using a pressure-sensitive needle inserted in the mid-lumbar discs of sixteen volunteers. In the next 20 years, the same authors continued their works and enlarged the number of subjects to 100 volunteers and investigated various postures (lying, sitting and standing) (Nachemson, 1966, 1981). In the following years, other researchers (Andersson et al., 1974; Okushima, 1970; Sato et al., 1999; Schultz et al., 1982; Takahashi et al., 2006; Wilke et al., 2001) also measured the IDP *in vivo* using different techniques. In addition, instrumented implants were inserted at L1 for four

patients and at level L3 for one patient to track magnitudes of the transmitted forces and moment in different directions (Rohlmann et al., 1999, 2013). Due to difficulties such as time, cost and the invasiveness associated with the aforementioned methods, alternative techniques were developed to measure spinal loads. For example, spinal shrinkage (Althoff et al., 1992; Eklund and Corlett, 1984; Rabinowitz et al., 1998; van Dieën et al., 1994) and Intra-abdominal pressure (IAP) (Davis, 1959; Davis and Troup, 1964; Hemborg et al., 1983) measurements were used to predict spinal loads. Also, the relationships between Erector Spinae muscle activity and extensor moments were explored (Dolan et al., 2001; Dolan and Adams, 1993). However, all these methods share major assumptions, including neglect of equipment intervention and anthropometric variations or oversimplification of IAP.

In order to circumvent the aforementioned limitations and take advantage of sophisticated computational technology, sensors, force plates as well as image capture systems, biomechanical models emerge as an indispensable and reliable tool in predicting trunk muscle forces and spinal load supported by each individual component (disc, ligament, facet joint). These models, however, either simulate the active components i.e. muscles accurately and simplify the passive structure (discs, ligaments, vertebrae), or vice versa.

2.3.3 Load sharing in lumbosacral spine

Spinal load-sharing is used as one of the popular means to describe the contribution of passive components (disc, ligament and facet joint) in resisting the imposed loads. A harmonic synergy between muscles and passive components in the spine subjected to various postures and external loads is of extreme importance to injury prevention and to maintain spinal health. Strength loss in any spinal components would lead to the compensation from other components, and long-term adaption to this situation would cause ultimate injury in spine (Naserkhaki et al., 2015). Thus, knowledge of load sharing is vital to understand and discriminate spine function and disorders. For example, a previous *in-vivo* experiment (Pollintine et al., 2004) revealed that the disc is able to carry out 92% of load and the neutral arch could resist the rest in a healthy function spine unit under neutral standing posture. In contrast, a degenerated disc plays a less important role in resisting the loads, and large portion of forces are transferred to the neutral arch under the same posture. However, the load sharing of discs is not affected by the status of the disc (healthy or degenerated) when the spine is subjected forward flexion posture.

Experimental studies that investigated load-sharing have tested cadaveric lumbar spines under flexion (Adams et al. 1980), extension (Adams et al. 1988), lateral bending (Schultz et al., 1979) and axial rotation (Adams and Hutton 1981), after sequential removal of the spinal structures (using superposition). Some Finite Element (FE) studies used a similar approach to investigate the influence of ligaments, partial/total facet joint removal, and nucleotomy on spinal rotational instabilities (Ivicsics et al., 2014; Noailly et al., 2007; Sharma et al., 1995). This approach, however, is not suitable to explain load-sharing in the intact/healthy spine, as it does not account for material and geometry nonlinearities of the various structures, nor for the sequence in which the nonlinear structures are removed, known to influence the spinal response to mechanical loading (Funabashi et al., 2015).

Other numerical studies have used models of the spinal unit L4-5 (Gudavalli and Triano, 1999) or multibody models (Abouhossein et al., 2011) to predict the load-sharing in extension or flexion. Naserkhaki et al. (2016a, 2016b) calculated load-sharing of intact lumbosacral spine in flexion and extension using forces of ligaments and facet joints predicted by a FE model together with disc forces and moments calculated using equilibrium conditions. Nevertheless, the load scenarios used in the abovementioned models were limited to a Follower Load (FL) of constant magnitude alone or combined with moment, which oversimplifies the realistic load supported by the spine during daily activities. Load sharing in *in vivo* condition remains unclear.

2.4 Musculoskeletal models

Musculoskeletal (MSK) models of the trunk, also called active models, utilize detailed muscle architecture to predict muscle forces under various postures and loading scenarios using different approaches, such as reduction method (Chaffin, 1969; Freivalds et al., 1984; McGill et al., 1996), EMG-assisted models (Granata and Marras, 1995; Hughes et al., 1994; Marras and Granata, 1997; McGill and Norman, 1986; Ning et al., 2012), optimization methods (Damsgaard et al., 2006; Park et al., 2012), hybrid EMG-optimization (Cholewicki et al., 1995; Cholewicki and McGill, 1996; Gagnon et al., 2001), and kinematic-driven model (Arjmand and Shirazi-Adl, 2006; Kiefer et al., 1997; Shirazi-Adl et al., 2002). The MSK models can include the IAP and predict joint reaction forces and moments under various static and dynamic postures (de Zee et al., 2007; El-Rich et al., 2014; Arjmand and Shirazi, 2006; Granata and Marras, 1995; Cholewicki et al., 1995). However, they are unable to predict stress and strain distribution in the

spinal structures, IDP in the discs etc. due to their simplified joints and bony structures. For instance, almost all MSK models simplified the intervertebral disc to a spherical rigid joint with 3 or more degrees of freedoms and consider the bony structures as rigid.

2.5 Finite element models

FE models of the spine include detailed geometry of the passive structures (disc, ligaments, facet joints, collagen fibres, annulus and nucleus) and consider more realistic material properties to predict IDP, stress/strain in the disc (Dreischarf et al., 2014; Naserkhaki et al., 2016a, 2016b; Rohlmann et al., 2009) as well as load-sharing of the passive components (Naserkhaki et al., 2016a, 2016b). Devoid of muscles, the FE models used *in-vitro* loading conditions such as pure moment (Heuer et al., 2007), FL or combination of both (Dreischarf et al., 2014; Naserkhaki et al., 2016b).

Table 2.1. Common loading scenarios used in FE models of the lumbar ligamentous spine

| Loading | FL (N) | Moment (N.m) | Reference |
|-----------------|--------|--------------|---------------------------|
| Flexion | 1175 | 7.5 | (Rohlmann et al., 2009) |
| Extension | 500 | 7.5 | (Rohlmann et al., 2009) |
| Lateral bending | 700 | 7.8 | (Dreischarf et al., 2012) |
| Axial rotation | 720 | 5.5 | (Dreischarf et al., 2011) |

This simplified load either overlooks or simplifies the muscle force and ignores the resulted shear forces. In addition, due to its constant magnitude, FL is not suitable to simulate the compressive force that varies along the spine (Shirazi-Adl and Parnianpour, 2000). Such models, thus, are not able to simulate *in-vivo* loading conditions. The most common loading scenarios used in FE models of the lumbar ligamentous spine are summarized in Table 2.1.

2.6 Combined MSK and FE models

In light of the aforementioned limitations of the current biomechanical models, developing a new computational tool that combines MSK model of the trunk to predict muscle forces and FE model of the spine that uses these muscle forces to predict spinal load including 3D distribution of strain and stress is imperative. Previous attempts of combining MSK (inverse static) and FE models quantified the discrepancy between the intervertebral rotations predicted by both models in flexion and extension. This discrepancy is due to differences in the Center of Rotation (CoR) definition and material properties used to model the bony structures in the FE model versus rigid

in the MSK model (Zhu et al., 2013). In addition, Toumanidou and Noailly (2015) explored IDP and disc swelling under muscle forces by coupling MSK model with passive resistance of the spinal tissues at L3-S1 level. Most recently, Azari et al. (2017) determined spinal load-sharing at level L4-5 by using a FE model subjected to gravity loads and muscle forces estimated by a trunk musculoskeletal model under 12 static activities. These studies, therefore, confirmed the feasibility of combining MSK and FE models to study spine biomechanics in *in-vivo* conditions. However, biomechanics of intact lumbosacral spine under *in vivo* conditions remain unclear.

The aim of the current study is to develop a numerical tool that allows the transfer of muscle forces predicted by a MSK model of the upper body in predefined postures to a detailed nonlinear FE model of the ligamentous lumbosacral spine to investigate spinal load and load-sharing as well as tissue-level stress/strain.

2.7 Summary

This chapter first presented an overview of spinal anatomy and muscle architecture, and then summarized the biomechanics of the lumbar spine, and further elaborated on the relationship between mechanical load and spinal force. Finally, state-of-the-art experimental and numerical models of the lumbar spine were reviewed.

In summary, the current MSK models of the trunk are faster and allow prediction of muscle forces and joint reaction forces while simplifying the discs to rigid joint with three rotational degrees of freedoms. In contrast, FE models of the spine are slower and consider detailed geometry and more realistic material properties but use simplified loading scenarios such as FL to predict magnitude and distribution of stress/strain in the passive components (discs, ligaments, facet joints). In conclusion, developing a model that is able to predict stress and strain magnitude and distribution in the passive structures under loading scenarios that simulate *in-vivo* conditions and account for muscle forces is imperative. The overall objective of the current research is to create such a model to predict spinal load and load-sharing in neutral standing and forward flexion postures, and loading scenarios.

Reference

- Abouhossein, A., Weisse, B., Ferguson, S.J., 2011. A multibody modelling approach to determine load sharing between passive elements of the lumbar spine. *Comput. Methods Biomech. Biomed. Engin.* 14, 527–537. <https://doi.org/10.1080/10255842.2010.485568>
- Adams, M.A., Dolan, P., Hutton, W.C., 1988. The lumbar spine in backward bending. *Spine* 13, 1019–1026.
- Adams, M.A., Hutton, W.C., 1981. The relevance of torsion to the mechanical derangement of the lumbar spine. *Spine* 6, 241–248.
- Adams, M.A., Hutton, W.C., Stott, J.R., 1980. The resistance to flexion of the lumbar intervertebral joint. *Spine* 5, 245–253.
- Althoff, I., Brinckmann, P., Frobin, W., Sandover, J., Burton, K., 1992. An improved method of stature measurement for quantitative determination of spinal loading. Application to sitting postures and whole body vibration. *Spine* 17, 682–693.
- Andersson, B.J., Ortengren, R., Nachemson, A., Elfström, G., 1974. Lumbar disc pressure and myoelectric back muscle activity during sitting. IV. Studies on a car driver's seat. *Scand. J. Rehabil. Med.* 6, 128–133.
- Arjmand, N., Shirazi-Adl, A., 2006. Model and in vivo studies on human trunk load partitioning and stability in isometric forward flexions. *J. Biomech.* 39, 510–521. <https://doi.org/10.1016/j.jbiomech.2004.11.030>
- Azari, F., Arjmand, N., Shirazi-Adl, A., Rahimi-Moghaddam, T., 2017. A combined passive and active musculoskeletal model study to estimate L4-L5 load sharing. *J. Biomech.* <https://doi.org/10.1016/j.jbiomech.2017.04.026>
- Breau, C., Shirazi-Adl, A., De Guise, J., 1991. Reconstruction of a human ligamentous lumbar spine using CT images-a three-dimensional finite element mesh generation. *Ann. Biomed. Eng.* 19, 291–302.
- Chaffin, D.B., 1969. A computerized biomechanical model-Development of and use in studying gross body actions. *J. Biomech.* 2, 429–441. [https://doi.org/10.1016/0021-9290\(69\)90018-9](https://doi.org/10.1016/0021-9290(69)90018-9)
- Cholewicki, J., McGill, S.M., 1996. Mechanical stability of the in vivo lumbar spine: implications for injury and chronic low back pain. *Clin. Biomech. Bristol Avon* 11, 1–15.

- Cholewicki, J., McGill, S.M., Norman, R.W., 1995. Comparison of muscle forces and joint load from an optimization and EMG assisted lumbar spine model: towards development of a hybrid approach. *J. Biomech.* 28, 321–331.
- Damsgaard, M., Rasmussen, J., Christensen, S.T., Surma, E., de Zee, M., 2006. Analysis of musculoskeletal systems in the AnyBody Modeling System. *Simul. Model. Pract. Theory, SIMS 2004* 14, 1100–1111. <https://doi.org/10.1016/j.simpat.2006.09.001>
- Davis, P.R., 1959. Posture of the trunk during the lifting of weights. *Br. Med. J.* 1, 87–89.
- Davis, P.R., Troup, J.D.G., 1964. Pressures in the trunk cavities when pulling, pushing and lifting. *Ergonomics* 7, 465–474. <https://doi.org/10.1080/00140136408930764>
- de Zee, M., Hansen, L., Wong, C., Rasmussen, J., Simonsen, E.B., 2007. A generic detailed rigid-body lumbar spine model. *J. Biomech.* 40, 1219–1227. <https://doi.org/10.1016/j.jbiomech.2006.05.030>
- Dolan, P., Adams, M.A., 1993. The relationship between EMG activity and extensor moment generation in the erector spinae muscles during bending and lifting activities. *J. Biomech.* 26, 513–522.
- Dolan, P., Kingma, I., De Looze, M.P., van Dieen, J.H., Toussaint, H.M., Baten, C.T., Adams, M.A., 2001. An EMG technique for measuring spinal loading during asymmetric lifting. *Clin. Biomech. Bristol Avon* 16 Suppl 1, S17-24.
- Dreischarf, M., Rohlmann, A., Bergmann, G., Zander, T., 2012. Optimised in vitro applicable loads for the simulation of lateral bending in the lumbar spine. *Med. Eng. Phys.* 34, 777–780. <https://doi.org/10.1016/j.medengphy.2012.04.002>
- Dreischarf, M., Rohlmann, A., Bergmann, G., Zander, T., 2011. Optimised loads for the simulation of axial rotation in the lumbar spine. *J. Biomech.* 44, 2323–2327. <https://doi.org/10.1016/j.jbiomech.2011.05.040>
- Dreischarf, M., Shirazi-Adl, A., Arjmand, N., Rohlmann, A., Schmidt, H., 2016. Estimation of loads on human lumbar spine: A review of in vivo and computational model studies. *J. Biomech.* 49, 833–845. <https://doi.org/10.1016/j.jbiomech.2015.12.038>
- Dreischarf, M., Zander, T., Shirazi-Adl, A., Puttlitz, C.M., Adam, C.J., Chen, C.S., Goel, V.K., Kiapour, A., Kim, Y.H., Labus, K.M., Little, J.P., Park, W.M., Wang, Y.H., Wilke, H.J., Rohlmann, A., Schmidt, H., 2014. Comparison of eight published static finite element

- models of the intact lumbar spine: predictive power of models improves when combined together. *J. Biomech.* 47, 1757–1766. <https://doi.org/10.1016/j.jbiomech.2014.04.002>
- Eklund, J.A., Corlett, E.N., 1984. Shrinkage as a measure of the effect of load on the spine. *Spine* 9, 189–194.
- El-Rich, M., Arnoux, P.-J., Wagnac, E., Brunet, C., Aubin, C.-E., 2009. Finite element investigation of the loading rate effect on the spinal load-sharing changes under impact conditions. *J. Biomech.* 42, 1252–1262. <https://doi.org/10.1016/j.jbiomech.2009.03.036>
- El-Rich, M., Shirazi-Adl, A., Arjmand, N., 2004. Muscle activity, internal loads, and stability of the human spine in standing postures: combined model and in vivo studies. *Spine* 29, 2633–2642.
- Freivalds, A., Chaffin, D.B., Garg, A., Lee, K.S., 1984. A dynamic biomechanical evaluation of lifting maximum acceptable loads. *J. Biomech.* 17, 251–262.
- Funabashi, M., El-Rich, M., Prasad, N., Kawchuk, G.N., 2015. Quantification of loading in biomechanical testing: the influence of dissection sequence. *J. Biomech.* 48, 3522–3526. <https://doi.org/10.1016/j.jbiomech.2015.06.020>
- Gagnon, D., Larivière, C., Loisel, P., 2001. Comparative ability of EMG, optimization, and hybrid modelling approaches to predict trunk muscle forces and lumbar spine loading during dynamic sagittal plane lifting. *Clin. Biomech.* 16, 359–372. [https://doi.org/10.1016/S0268-0033\(01\)00016-X](https://doi.org/10.1016/S0268-0033(01)00016-X)
- Granata, K.P., Marras, W.S., 1995. An EMG-assisted model of trunk loading during free-dynamic lifting. *J. Biomech.* 28, 1309–1317.
- Gudavalli, M.R., Triano, J.J., 1999. An analytical model of lumbar motion segment in flexion. *J. Manipulative Physiol. Ther.* 22, 201–208.
- Hemborg, B., Moritz, U., Hamberg, J., Löwing, H., Akesson, I., 1983. Intraabdominal pressure and trunk muscle activity during lifting-effect of abdominal muscle training in healthy subjects. *Scand. J. Rehabil. Med.* 15, 183–196.
- Heuer, F., Schmidt, H., Klezl, Z., Claes, L., Wilke, H.J., 2007. Stepwise reduction of functional spinal structures increase range of motion and change lordosis angle. *J. Biomech.* 40, 271–280. <https://doi.org/10.1016/j.jbiomech.2006.01.007>
- Hoogendoorn, W.E., Bongers, P.M., de Vet, H.C., Douwes, M., Koes, B.W., Miedema, M.C., Ariëns, G.A., Bouter, L.M., 2000. Flexion and rotation of the trunk and lifting at work are

- risk factors for low back pain: results of a prospective cohort study. *Spine* 25, 3087–3092.
- Hughes, R.E., Chaffin, D.B., Lavender, S.A., Andersson, G.B., 1994. Evaluation of muscle force prediction models of the lumbar trunk using surface electromyography. *J. Orthop. Res. Off. Publ. Orthop. Res. Soc.* 12, 689–698. <https://doi.org/10.1002/jor.1100120512>
- Ivicsics, M.F., Bishop, N.E., Püschel, K., Morlock, M.M., Huber, G., 2014. Increase in facet joint loading after nucleotomy in the human lumbar spine. *J. Biomech.* 47, 1712–1717. <https://doi.org/10.1016/j.jbiomech.2014.02.021>
- Kiefer, A., Shirazi-Adl, A., Parnianpour, M., 1997. Stability of the human spine in neutral postures. *Eur. Spine J. Off. Publ. Eur. Spine Soc. Eur. Spinal Deform. Soc. Eur. Sect. Cerv. Spine Res. Soc.* 6, 45–53.
- Manchikanti, L., 2000. Epidemiology of low back pain. *Pain Physician* 3, 167–192.
- Marras, W.S., Granata, K.P., 1997. The development of an EMG-assisted model to assess spine loading during whole-body free-dynamic lifting. *J. Electromyogr. Kinesiol. Off. J. Int. Soc. Electrophysiol. Kinesiol.* 7, 259–268.
- McGill, S.M., Norman, R.W., 1986. Partitioning of the L4-L5 dynamic moment into disc, ligamentous, and muscular components during lifting. *Spine* 11, 666–678.
- McGill, S.M., Norman, R.W., Cholewicki, J., 1996. A simple polynomial that predicts low-back compression during complex 3-D tasks. *Ergonomics* 39, 1107–1118. <https://doi.org/10.1080/00140139608964532>
- Nachemson, A., Morris, J.M., 1964. In vivo measurement of intradiscal pressure. discometry, a method for the determination of pressure in the lower lumbar discs. *J. Bone Joint Surg. Am.* 46, 1077–1092.
- Nachemson, A., 1966. The load on lumbar disks in different positions of the body. *Clin. Orthop.* 45, 107–122.
- Nachemson, A.L., 1981. Disc pressure measurements. *Spine* 6, 93–97.
- Naserkhaki, S., Jaremko, J.L., Adeeb, S., El-Rich, M., 2016a. On the load-sharing along the ligamentous lumbosacral spine in flexed and extended postures: Finite element study. *J. Biomech.* 49, 974–982. <https://doi.org/10.1016/j.jbiomech.2015.09.050>

- Naserkhaki, S., Jaremko, J.L., El-Rich, M., 2016b. Effects of inter-individual lumbar spine geometry variation on load-sharing: Geometrically personalized Finite Element study. *J. Biomech.* 49, 2909–2917. <https://doi.org/10.1016/j.jbiomech.2016.06.032>
- Naserkhaki, S., 2015. On the lumbosacral spine geometry variation and spinal load-sharing: personalized finite element modelling. Ph. D. thesis, University of Alberta. Canada.
- Ning, X., Jin, S., Mirka, G.A., 2012. Describing the active region boundary of EMG-assisted biomechanical models of the low back. *Clin. Biomech. Bristol Avon* 27, 422–427.
- Noailly, J., Wilke, HJ., Planell, J.A., Lacroix, D., 2007. How does the geometry affect the internal biomechanics of a lumbar spine bi-segment finite element model? Consequences on the validation process. *J. Biomech.* 40, 2414–2425.
- Okushima, H., 1970. [Study on hydrodynamic pressure of lumbar intervertebral disc]. *Nihon Geka Hokan Arch. Jpn. Chir.* 39, 45–57.
- Panjabi, M.M., 1992. The stabilizing system of the spine. Part I. Function, dysfunction, adaptation, and enhancement. *J. Spinal Disord.* 5, 383–389; discussion 397.
- Park, W.M., Wang, S., Kim, Y.H., Wood, K.B., Sim, J.A., Li, G., 2012. Effect of the intra-abdominal pressure and the center of segmental body mass on the lumbar spine mechanics—a computational parametric study. *J. Biomech. Eng.* 134, 011009.
- Pollintine, P., Dolan, P., Tobias, J.H., Adams, M.A., 2004. Intervertebral disc degeneration can lead to “stress-shielding” of the anterior vertebral body: a cause of osteoporotic vertebral fracture? *Spine* 29, 774–782.
- Rabinowitz, D., Bridger, R.S., Lambert, M.I., 1998. Lifting technique and abdominal belt usage: a biomechanical, physiological and subjective investigation. *Saf. Sci.* 28, 155–164.
- Rohlmann, A., Bergmann, G., Graichen, F., 1999. Loads on internal spinal fixators measured in different body positions. *Eur. Spine J.* 8, 354–359. <https://doi.org/10.1007/s005860050187>
- Rohlmann, A., Dreischarf, M., Zander, T., Graichen, F., Strube, P., Schmidt, H., Bergmann, G., 2013. Monitoring the load on a telemeterised vertebral body replacement for a period of up to 65 months. *Eur. Spine J.* 22, 2575–2581. <https://doi.org/10.1007/s00586-013-3057-1>
- Rohlmann, A., Zander, T., Rao, M., Bergmann, G., 2009. Realistic loading conditions for upper body bending. *J. Biomech.* 42, 884–890. <https://doi.org/10.1016/j.jbiomech.2009.01.017>

- Sato, K., Kikuchi, S., Yonezawa, T., 1999. In vivo intradiscal pressure measurement in healthy individuals and in patients with ongoing back problems. *Spine* 24, 2468–2474.
- Schmidt, H., Heuer, F., Simon, U., Kettler, A., Rohlmann, A., Claes, L., Wilke, H.-J., 2006. Application of a new calibration method for a three-dimensional finite element model of a human lumbar annulus fibrosus. *Clin. Biomech.* 21, 337–344.
- Schultz, A., Andersson, G., Ortengren, R., Haderspeck, K., Nachemson, A., 1982. Loads on the lumbar spine. Validation of a biomechanical analysis by measurements of intradiscal pressures and myoelectric signals. *J. Bone Joint Surg. Am.* 64, 713–720.
- Schultz, A.B., Warwick, D.N., Berkson, M.H., Nachemson, A.L., 1979. Mechanical properties of human lumbar spine motion segments. *J Biomech Eng* 101, 46–52.
- Sharma, M., Langrana, N.A., Rodriguez, J., 1995. Role of ligaments and facets in lumbar spinal stability. *Spine* 20, 887–900.
- Shirazi-Adl, A., Parnianpour, M., 2000. Load-bearing and stress analysis of the human spine under a novel wrapping compression loading. *Clin. Biomech. Bristol Avon* 15, 718–725.
- Shirazi-Adl, A., Sadouk, S., Parnianpour, M., Pop, D., El-Rich, M., 2002. Muscle force evaluation and the role of posture in human lumbar spine under compression. *Eur. Spine J. Off. Publ. Eur. Spine Soc. Eur. Spinal Deform. Soc. Eur. Sect. Cerv. Spine Res. Soc.* 11, 519–526. <https://doi.org/10.1007/s00586-002-0397-7>
- Takahashi, I., Kikuchi, S., Sato, K., Sato, N., 2006. Mechanical load of the lumbar spine during forward bending motion of the trunk—a biomechanical study. *Spine* 31, 18–23.
- Thiese, M.S., Hegmann, K.T., Wood, E.M., Garg, A., Moore, J.S., Kapellusch, J., Foster, J., Ott, U., 2014. Prevalence of low back pain by anatomic location and intensity in an occupational population. *BMC Musculoskelet. Disord.* 15, 283. <https://doi.org/10.1186/1471-2474-15-283>
- Toumanidou, T., Noailly, J., 2015. Musculoskeletal Modeling of the Lumbar Spine to Explore Functional Interactions between Back Muscle Loads and Intervertebral Disk Multiphysics. *Front. Bioeng. Biotechnol.* 3, 111.
- van Dieën, J.H., Creemers, M., Draisma, I., Toussaint, H.M., Kingma, I., 1994. Repetitive lifting and spinal shrinkage, effects of age and lifting technique. *Clin. Biomech.* 9, 367–374. <https://doi.org/10.1016/j.jbiomech.2013.03.003>

- Wilke, H., Neef, P., Hinz, B., Seidel, H., Claes, L., 2001. Intradiscal pressure together with anthropometric data-a data set for the validation of models. *Clin. Biomech.* Bristol Avon 16 Suppl 1, S111-126.
- Zhu, R., Zander, T., Dreischarf, M., Duda, G.N., Rohlmann, A., Schmidt, H., 2013. Considerations when loading spinal finite element models with predicted muscle forces from inverse static analyses. *J. Biomech.* 46, 1376–1378. <https://doi.org/10.1016/j.jbiomech.2013.03.003>

Chapter 3

Load-Sharing in the Lumbosacral Spine in Neutral Standing & Flexed Postures-A combined Finite Element and Inverse Static Study

This chapter has been published as Liu, T., Khalaf, K., Naserkhaki, S., El-Rich, M., 2018. Load-sharing in the lumbosacral spine in neutral standing & flexed postures - A combined finite element and inverse static study. J. Biomech. <https://doi.org/10.1016/j.jbiomech.2017.10.033>.

Abstract

Understanding load-sharing in the spine during *in-vivo* conditions is critical for better spinal implant design and testing. Previous studies of load-sharing that considered actual spinal geometry applied compressive follower load, with or without moment, to simulate muscle forces. Other studies used musculoskeletal models, which include muscle forces, but model the discs by simple beams or spherical joints and ignore the articular facet joints.

This study investigated load-sharing in neutral standing and flexed postures using a detailed Finite Element (FE) model of the ligamentous lumbosacral spine, where muscle forces, gravity loads and intra-abdominal pressure, as predicted by a musculoskeletal model of the upper body, are input into the FE model. Flexion was simulated by applying vertebral rotations following spine rhythm measured in a previous *in-vivo* study, to the musculoskeletal model. The FE model predicted intradiscal pressure (IDP), strains in the annular fibers, contact forces in the facet joints, and forces in the ligaments. The disc forces and moments were determined using equilibrium equations, which considered the applied loads, including muscle forces and IDP, as well as forces in the ligaments and facet joints predicted by the FE model. Load-sharing was calculated as the portion of the total spinal load carried along the spine by each individual spinal structure. The results revealed that spinal loads which increased substantially from the upright to the flexed posture were mainly supported by the discs in the upright posture, whereas the ligaments' contribution in resisting shear and moment was more significant in the flexed posture.

Keywords: Load-sharing, *In-vivo* loading conditions, Neutral standing, Forward flexion, Finite element analysis, Musculoskeletal model, Inverse static analysis

3.1 Introduction

Understanding the mechanical function of the spine requires a solid knowledge of the interaction between the various spinal components and their role in sharing the load during daily activities. This information is of prime importance in spinal implant design and testing, as well as effective injury prevention and rehabilitation/treatment programs. Spinal load-sharing is used as one of the means to describe the contribution of each spinal component in resisting the imposed loads. Previous experimental studies that investigated load-sharing have tested cadaveric lumbar spines under flexion (Adams et al. 1980), extension (Adams et al. 1988), lateral bending (Schultz et al., 1979) and axial rotation (Adams and Hutton 1981), after sequential removal of the spinal structures (using superposition). Some FE studies used a similar approach to investigate the influence of ligaments, partial/total facet joint removal, and nucleotomy on spinal rotational instabilities (Ivicsics et al., 2014; Noailly et al., 2007; Sharma et al., 1995). This approach, however, is not suitable to explain load-sharing in the intact/healthy spine, as it does not account for material and geometry nonlinearities of the various structures, nor of the sequence in which the nonlinear structures are removed, known to influence the spinal response to mechanical loading (Funabashi et al., 2015).

Other numerical studies have used models of the spinal unit L4-5 (Gudavalli and Triano, 1999) or multibody models (Abouhossein et al., 2011) to predict the load-sharing in extension or flexion. Strains of ligaments were also investigated in spinal units (El-Rich et al., 2009; Mustafy et al., 2014) and in the entire lumbar structure (Gudavalli and Triano, 1999). Naserkhaki et al. (2016a, b) calculated load-sharing of intact lumbosacral spine in flexion and extension using forces of ligaments and facet joints predicted by a FE model together with disc forces and moments calculated using equilibrium conditions. In addition, Naserkhaki et al. (2017) investigated the effects of different ligament properties on biomechanics of the lumbar Functional Spinal L4-5 including spinal force- and moment-sharing. Nevertheless, the load scenarios used in the abovementioned models were limited to a Follower Load (FL) of constant magnitude alone or combined with moment, which oversimplifies the realistic load supported by

the spine during daily activities. More recently, Azari et al. (2017) determined spinal load-sharing at level L4-5 using a FE model subjected to gravity loads and muscle forces estimated by a trunk musculoskeletal model under twelve static activities.

For realistic spinal loading assessment, load-sharing must be evaluated during *in-vivo* conditions, and must include muscles, in addition to the various passive structures of the spine Azari et al. (2017). This study used the AnyBody musculoskeletal (MSK) model of the trunk, in conjunction with a 3D FE model of a ligamentous lumbosacral spine, to investigate load-sharing in neutral standing and 60° forward flexion postures. The MSK model was used to determine muscle forces and intra-abdominal pressure (IAP) due to gravitational loads in both postures, which were then applied to the FE model to predict load-sharing.

3.2 Methods

3.2.1 MSK model

The model was set up assuming a standard male height of 168cm and a weight of 70kg. The upper body included the skull, upper arms and thorax; the lumbar region included five rigid vertebrae and a pelvis with sacrum (version 6.0, AnyBody Technology A/S, Denmark) (Fig. 3.1). The discs were modeled as rigid joints with three rotational degrees of freedom (DOF) (Han et al., 2012) and transitional DOF constrained in all directions (Zhu et al., 2013). Therefore, the MSK model had fixed centers of rotation located at the centers of the rigid joints, which are considered as the average positions of instantaneous axes of rotation from extension to flexion (Pearcy and Bogduk, 1988). Flexural stiffness of these joints used by the default MSK model is linear (Fig. 3.2) and similar at all spinal levels. It was obtained experimentally by using linear regression curve (Schmidt et al., 1998). However, the current MSK model used nonlinear stiffness curves predicted by FE models of functional spinal units devoid of ligaments and facet joints and subjected to flexion and extension moments.

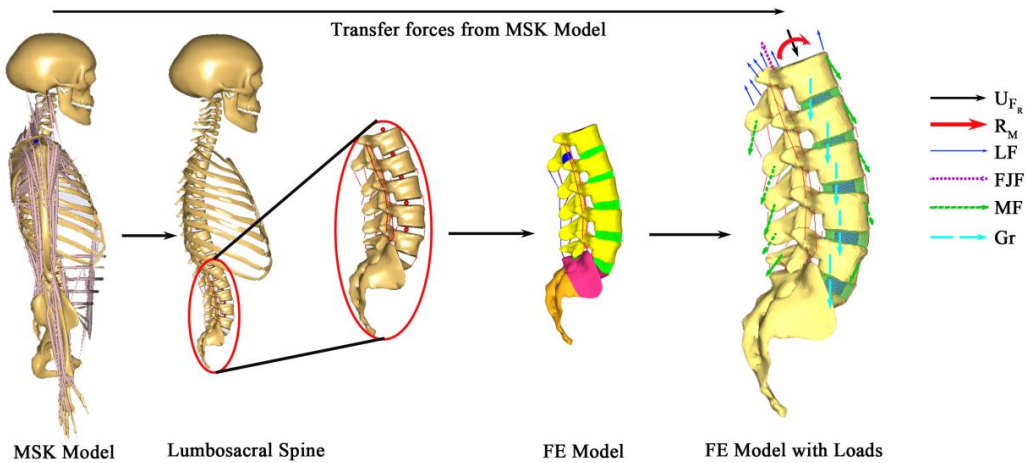


Fig. 3.1. Load Transfer from the MSK model to the FE model. U_{FR} : Translation in the direction of the reaction force at T12-L1; R_M : Reaction moment at joint T12-L1; LF : Ligament forces; FJF : Facet joint forces; MF : Muscle forces; Gr : Gravitational force for each spinal level.

The model musculature included 188 muscle fascicles (Chapter 4) attached to the upper body. The muscles were modeled using three different forms: a straight line connecting insertion and origin points, via-points muscles, and nonlinear wrapping muscles. Each muscle was assumed to resist only tensile forces. The muscle strength was equal to the product of the physiological cross-sectional area and predefined muscle tension. Muscle forces were calculated by minimizing the objective function taken as the sum of the square of the ratios of muscle force to muscle strength (de Zee et al., 2007).

Since the default MSK model only includes the Anterior Longitudinal Ligament (ALL), Posterior Longitudinal Ligament (PLL), Intertransverse Ligament (ITL), Ligamentum Flavum (LF), Supraspinous Ligament (SSL), and Interspinous Ligament (ISL), the Capsular Ligament (CL) was added to the articular facet joints. The force-deformation relationship of the ligaments was assumed as a fourth order polynomial function of the strain. All ligaments were modelled with springs that can resist only tension. The stiffness of the ligaments was modified to match the nonlinear force-displacement curve (Rohmann et al., 2006) and to vary with the spinal levels according to the literature (Pintar et al., 1992). All ligaments had zero forces at neutral standing

position.

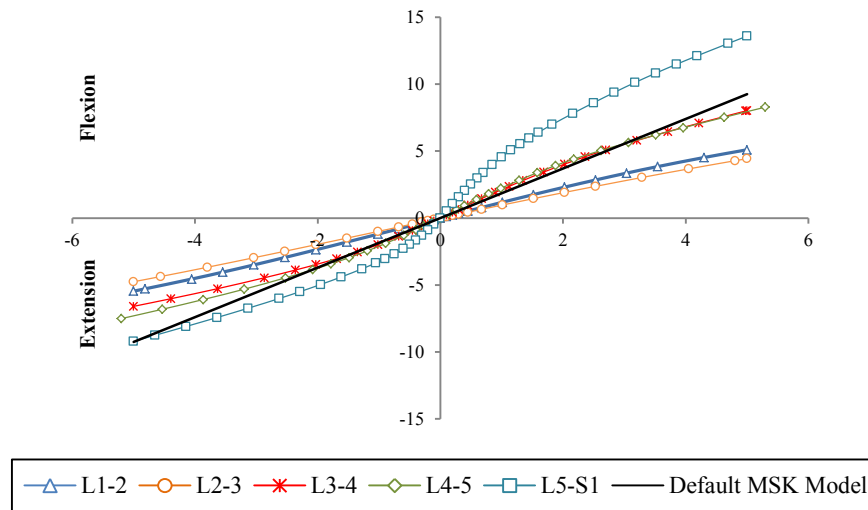


Fig. 3.2. Nonlinear flexural stiffness of the discs predicted by FE models of functional spinal units and used in the modified MSK model versus the original stiffness of the joints used in the default MSK model.

The IAP was modelled using a cylinder with constant volume and pressure with a magnitude limited to 26.6kPa (Essendrop, 2003). It was produced by the force of the transverse muscles which changed the volume of the cylinder under flexion (Arshad et al., 2016). The predicted lower and upper bounds of IAP were 2.2 and 4.4kPa (Schultz et al., 1982), respectively, during the simulations.

Flexion was simulated using a spine rhythm in which the intervertebral rotations (IVRs) were defined as a percentage of the total rotation (Arjmand and Shirazi-Adl, 2006a): 8% at T12-L1, 13% at L1-2, 16% at L2-3, 23% at L3-4, 26% at L4-5, and 14% at L5-S1. The Average lumbo-pelvic ratio were also applied based on in vivo measurement. The range of flexion (60°) is composed of lumbar flexion (36°) and sacrum rotation (24°).

3.2.2 FE model

Geometry acquisition

Three-dimensional geometry of the lumbar vertebrae and sacrum of the MSK model (Nissan and

Gilad, 1986), corresponding to standing posture, was used to construct the FE model after cleaning from spikes and sharp edges using Geomagic software (Geomagic Studio 2014).

Mesh

The endplates were meshed using 4-node shell elements using the software Hypermesh (Hyperworks 14.0). The mesh of all endplates followed a similar pattern and included an equal number of elements. The elements of the endplates were then extruded to construct 8-node brick elements simulating the discs, which in turn were divided into nucleus and annulus with volume ratio of 44% and 56%, respectively (El-Rich et al., 2009; Schmidt et al., 2007). The total disc cross section at L4-5 was $\sim 1190 \text{ mm}^2$. The annulus was strengthened by collagen fibers, modeled with tension only nonlinear springs, distributed in concentric lamellae with a crosswise pattern close to $\pm 35^\circ$ (El-Rich et al., 2009; Schmidt et al., 2007). The articular facets were meshed with relatively small 3-node shell elements, and a frictionless surface-to-surface contact was established between adjacent facets with a minimal gap of 1.5mm. The FE model included the same ligaments as the MSK model, which were constructed using nonlinear springs that only resist tension. The insertion and origin points were matched exactly with their counterparts in the MSK model. The cortical and cancellous bone of the posterior elements and the vertebral bodies were meshed with 3-node shell elements, and 4-node solid elements, respectively.

Table 3.1. Material properties of the FE model

| Spinal components | Material behavior | Mechanical properties | Reference |
|--------------------------|------------------------------------|-----------------------------|---------------------------|
| Cortical bone | Linear elastic | E=12,000 MPa, v=0.3 | Naserkhaki et al. (2016a) |
| Cartilaginous endplate | | E=23.8 MPa, v=0.4 | |
| Cancellous bone | E=200 MPa, v=0.25 | | |
| Annulus ground substance | Hyper-Elastic (Mooney-Rivlin) | $C_{10}=0.18, C_{01}=0.045$ | |
| Nucleus pulposus | Nonlinear force-displacement curve | $C_{10}=0.12, C_{01}=0.030$ | Schmidt et al. (2006) |
| Collagen fibers | | | Shirazi-Adl et al. (1986) |

Material properties

Cartilaginous endplates and bones were assumed to be linear elastic. The annulus ground and nucleus pulposus were modeled using the hyper-elastic Mooney-Rivlin model (El-Rich et al., 2009; Naserkhaki et al., 2016a,b) (Table 3.1). The force-displacement curve for ligaments varied with spinal levels (Table 3.2) and it was adopted from literature (Pintar et al., 1992; Rohlmann et al., 2006). The nonlinear behavior of the annular fibres with increasing stiffness from inner to outer lamella (Schmidt et al., 2006; Shirazi-Adl et al., 1986) was adopted. All analyses were performed using the FE solver Abaqus. The sacrum was completely fixed during neutral standing posture and was rotated based on the lumbo-pelvic ration used during forward flexion.

3.2.3 Model testing and validation

MSK model

As stiffnesses of the discs and ligaments of the default MSK model were modified, and the ligament CL was added, the model was tested in both neutral standing and flexion postures by comparing the compressive force in the joint L4-5 to the value reported *in-vivo* (Wilke et al., 2001). The muscle forces were also compared to other numerical (Arjmand et al., 2010) data. The IDP measured in the disc L4-5 (Wilke et al., 2001) was converted to a compressive force by multiplying the product of the area of disc ($\sim 1190 \text{ mm}^2$) and a coefficient (0.66 ± 0.11) that varies with the inclination of the upper body (Dreischarf et al., 2013). The compressive force predicted by the MSK model increased with the upper body inclination from 395N in neutral standing to 1517N at 60° flexion, in alignment with the reported *in-vivo* range (Fig. 3.3).

The local muscle forces were summed up as well as the global muscle forces (Arshad et al., 2016) and compared to the values reported by Arjmand et al., (2010), who used a multi-joint Kinematics-driven (KD) model. The local muscle forces increased from $\sim 152\text{N}$ to $\sim 1108\text{N}$ when the posture changed from standing to 60° flexion, are in agreement with the KD model prediction.

However, the current model yielded greater forces in the whole simulation (Fig. 3.4). Although both the MSK and KD models showed similar trend in global muscle force, the current model

predicted a slightly smaller global muscle forces between 8% and 20% of total body inclination and greater forces for the rest flexion.

Table 3.2. Material properties of the ligaments

| Level | Ligaments | Strain (%) | Stiffness (N/mm) | Strain (%) | Stiffness (N/mm) | Reference |
|-------|-----------|------------------------|------------------|-----------------------|------------------|------------------------|
| L1-L2 | ALL | $0 < \epsilon < 17.95$ | 277.6 | $17.95 \leq \epsilon$ | 1491.2 | |
| | PLL | $0 < \epsilon < 21.14$ | 14.0125 | $21.14 \leq \epsilon$ | 112.1 | |
| | CL | $0 < \epsilon < 28.23$ | 36 | $28.23 \leq \epsilon$ | 384 | Rohlmann et al. (2006) |
| | ISL | $0 < \epsilon < 19.95$ | 0.77 | $19.95 \leq \epsilon$ | 8.085 | Pintar et al. (1992) |
| | LF | $0 < \epsilon < 47.39$ | 5.519 | $47.39 \leq \epsilon$ | 38.994 | |
| | SSL | $0 < \epsilon < 24.56$ | 1.65 | $24.56 \leq \epsilon$ | 22.44 | |
| | ITL | $0 < \epsilon < 22.56$ | 0.3 | $22.56 \leq \epsilon$ | 10.7 | Rohlmann et al. (2006) |
| L2-L3 | ALL | $0 < \epsilon < 17.95$ | 178.358 | $17.95 \leq \epsilon$ | 958.096 | |
| | PLL | $0 < \epsilon < 21.14$ | 29.5 | $21.14 \leq \epsilon$ | 236 | |
| | CL | $0 < \epsilon < 28.23$ | 28.728 | $28.23 \leq \epsilon$ | 306.432 | Rohlmann et al. (2006) |
| | ISL | $0 < \epsilon < 19.95$ | 0.742 | $19.95 \leq \epsilon$ | 7.791 | Pintar et al. (1992) |
| | LF | $0 < \epsilon < 47.39$ | 5.6056 | $47.39 \leq \epsilon$ | 42.37 | |
| | SSL | $0 < \epsilon < 24.56$ | 1.7825 | $24.56 \leq \epsilon$ | 24.242 | |
| | ITL | $0 < \epsilon < 22.56$ | 0.3 | $22.56 \leq \epsilon$ | 10.7 | Rohlmann et al. (2006) |
| L3-L4 | ALL | $0 < \epsilon < 17.95$ | 340.06 | $17.95 \leq \epsilon$ | 1826.72 | |
| | PLL | $0 < \epsilon < 21.14$ | 8.555 | $21.14 \leq \epsilon$ | 68.44 | |
| | CL | $0 < \epsilon < 28.23$ | 27.36 | $28.23 \leq \epsilon$ | 291.84 | Rohlmann et al. (2006) |
| | ISL | $0 < \epsilon < 19.95$ | 1.4 | $19.95 \leq \epsilon$ | 14.7 | Pintar et al. (1992) |
| | LF | $0 < \epsilon < 47.39$ | 7.7 | $47.39 \leq \epsilon$ | 58.2 | |
| | SSL | $0 < \epsilon < 24.56$ | 2.5 | $24.56 \leq \epsilon$ | 34 | |
| | ITL | $0 < \epsilon < 22.56$ | 0.3 | $22.56 \leq \epsilon$ | 10.7 | Rohlmann et al. (2006) |
| L4-L5 | ALL | $0 < \epsilon < 17.95$ | 347 | $17.95 \leq \epsilon$ | 1864 | |
| | PLL | $0 < \epsilon < 21.14$ | 20.65 | $21.14 \leq \epsilon$ | 165.2 | |
| | CL | $0 < \epsilon < 28.23$ | 25.92 | $28.23 \leq \epsilon$ | 276.48 | Rohlmann et al. (2006) |
| | ISL | $0 < \epsilon < 19.95$ | 0.672 | $19.95 \leq \epsilon$ | 7.056 | Pintar et al. (1992) |
| | LF | $0 < \epsilon < 47.39$ | 6.0676 | $47.39 \leq \epsilon$ | 45.86 | |
| | SSL | $0 < \epsilon < 24.56$ | 1.2925 | $24.56 \leq \epsilon$ | 17.578 | |
| | ITL | $0 < \epsilon < 22.56$ | 0.3 | $22.56 \leq \epsilon$ | 10.7 | Rohlmann et al. (2006) |
| L5-S1 | ALL | $0 < \epsilon < 17.95$ | 113.122 | $17.95 \leq \epsilon$ | 607.664 | |
| | PLL | $0 < \epsilon < 21.14$ | 17.7 | $21.14 \leq \epsilon$ | 141.6 | |
| | CL | $0 < \epsilon < 28.23$ | 25.2 | $28.23 \leq \epsilon$ | 268.8 | Rohlmann et al. (2006) |
| | ISL | $0 < \epsilon < 19.95$ | 1.26 | $19.95 \leq \epsilon$ | 13.23 | Pintar et al. (1992) |
| | LF | $0 < \epsilon < 47.39$ | 4.543 | $47.39 \leq \epsilon$ | 34.338 | |
| | SSL | $0 < \epsilon < 24.56$ | 1.275 | $24.56 \leq \epsilon$ | 17.34 | |
| | ITL | $0 < \epsilon < 22.56$ | 0.3 | $22.56 \leq \epsilon$ | 10.7 | Rohlmann et al. (2006) |

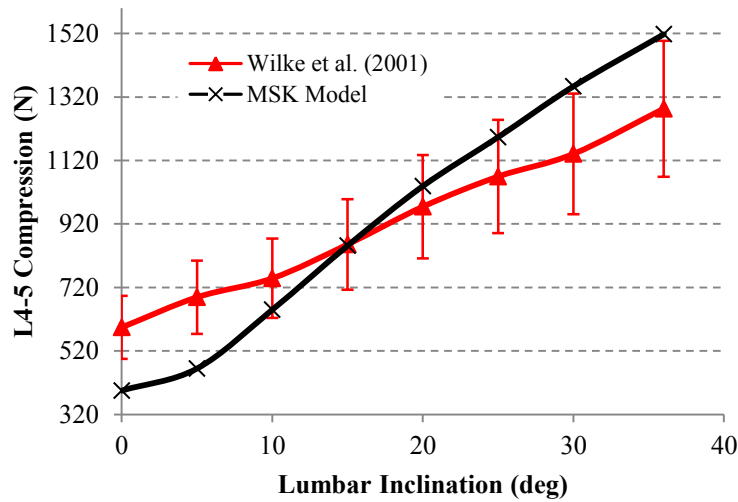


Fig. 3.3. Comparison between the compressive force predicted by the MSK model and the one calculated using the IDP value measured at L4-5.

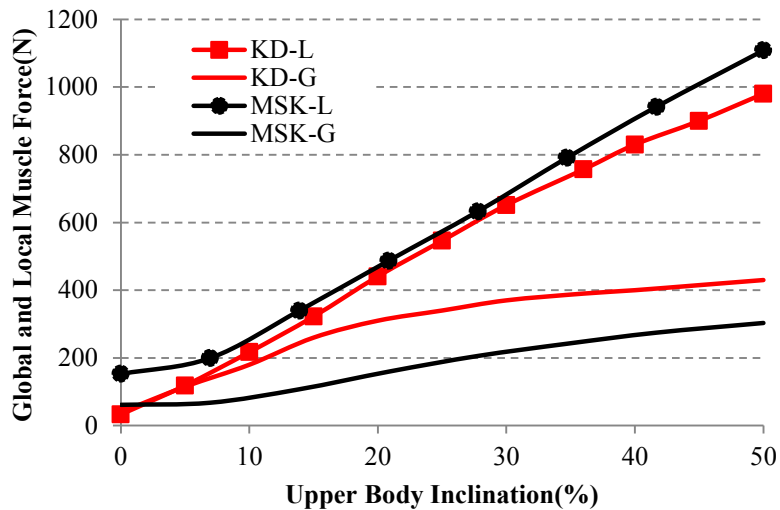


Fig. 3.4. Comparison of total global (G) muscle forces and total local (L) muscle forces predicted by the current MSK model and the KD model of Arjmand et al. (2010).

FE model

Only the lumbar spine (L1-5) was used to test the FE model as the literature lacks experimental data of the lumbosacral spine. The model was fixed in all directions at the L5 level. Rotation of L1 with respect to L5 under 7.5Nm flexion and extension moments was compared to *in-vitro* (Rohlmann et al., 2001) and other numerical (Dreischarf et al., 2014; Naserkhaki et al., 2016a)

data. The moments were applied to the upper endplate of the L1, which was made rigid. The results showed very good agreement with the *in-vitro* data in extension, although more stiff response was observed in flexion, similar to other reported computational data (Fig. 3.5).

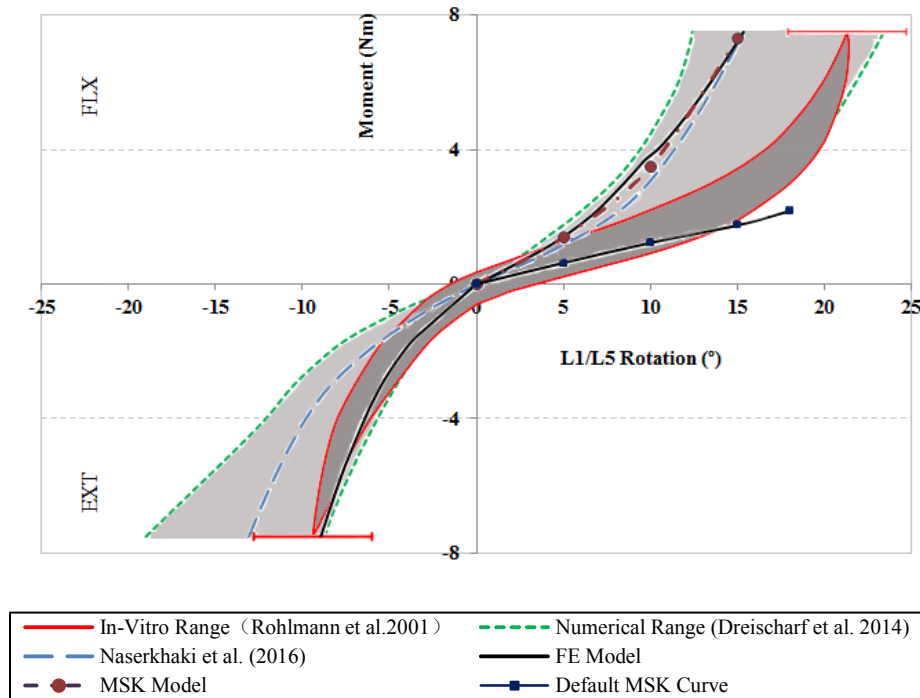


Fig. 3.5. Comparison of moment-rotation curves of the current FE model, the default and the modified MSK models as well as other *in-vitro* and numerical studies.

3.2.4 Loading transfer from the MSK model to the FE model

The reaction moment, ligament forces, and facet joint forces obtained at the junction T12-L1 of the MSK model were applied to vertebra L1 of the FE model. The muscle forces and gravitational forces were also added to vertebra at all levels. These loads resulted from the upper body weight and muscle forces and accounted for the IAP.

All the external forces will act on the reference points (detailed coordinates are specified in Appendix A) that represent the muscle insertion points and are exactly the same as the insertion points used in the MSK model in the form of concentrated load. Each reference point is attached to the corresponding deformable vertebra surface through continuum distribution coupling

constraints with minimum influence radius (specified in Appendix A) in order to reduce the computational cost. Distributing coupling constraints the motion of the coupling nodes to the translation and rotation of the reference nodes and the force and moment acting on the reference node are distributed among coupled nodes based on the default uniform weighting method and equilibrium. The detailed coordinates of each reference point together with its minimum influence radius are specified in Appendix A, and the constrained FE model with all reference points are shown in Fig 3.6.

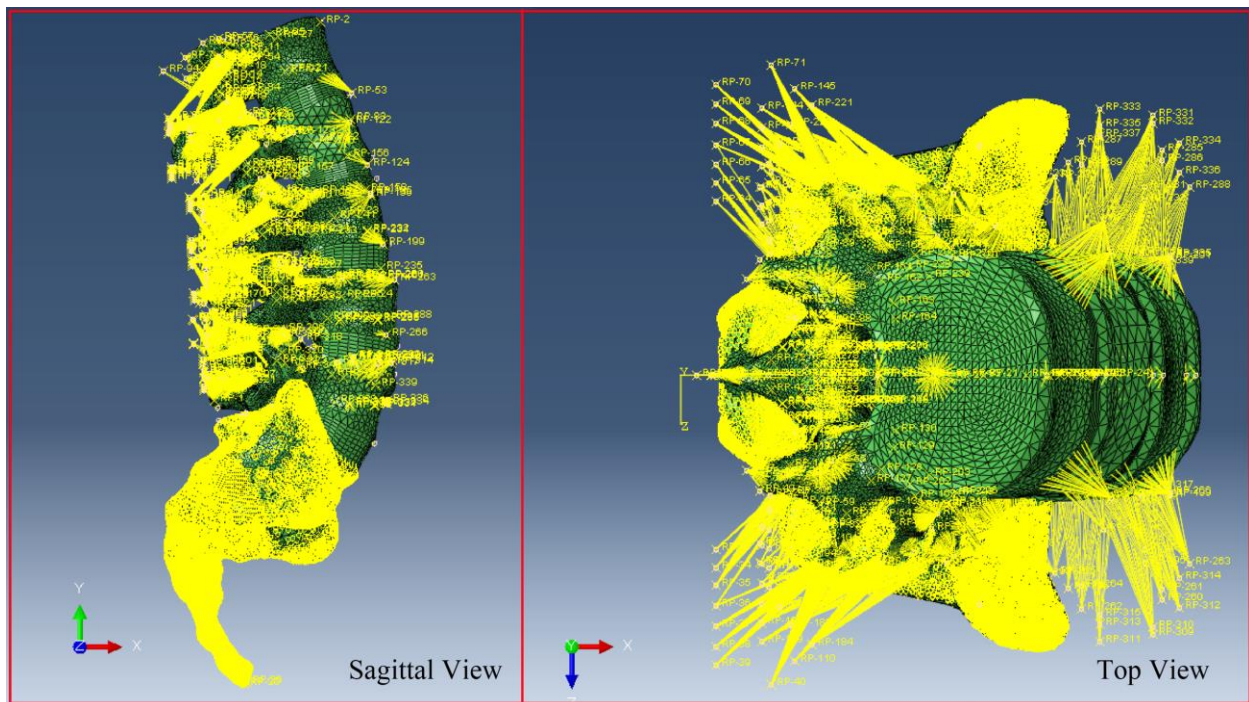


Fig. 3.6 Sagittal and top view of the FE model with the continuum distributing coupling constraints used to apply muscle forces.

Since the discs in the MSK model were simulated as rotational rigid joints that allow neither axial nor shear deformations, while they were deformable in the FE model, the deformed position of the spine in the FE model differed slightly from the one in the MSK model (Fig. 3.7). Therefore, instead of applying the reaction force F_R at T12-L1 that was predicted by the MSK model, L1 vertebra was subjected to a translation in the direction of the force F_R equal to the one predicted by the MSK model in addition to the aforementioned loads. This also ensured

quick convergence of the FE model to the same position predicted by the MSK model. The reaction force R_F resulting from this applied translation in the FE model was then compared to the force F_R at the same level. If the difference between the magnitudes of R_F and F_R was greater than predefined tolerances (1.5% for standing and 2.6% for flexion), the applied translation was adjusted. This procedure was repeated until convergence (the error was smaller or equal to the predefined tolerances) (Fig. 3.8).

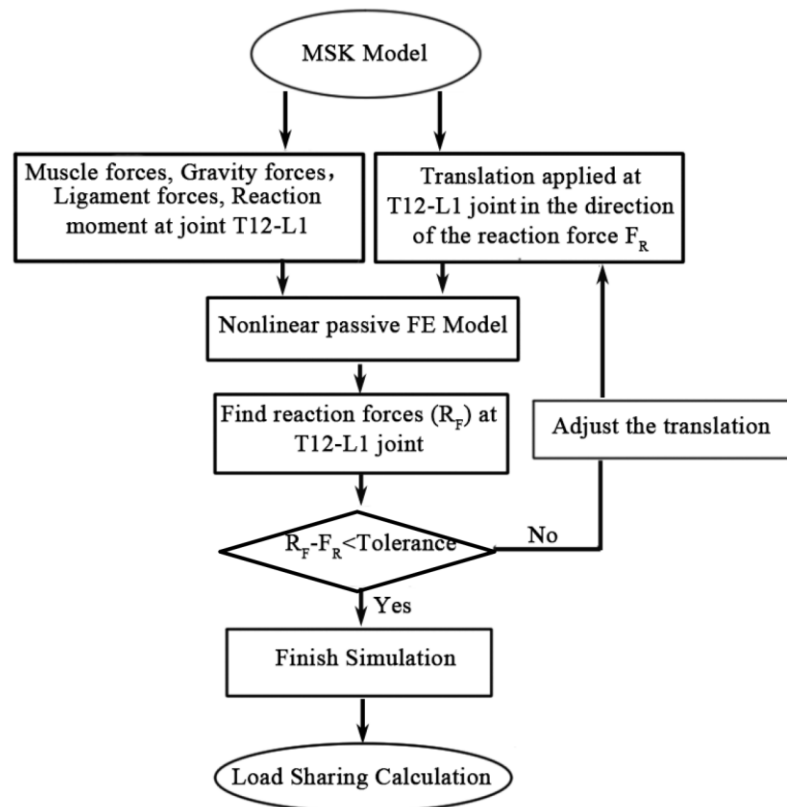


Fig. 3.7. Flowchart of the loading scenario applied to the FE model.

All muscle forces obtained from the MSK model were applied to the FE model at the insertion points as force vectors. It should be noted that the coordinates of these insertion points were adopted from the MSK model. In addition, the gravity load of each vertebra was treated as a concentrated force applied at the centroid of that vertebra. The forces in the ligaments of the segment T12-L1 were also applied as concentrated loads acting along the direction of the ligaments (Fig. 3.1).

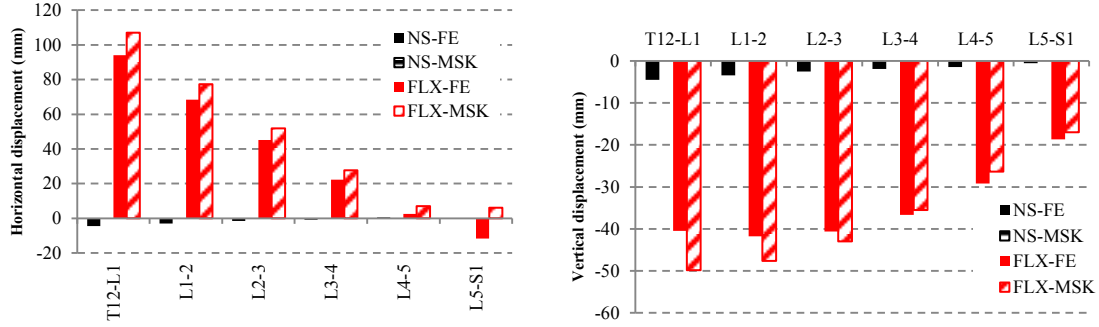


Fig. 3.8. Comparison of intersegmental horizontal (+ve: anterior) and total vertical (+ve: inferior) displacements predicted by the FE model and MSK model in standing and forward flexion postures.

3.2.5 Mathematical background of load sharing

Load sharing was calculated at each spinal level in the deformed configuration using equations of equilibrium (Naserkhaki et al., 2016a, 2016b). An imaginary plane passing through the disc at each spinal joint level was created to calculate the internal force and moment in the disc. The moment was calculated at a location similar to the joint location in the MSK model. The muscle forces, facet joint forces and ligament forces were expressed as vectors. The direction of the muscle forces in the deformed configurations of the FE model was unchanged from the MSK model. The facet joint forces were perpendicular to the articular surface at each contact node. The internal force and moment in the disc at a given spinal level were calculated as follows:

$$\sum \vec{F} = \vec{0} \rightarrow \vec{D}_F = \sum \vec{M}_i \vec{F} + \sum \vec{L}_i \vec{F} + \vec{F} \vec{J} \vec{F} + \vec{G} \vec{r} + \vec{R}_F$$

$$\sum \vec{M} = \vec{0} \rightarrow \vec{D}_M = \sum \vec{r}_{M_i F} \times \vec{M}_i \vec{F} + \sum \vec{r}_{L_i F} \times \vec{L}_i \vec{F} + \vec{r}_{F J F} \times \vec{F} \vec{J} \vec{F} + \vec{r}_{G r} \times \vec{G} \vec{r} + \vec{r}_{R_F} \times \vec{R}_F$$

Where:

\rightarrow : Force vector expressed in global Cartesian coordinate system;

DF : Disc force

DM : Disc moment

$M_i F$: Muscle i force

$L_i F$: Ligament i force

FJF : Facet joint force at each contact node

Gr : Gravity force

R_F : Reaction force from upper adjacent level in FE model

$\overrightarrow{r_{M_iF}}$: The position vector of each muscle force

$\overrightarrow{r_{FJF}}$: The position vector of facet joint force

$\overrightarrow{r_{Gr}}$: The position vector of gravity force

$\overrightarrow{r_{RF}}$: The position vector of reaction force

$\overrightarrow{r_{L_iF}}$: The position vector of ligament force

All position vectors were measured in global coordinate system. At a given level, all moments were calculated about a point in the disc similar to the joint position in the MSK model at that level.

The disc force and moment vectors were transformed to the local (disc) coordinate system in order to obtain the anterior-posterior shear and compressive forces supported by the disc. Spinal load-sharing was determined as the percentage of the total internal force/moment that each spinal component supported at a given level. The total internal force sharing can be expressed as follows:

$$Total\ Internal\ Force = |\overrightarrow{DF}|_{dir} + \sum |\overrightarrow{L_iF}|_{dir} + |\overrightarrow{FJF}|_{dir}$$

$$Disc\ Force - Share = 100 \left(\frac{|\overrightarrow{DF}|_{dir}}{Total\ Internal\ Force} \right)$$

$$Ligament\ Force - Share = 100 \left(\frac{\sum |\overrightarrow{L_iF}|_{dir}}{Total\ Internal\ Force} \right)$$

$$FJ\ Force - Share = 100 \left(\frac{|\overrightarrow{FJF}|_{dir}}{Total\ internal\ Force} \right)$$

Where:

dir : Direction of forces (either along compression or shear in the disc system)

The shear force sharing and compressive force sharing can be calculated separately using the

above formulae. This method allows identifying the contribution of each spinal component along the compressive force and shear force directions in the disc local coordinate system. The moment-sharing was estimated using similar equations without taking the direction into consideration since the flexion axis is similar in both the disc local and the global coordinates system. The moment of individual spinal component was evaluated at the joint between the adjacent vertebrae.

3.3 Results of the FE model

3.3.1 IDP

The magnitude of the IDP in neutral standing posture varied slightly along the spinal levels. The average magnitude was 0.48MPa. In the flexion posture, the IDP increased significantly particularly at lower-levels of the spine, reaching 1.98MPa at levels L5-S1 (Fig. 3.9).

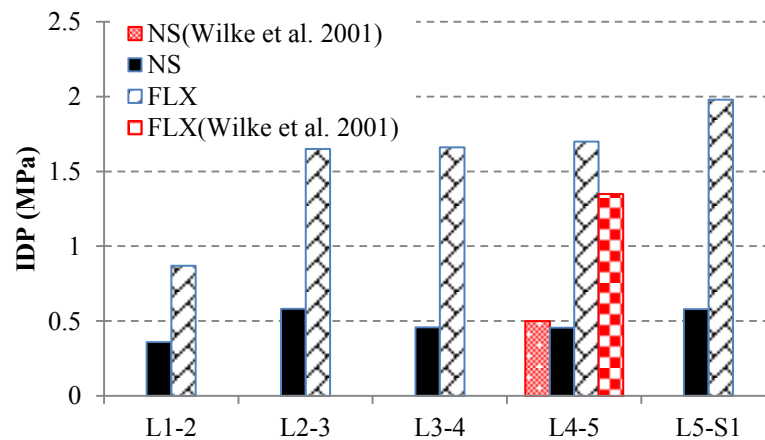


Fig. 3.9. IDP at each spinal level predicted by the FE model. Magnitude at level L4-5 is compared to *in-vivo* value reported by Wilke et al. (2001). NS: neutral stand; FLX: forward flexion.

3.3.2 Spinal loads

The total internal force at each spinal level was determined by summing the forces in the disc, ligaments and facet joints at each of these levels. The total internal moment at each spinal level was calculated by summing the disc moment and the moments about a point in the disc similar to the joint position in the MSK model of the ligament and facet joint forces. In the standing

posture, the total force and moment increased from L1 to S1 reaching 570 N and 7 Nm, respectively, at level L5-S1. A similar trend was found in the flexion posture with a significant increase in the force and moment at each level, as compared to the standing posture, where the magnitudes of the force and moment reached 1721 N and 36.15 Nm, respectively, at level L5-S1 (Fig. 3.10).

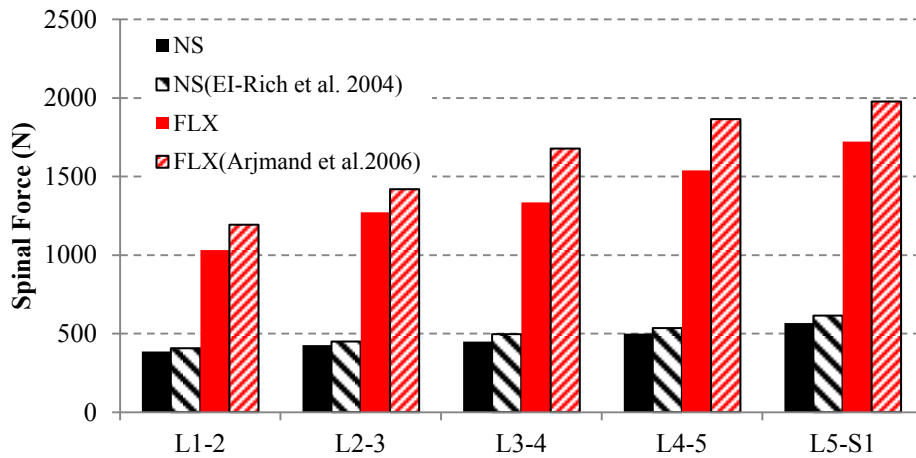


Fig. 3.10. Total internal force and moment at each spinal level predicted by the FE model for neutral standing (NS) and forward flexion (FLX).

3.3.3 Disc force and moment

While the compressive force in the discs varied slightly (average ~390 N) along the spine in neutral standing, it increased significantly at all levels, particularly at L5-S1 (~ 1226 N) in flexion. Shear increased similarly at all levels and it changed direction from posterior to anterior at L5-S1. The greatest shear value occurred at L1-2 (~630 N) (Fig. 3.11).

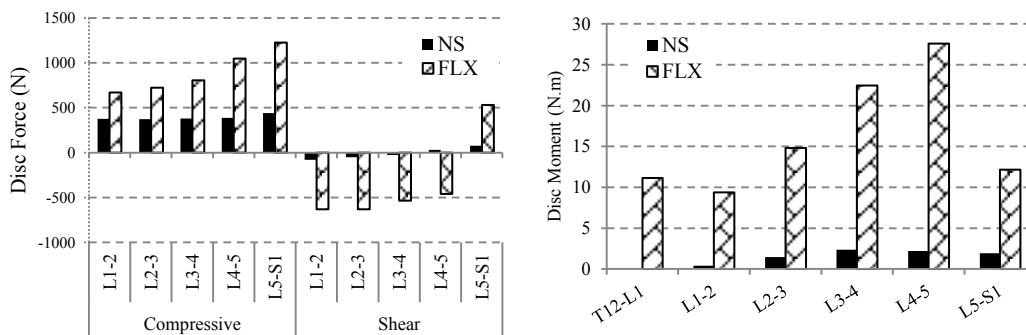


Fig. 3.11. Internal disc forces and moment (shear force: +ve in anterior direction, sagittal moment: +ve in flexion).

The disc moment was relatively small in neutral standing (< 1.5 Nm for L1-3 and ~ 2 Nm for L3-5), but significantly increased in flexion, particularly at mid-levels. The greatest magnitude reached 27.6 Nm in flexion at level L4-5.

3.3.4 Strain in annular fibers

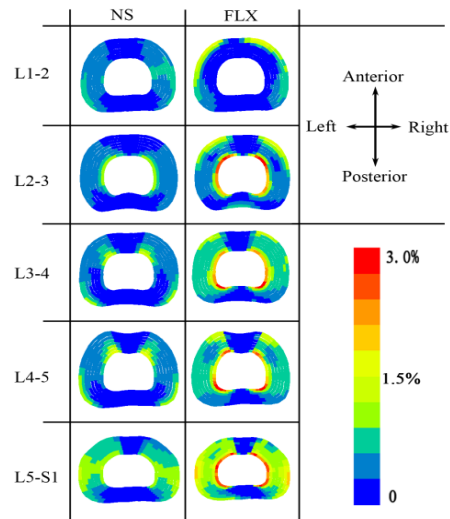


Fig. 3.12. Tensile stain distributions in the annular fibres at L1-S1 levels (NS: neutral standing; FLX: forward flexion).

The fibers at L5-S1 experienced a larger strain as compared to other levels in standing posture. The maximum strain (1.29%) occurred in the lateral (right and left) inner lamellae of the annulus. The posterior outermost lamella and the anterior innermost lamellae of L3-5 discs experienced higher strain, while the greatest strain at L2-3 was located in the innermost lamella of the lateral regions of the annulus. The annulus L1-2 experienced the lowest strain (Fig. 3.12). In flexion, strain increased significantly at L2-3 level. The maximum values ($\sim 3\%$) were found in the whole innermost lamella at L2-3 and L5-S1, as well as in the posterior innermost lamella at L3-5. The strain also increased in the anterior outmost lamella of the disc at L1-2. However, a sharp increase of the strain was observed at the L5-S1 level.

3.3.5 Load-sharing

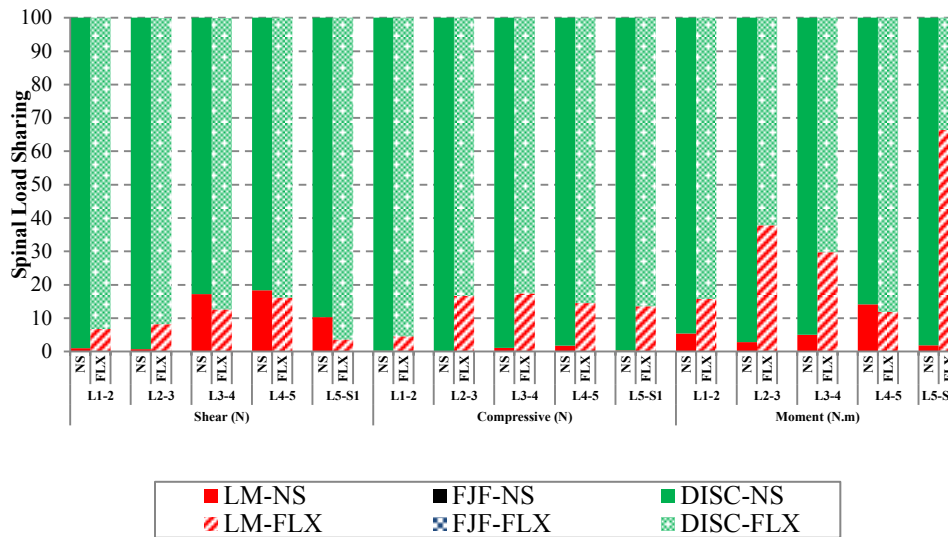


Fig. 3.13. Spinal load sharing in neutral standing (NS) and forward flexion posture (FLX) (LM: Ligaments; FJF: Facet joints; DISC: Discs).

In the standing posture, the compressive force was entirely resisted by the discs at all levels (Fig. 3.13). Shear and moment were also supported by the discs alone at levels L1-3 and L5-1, respectively. Contribution of the ligaments in resisting shear was observed at levels L3-S1, where the maximum force-sharing reached 18% at levels L3-5. The role of the ligaments in supporting the moment was minor, except at level L4-5, where the moment-sharing reached 14%. The facet joints had no contribution at all.

In flexion, the role of ligaments in resisting the compressive and shear forces, as well as moment, become more important, which alleviated the discs. For instance, the ligaments resisted 16.13% of shear at level L4-5, 17.36% of compression at L3-4, and 66.35% of the moment at L5-S1. The facet joints again had no role in supporting the load in flexion.

3.4 Discussions

We investigated spinal load-sharing in neutral standing and flexion postures using a FE model of the ligamentous lumbosacral spine in conjunction with muscle forces predicted by a MSK model. Flexion was simulated using a spine rhythm measured *in-vivo* (Arjmand and Shirazi-Adl, 2006a). The muscle forces predicted by the MSK model considered the IAP.

3.4.1 Models validation

The MSK model was tested by comparing the compressive force at L4-5 and the global and local spinal muscle forces, to experimental and computational data available in literature (Fig. 3.3). Using the vertebrae of the MSK model to create geometry of the FE model resulted in disc L4-5 with size smaller than the one reported by Wilke et al., (2001). Despite these discrepancies the compressive force demonstrated good agreement with values calculated using *in-vivo* magnitudes of the IDP (Wilke et al. 2001). The muscle forces were also in acceptable agreement with Arjmand et al. (2010). However, it is important to mention that the results were evaluated to get feedback on the MSK model, after modifying the joint stiffness and adding the CL to the model, rather than performing a thorough comparison with published data. For instance, the discrepancy between the global muscle forces predicted by the MSK model and reported values might be due to the difference in disc modeling and muscle attachment. While rigid joints were used in the current model, Arjmand et al. (2010) utilized 3D deformable beams to simulate the discs, not to mention the different optimization algorithms used in the muscle forces calculation.

The FE model was tested by comparing the spinal rotation in forward flexion and extension to *in-vitro* (Rohlmann et al. 2001) and numerical (Naserkhaki et al., 2016a; Dreischarf et al., 2014) data (Fig. 3.5). In alignment with other computational models, the current model predicted a stiff response to flexion, as compared to *in-vitro* data, which might be due to the properties of the ligaments used in this study (Naserkhaki et al., 2017). Nevertheless, the response to extension fell within the *in-vitro* range. When compared to *in-vivo* values, the IDP showed good agreement in neutral standing in flexion.

3.4.2 Spinal load and load-sharing

The FE model predicted spinal force in good agreement with results reported by El-Rich et al., (2004) in standing posture and Arjmand and Shirazi-Adl (2006a, b) in forward flexion at all spinal levels. Spinal moments, however, were not compared as our FE model and the ones used in the aforementioned studies did not calculate them the same location. Our results revealed that during neutral standing, the discs resisted almost the entire spinal forces and moments while the

ligaments made small contribution and the facet joints were silent. This is due to the small IVRs produced by gravity in standing posture. In contrast, the ligaments played a much more important role during flexion which reduced the disc contribution, where the compressive force- and moment-sharing of the ligaments reached 17.36% and 66.35% of the total load, respectively. This is reasonable since flexion is expected to lengthen the ligaments. In alignment with literature, flexion activated more ligament forces which added compression and shear to the spine at all levels (Naserkhaki et al., 2016a). The moment-sharing during standing again revealed the very important role of the disc in resisting the moment produced by muscle force. The ligaments, however, had less influence on the moment-sharing. We hence conclude, based on the aforementioned findings that the role of the discs and ligaments in resisting spinal load varies along the spine and depends on the posture.

3.4.3 Methodological issues and limitations

The MSK model did not consider abdominal muscle co-activation, known to increase the stability of the lumbar spine especially in standing posture (El-Rich et al., 2004). None of the MSK and FE models included ligaments pre-tensioning. The MSK model predicted total muscle force including passive and active components. This total force was applied as external load to the FE model. It is, however, recommended to determine the passive component and include it in the load-sharing calculation, particularly in flexion as the passive resistance of the trunk musculature played an important role in the spine equilibrium and stability as the trunk flexion increased (Arjmand and Shirazi-Adl, 2006a). Due to lack of geometry of unloaded spine, the FE model used the geometry of the MSK model's spine which loaded with gravity as initial geometry.

3.4.4 Conclusions

The current study presents a novel methodology for combining MSK and FE modeling towards comprehensive quantitative analysis of spinal biomechanics *in-vivo*. The results, in good overall agreement with literature, showed that the disc forces and moments, as well as IDP, increased substantially from an upright to a flexed posture. Spinal forces and moments were mainly

supported by the discs in the upright posture, whereas the contribution of the ligaments in resisting shear and moment was more significant in the flexed position. Detailed understanding of spinal load-sharing and the contribution of each of the spinal components during *in-vivo* conditions remains elusive. Solving this, as well as other challenges in spinal biomechanics, is invaluable for both research and clinical communities alike, towards devising more effective therapeutic and rehabilitation modalities, and for shedding light on the aetiology of the spine.

Conflict of interest statement

The authors have no conflicts of interest concern.

Acknowledgment

This study is financially supported by the China Scholarship Council (201506080013) and NSERC Discovery Grant (402046-2013), Canada.

References

- Abouhossein, A., Wisse, B., Ferguson, S.J., 2011. A multibody modelling approach to determine load sharing between passive elements of the lumbar spine. *Comput. Methods Biomech. Biomed. Eng.* 14,527-537.
- Adams, M. A., Hutton W. C., Stott J.R., 1980. The resistance to flexion of the lumbar intervertebral joint. *Spine.* 5(3):245-253.
- Adams, M. A., Hutton W. C., 1981. The relevance of torsion to the mechanical derangement of the lumbar spine. *Spine.* 6(3):241-248.
- Adams, M. A., Dolan, P., Hutton, W.C., 1988. The lumbar spine in backward bending. *Spine* 13, 1019-1026
- Arjmand, N., Gagnon, D., Plamondon, A., Shirazi-Adl, A., Larivière, C., 2010. A comparative study of two trunk biomechanical models under symmetric and asymmetric loadings. *J. Biomech.* 43, 485–491. doi:10.1016/j.jbiomech.2009.09.032
- Arjmand, N., Shirazi-Adl, A., 2006a. Model and in vivo studies on human trunk load partitioning and stability in isometric forward flexions. *J. Biomech.* 39, 510–521. doi:10.1016/j.jbiomech.2004.11.030
- Arjmand, N., Shirazi-Adl, A., 2006b. Sensitivity of kinematics-based model predictions to optimization criteria in static lifting tasks. *Med. Eng. Phys.* 28, 504–514. doi:10.1016/j.medengphy.2005.10.001
- Arshad, R., Zander, T., Dreischarf, M., Schmidt, H., 2016. Influence of lumbar spine rhythms and intra-abdominal pressure on spinal loads and trunk muscle forces during upper body inclination. *Med. Eng. Phys.* 38, 333–338. doi:10.1016/j.medengphy.2016.01.013
- Azari, F., Arjmand, N., Shirazi-Adl, A., Rahimi-Moghaddam, T., 2017. A combined passive and active musculoskeletal model study to estimate L4-L5 load sharing.
- de Zee, M., Hansen, L., Wong, C., Rasmussen, J., Simonsen, E.B., 2007. A generic detailed rigid-body lumbar spine model. *J. Biomech.* 40, 1219–1227. doi:10.1016/j.jbiomech.2006.05.030
- Dreischarf, M., Rohlmann, A., Zhu, R., Schmidt, H., Zander, T., 2013. Is it possible to estimate

- the compressive force in the lumbar spine from intradiscal pressure measurements? A finite element evaluation. *Med. Eng. Phys.* 35, 1385–1390. doi:10.1016/j.medengphy.2013.03.007
- Dreischarf, M., Zander, T., Shirazi-Adl, A., Puttlitz, C.M., Adam, C.J., Chen, C.S., Goel, V.K., Kiapour, A., Kim, Y.H., Labus, K.M., Little, J.P., Park, W.M., Wang, Y.H., Wilke, H.J., Rohlmann, A., Schmidt, H., 2014. Comparison of eight published static finite element models of the intact lumbar spine: predictive power of models improves when combined together. *J. Biomech.* 47, 1757–1766. doi:10.1016/j.jbiomech.2014.04.002
- El-Rich, M., Shirazi-Adl a., Arjmand, N., 2004. Muscle activity, Internal loads, and Stability of the Human Spine in Standing Postures: Combined Model and *in vivo* studies. *Spine* 29, 2633-2642.
- El-Rich, M., Arnoux, P.J., Wagnac, E., Brunet, C., Aubin, C.E., 2009. Finite element investigation of the loading rate effect on the spinal load-sharing changes under impact conditions. *J. Biomech.* 42, 1252–1262. doi:10.1016/j.jbiomech.2009.03.036
- Essendrop, M., 2003. Significance of intra-abdominal pressure in work related trunk-loading. Ph. D. thesis, University of Copenhagen, Denmark.
- Funabashi, M., El-Rich, M., Prasad, N., Kawchuk, G.N., 2015. Quantification of loading in biomechanical testing: the influence of dissection sequence. *J. Biomech.* 48, 3522–3526. doi:10.1016/j.jbiomech.2015.06.020
- Gudavalli, M.R., Triano, J.J., 1999. An analytical model of lumbar motion segment in flexion. *J. Manipulative Physiol. Ther.* 22, 201–208.
- Han, K.-S., Zander, T., Taylor, W.R., Rohlmann, A., 2012. An enhanced and validated generic thoraco-lumbar spine model for prediction of muscle forces. *Med. Eng. Phys.* 34, 709–716. doi:10.1016/j.medengphy.2011.09.014
- Ivicsics, M.F., Bishop, N.E., Püschel, K., Morlock, M.M., Huber, G., 2014. Increase in facet joint loading after nucleotomy in the human lumbar spine. *J. Biomech.* 47, 1712–1717. doi:10.1016/j.jbiomech.2014.02.021

- Mustafy, T., El-Rich, M., Mesfar, W., Moglo, K., 2014. Investigation of impact loading rate effects on the ligamentous cervical spinal load-partitioning using finite element model of functional spinal unit C2–C3. *J. Biomech.* 47, 2891–2903. doi:10.1016/j.jbiomech.2014.07.016
- Naserkhaki, S., Arjmand, N., Shirazi-Adl, A., Farahmand, F., El-Rich, M., 2017. Effects of eight different ligament property datasets on biomechanics of a lumbar L4-L5 finite element model. *J. Biomech.* doi:10.1016/j.jbiomech.2017.05.003
- Naserkhaki, S., Jaremko, J.L., Adeeb, S., El-Rich, M., 2016a. On the load-sharing along the ligamentous lumbosacral spine in flexed and extended postures: finite element study. *J. Biomech.* 49, 974–982. doi:10.1016/j.jbiomech.2015.09.050
- Naserkhaki, S., Jaremko, J.L., El-Rich, M., 2016b. Effects of inter-individual lumbar spine geometry variation on load-sharing: Geometrically personalized finite element study. *J. Biomech.* 49, 2909–2917. doi:10.1016/j.jbiomech.2016.06.032
- Nissan, M., Gilad, I., 1986. Dimensions of human lumbar vertebrae in the sagittal plane. *J. Biomech.* 19, 753757–755758.
- Noailly, J., Wilke, HJ., Planell, J.A., Lacroix, D., 2007. How does the geometry affect the internal biomechanics of a lumbar spine bi-segment finite element model? Consequences on the validation process. *J. Biomech.* 40, 2414–2425. doi:10.1016/j.jbiomech.2006.11.021
- Pearcy, M.J., Bogduk, N., 1999. Instantaneous axes of rotation of the lumbar intervertebral joints. *Spine* 13, 1033-1041.
- Pintar, F.A., Yoganandan, N., Myers, T., Elhagediab, A., Sances, A., 1992. Biomechanical properties of human lumbar spine ligaments. *J. Biomech.* 25, 1351–1356.
- Rohlmann, A., Bauer, L., Zander, T., Bergmann, G., Wilke, HJ., 2006. Determination of trunk muscle forces for flexion and extension by using a validated finite element model of the lumbar spine and measured in vivo data. *J. Biomech.* 39, 981–989. doi:10.1016/j.jbiomech.2005.02.019

- Rohlmann, A., Neller, S., Claes, L., Bergmann, G., Wilke, H.-J., 2001. Influence of a follower load on intradiscal pressure and intersegmental rotation of the lumbar spine. *Spine* 26, E557–E561.
- Schmidt, H., Heuer, F., Simon, U., Kettler, A., Rohlmann, A., Claes, L., Wilke, H.-J., 2006. Application of a new calibration method for a three-dimensional finite element model of a human lumbar annulus fibrosus. *Clin. Biomech.* 21, 337–344.
- Schmidt, H., Kettler, A., Heuer, F., Simon, U., Claes, L., Wilke, H.-J., 2007. Intradiscal pressure, shear strain, and fiber strain in the intervertebral disc under combined loading. *Spine* 32, 748–55. doi:10.1097/01.brs.0000259059.90430.c2
- Schmidt, T.A., An, H.S., Lim, T.H., Nowicki, B.H., Haughton, V.M., 1998, The Stiffness of lumbar spinal motion segments with a high-intensity zone in the anulus fibrosus. *Spine* 23, 2167-2173.
- Schultz, A., Andersson, G., Ortengren, R., Haderspeck, K., Nachemson, A., 1982. Loads on the lumbar spine. Validation of a biomechanical analysis by measurements of intradiscal pressures and myoelectric signals. *J. Bone Joint Surg. Am.* 64, 713–720.
- Schultz, A.B., Warwick, D.N., Berkson, M.H., Nachemson, A.L., 1979. Mechanical properties of human lumbar spine motion segments. *J Biomech Eng* 101, 46–52.
- Sharma, M., Langrana, N.A., Rodriguez, J., 1995. Role of ligaments and facets in lumbar spinal stability. *Spine* 20, 887–900.
- Shirazi-Adl, A., Ahmed, A.M., Shrivastava, S.C., 1986. Mechanical response of a lumbar motion segment in axial torque alone and combined with compression. *Spine* 11, 914–927.
- Wilke, H., Neef, P., Hinz, B., Seidel, H., Claes, L., 2001. Intradiscal pressure together with anthropometric data-a data set for the validation of models. *Clin. Biomech.* Bristol Avon 16 Suppl 1, S111-126.
- Zhu, R., Zander, T., Dreischarf, M., Duda, G.N., Rohlmann, A., Schmidt, H., 2013. Considerations when loading spinal finite element models with predicted muscle forces from inverse static analyses. *J. Biomech.* 46, 1376–1378.

Chapter 4

Effects of Lumbo-Pelvic Rhythm on Trunk Muscle Forces and Disc Loads during Forward Flexion: A Combined Musculoskeletal and Finite Element Simulation Study

This chapter has been published as Liu, T., Khalaf, K., Adeb S., El-Rich, M., 2018. Effects of Lumbo-Pelvic Rhythm on Trunk Muscle Forces and Disc Loads during Forward Flexion: A Combined Musculoskeletal and Finite Element Simulation Study. J. Biomech.

Abstract

Previous *in-vivo* studies suggest that the ratio of total lumbar rotation over pelvic rotation (lumbo-pelvic rhythm) during trunk sagittal movement is essential to evaluate spinal loads and discriminate between low back pain (LBP) and asymptomatic population. Similarly, there is also evidence that the lumbo-pelvic rhythm is key for evaluation of realistic muscle and joint reaction forces and moments predicted by various computational musculoskeletal (MSK) models. This study investigated the effects of three lumbo-pelvic rhythms defined based on *in-vivo* measurements on the spinal response during moderate forward flexion (60°) using a combined approach of MSK modeling of the upper body and Finite Element (FE) model of the lumbosacral spine. The muscle forces and joint loads predicted by the MSK model, together with the gravitational forces, were applied to the FE model to compute the disc force and moment, intradiscal pressure (IDP), annular fibers strain, and load-sharing. The results revealed that a rhythm with high pelvic rotation and low lumbar flexion involves more global muscles and increases the role of the disc in resisting spinal loads, while its counterpart, with low pelvic rotation, recruits more local muscles and engages the ligaments to lower the disc loads. On the other hand, a normal rhythm that has balanced pelvic and lumbar rotations yields almost equal disc and ligament load-sharing and results in more balanced synergy between global and local muscles. The lumbo-pelvic rhythm has less effect on the IDP and annular fibers strain. This work demonstrated that the spinal response during forward flexion is highly dependent on the lumbo-pelvic rhythm. It is therefore, essential to adapt this parameter instead of using the default parameters in MSK modeling for accurate prediction of muscle forces and joint reaction forces and moments. The findings provided by this work are expected to improve knowledge of spinal response during forward flexion, and are clinically relevant towards LBP treatment and disc injury prevention.

Keywords: Lumbo-pelvic rhythm, Finite element analysis, Musculoskeletal model, Flexion, Muscle forces, Load-sharing, Spinal load, Center of mass, Posture

4.1 Introduction

Forward flexion includes a combination of lumbar flexion and pelvic rotation, also referred to as, lumbo-pelvic coordination or rhythm (Granata and Sanford, 2000; Tafazzol et al., 2014). *In vivo* investigations, through measuring the kinematics of the lumbar spine (Arjmand and Shirazi-Adl, 2006; Granata and Sanford, 2000) and the lumbo-pelvic rhythm during flexion, have demonstrated discrepancies in the variation of both rhythms in different experiments (Esola et al., 1996; Porter and Wilkinson, 1997; Tafazzol et al., 2014; Rose et al., 1988). Furthermore, the lumbo-pelvic rhythm was found different between healthy subjects and LBP patients (Kim et al. 2013). A recent study revealed that the lumbar contribution to the lumbo-pelvic rhythm during flexion was about 22% smaller in chronic LBP patients as compared to control (Laird et al, 2016). Subjects with a history of LBP exhibited different lumbo-pelvic rhythms (Esola et al 1996), yet reduced mobility (20%) of the pelvis as compared to asymptomatic subjects (Porter and Wilkinson 1997), indicating that LBP can potentially be reduced by greater pelvic rotation. On the contrary, Vazirian et al. (2016) found that the magnitude of lumbar contribution decreases in LBP patients, the elderly and females, as well as with greater pace of motion, but increases with greater external load and back muscle fatigue.

MSK modeling, which allows the evaluation of muscle forces and joint reaction forces and moments, during forward flexion for instance requires accurate lumbar and pelvic rotation input for realistic predictions (Arjmand et al., 2011; Arjmand and Shirazi-Adl, 2006; Fathallah et al., 1999; Cholewicki and McGill, 1996). Arshad et al. (2016) reported that spine rhythms affects the shear and compression forces in the L4-5 disc as well as the global and local trunk muscle forces at maximum flexion position. Tafazzol et al. (2014) found that the lumbar spine contributed more to the trunk rotation during early forward flexion, while the pelvis contributed more during the final stage. The aforementioned research sheds light on the interactions between the lumbar spine and pelvic rotations and spinal forces. However, the effects of the lumbo-pelvic rhythm on load-sharing or IDP along the spine remain unknown.

This study, hence, aims to quantify the effects of three different lumbo-pelvic rhythms defined based on *in-vivo* data taken from the literature on the response of the lumbosacral spine during moderate forward flexion (up to 60°) using a combined MSK modelling and FE analysis.

4.2 Methods

4.2.1 Musculoskeletal model

A previously-validated MSK model (Liu et al., 2018) was employed to calculate trunk local and global muscle forces during 60° forward flexion. The model was adjusted to average height and weight of 168cm and 70kg, respectively. The MSK model (version 6.0, AnyBody Technology A/S, Denmark) included the skull, upper arms, thorax, and lumbosacral spine. The lumbosacral spine L1-S1 included five rigid vertebrae (L1-5), five discs modeled as rigid joints with rotational degrees of freedom only and nonlinear flexural stiffness, seven ligaments, the sacrum, and the pelvis.

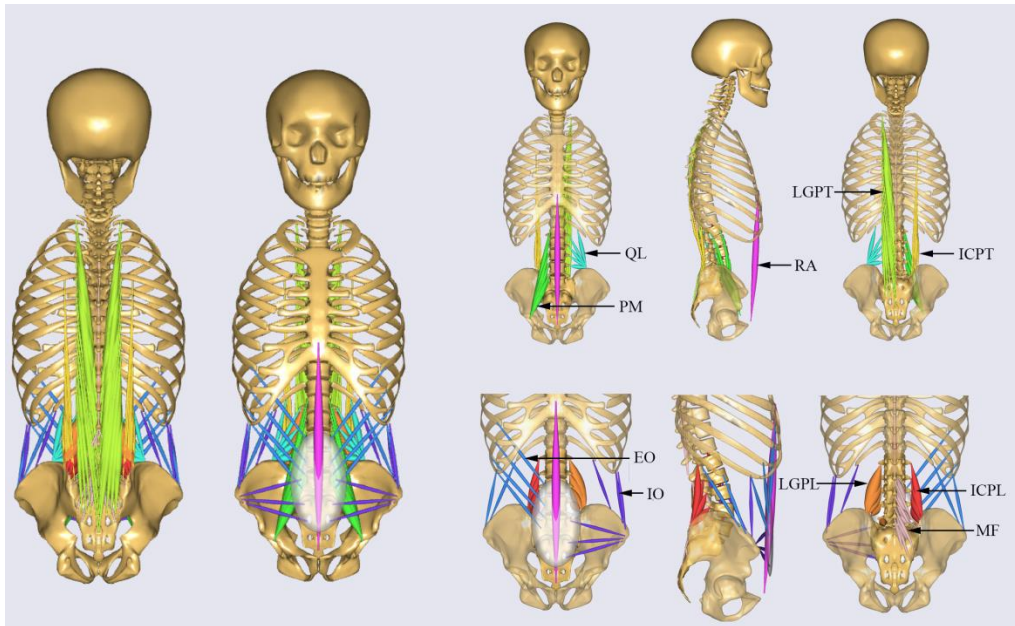


Fig. 4.1. Trunk muscle architecture in Anybody and individual muscle groups. Global muscles(1 rectus abdominis (RA), 12 internal oblique (IO), 12 external oblique (EO), 16 iliocostalis lumborum pars thoracic (ICPT), 24 longissimus thoracis pars thoracic (LGPT)) and Local muscles (8 iliocostalis lumborum pars lumborum (ICPL), 10 longissimus thoracis pars lumborum (LGPL), 22 psoas major (PM), 38 multifidus (MF) and 10 quadratus lumborum muscle fascicles (QL)) (Arshad et al. 2016).

The ligaments were simulated by springs for which the force is calculated as the product of the stiffness and length change during simulation. The facet joints were activated and the contact force was produced by detecting the distance between the contact points located between adjacent facet surfaces (Liu et al., 2018). The overall musculature of the MSK model included 188 muscle fascicles grouped into global and local muscles (Fig. 4.1). The muscles were

modelled in the following three forms embedded in Anybody: a straight line connecting insertion and origin points, via-points muscles, and nonlinear wrapping muscles. Muscle strength was defined as the product of the maximum muscle stress to the physiological cross-sectional area (de Zee et al., 2007). Muscle forces were evaluated by minimizing the sum of the square of the ratios of muscle force and muscle strength (de Zee et al., 2007, Damsgaard et al., 2006). The MSK model also considered the intra-abdominal pressure (IAP), with magnitude fluctuating between 2.2 kPa to 4.4 kPa, during the simulations. The spine rhythm measured by Granata and Sanford (2000) was applied to the model as follows : 8% at T12-L1, 13% at L1-2, 16% at L2-3, 23% at L3-4, 26% at L4-5, and 14% at L5-S1. These percentages express the intersegmental rotations as a percentage of the total lumbar flexion.

4.2.2 Passive FE model

The 3D geometry of the L1-S1 bony structures was directly obtained from the MSK model, cleaned from spikes and sharp edges using Geomagic software (Geomagic Studio 2014), then meshed in Hypermesh (Hyperworks 14.0). The disc was created between two intervening endplates and divided into nucleus pulposus (NP) and annulus fibrosus (AF) reinforced by collagen fibers with nonlinear tension force-length relationship, with a volume ratio of 44% and 56%, respectively (El-Rich et al., 2009; Schmidt et al., 2006). The fibers were distributed in concentric lamellae with a crosswise pattern close to $\pm 35^\circ$ (El-Rich et al., 2009; Schmidt et al., 2007). A frictionless surface-to-surface contact was established between all facet joints with a minimal gap of 1.5mm. The ligament force had the same force-length relationship and insertion points as those in the MSK model. The cartilaginous endplates and bones were assumed to be linear elastic while the annulus ground and NP were modeled using the hyper-elastic Mooney-Rivlin model. Details on material properties were provided elsewhere (Liu et al., 2018). All simulations were performed using Abaqus software (Abaqus 6.13-4). The sacrum was rotated based on the lumbo-pelvic ratios investigated in this study.

4.2.3 Load transfer from the MSK model to the FE model

The reaction moment, ligament forces, and facet joint forces obtained at the level T12-L1 together with muscle forces at all levels of the MSK model were applied to the FE model. These loads resulted from the upper body weight and muscle forces and accounted for the IAP (Liu et al., 2018). To correct the small discrepancy in the deformed positions predicted by the MSK

model and the FE model due to the difference in the modeling of the disc, the L1 vertebra was subjected to a slight anterior-posterior translation, in addition to the aforementioned loads. All muscle forces obtained from the MSK model were applied to the FE model at the insertion points as force vectors. The gravity force of each vertebra and the forces in the ligaments of the segment T12-L1 were applied as concentrated forces (Fig. 4.2).

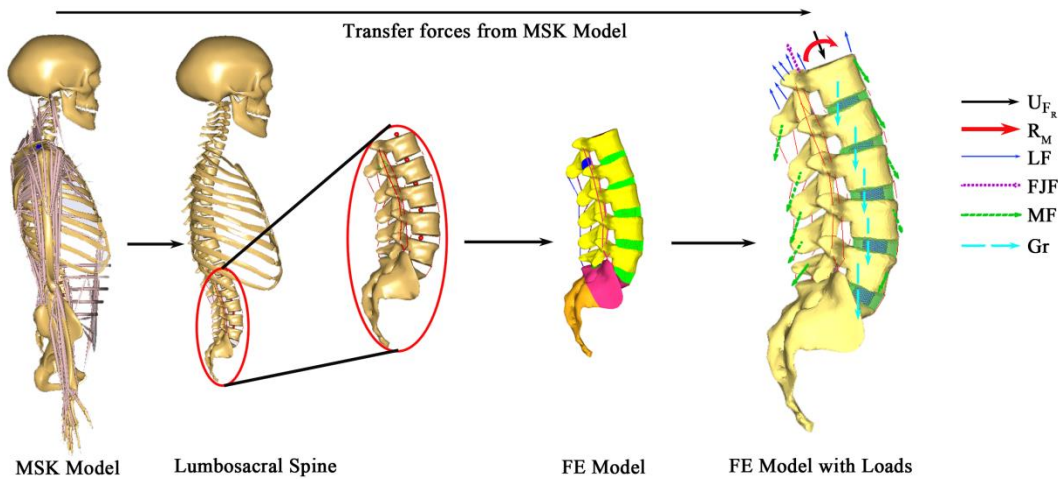


Fig. 4.2. The process of transferring forces from the MSK model to FE model. (U_{F_R} : Translation in the direction of the reaction force at T12-L1; R_M : Reaction moment at joint T12-L1; LF: Ligament forces; FJF: Facet joint forces; MF: Muscle forces; Gr: Gravitational force for each vertebra).

4.2.4 Validation

The MSK model and passive FE model have been validated in our previous study (Liu et al., 2018). The MSK model was tested in neutral standing and flexion postures by comparing the compressive force in the joint L4-5 indirectly to the *in-vivo* measured IDP at the same level (Wilke et al., 2001). The FE model was also tested by comparing total rotation of L1 with respect to L5 produced by flexion and extension moments to other numerical (Dreischarf et al., 2014, Naserkhaki et al., 2016) and *in-vitro* (Rohlmann et al. 2001) data. The method of transferring the muscle forces from the MSK model to FE model, as well as simulation process, are also elaborated at length in our previous work (Liu et al., 2018).

4.2.5 Simulated tasks

Sixty degrees forward trunk flexion was simulated using three lumbo-pelvic rhythms as summarized in Table 4.1. These rhythms were defined based on the peak *in-vivo* ranges measured in previous studies (Rose et al., 1988; Esola et al., 1996; Porter and Wilkinson, 1997; Tafazzol et al., 2014,).

Table 4.1. The lumbo-pelvic rhythms applied to the model

| Lumbo-Pelvic Rhythm Models* | Lumbar Rotation Angle/Pelvic Rotation Angle | Lumbar (L1-S1) Rotation (°) | Pelvis Rotation (°) |
|-----------------------------|---|-----------------------------|---------------------|
| L20P40 | 0.5 | 20 | 40 |
| L36P24 | 1.5 | 36 | 24 |
| L45P15 | 3 | 45 | 15 |

* LnPm: n is the lumbar rotation, m is the pelvis rotation, $n + m = 60^\circ$ (total flexion rotation).

4.3 Results

4.3.1 Posture and Center of Mass

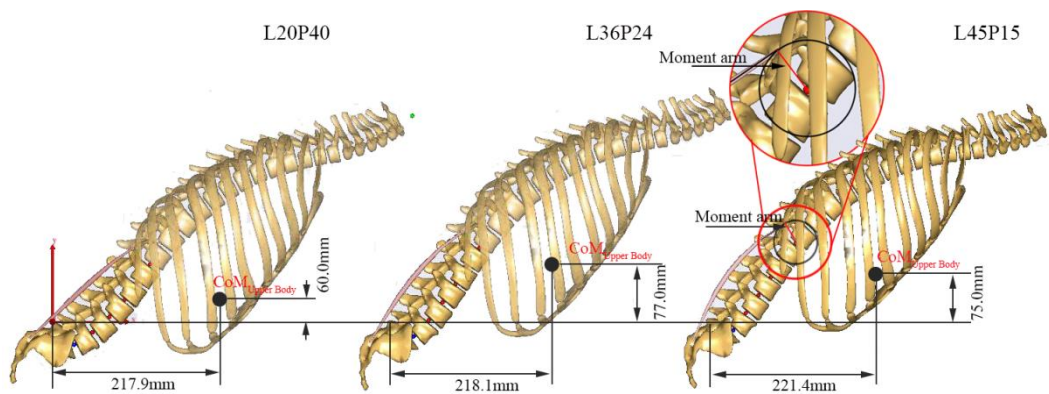


Fig. 4.3. Variation of posture and Center of Mass (CoM) of the upper body at 60° flexion with lumbo-pelvic rhythms.

The thorax and lumbar spine postures, as well the lever arms and the vertical positions of the gravity forces, varied with the lumbo-pelvic rhythm (Fig. 4.3). The CoM for the entire upper body was closer to the sacrum (217.9mm) and was lower (60mm) in the L20P40 model than in the other models. The L45P15 model, however, yielded posture with greater lever arms (221.4mm) of the gravity forces and higher CoM (75mm). The L36P24 model produced posture with greatest vertical distance of the CoM (77mm). The reference frame of all CoMs is located at the posteriorly distal point of the sacrum.

4.3.2 Trunk muscle force

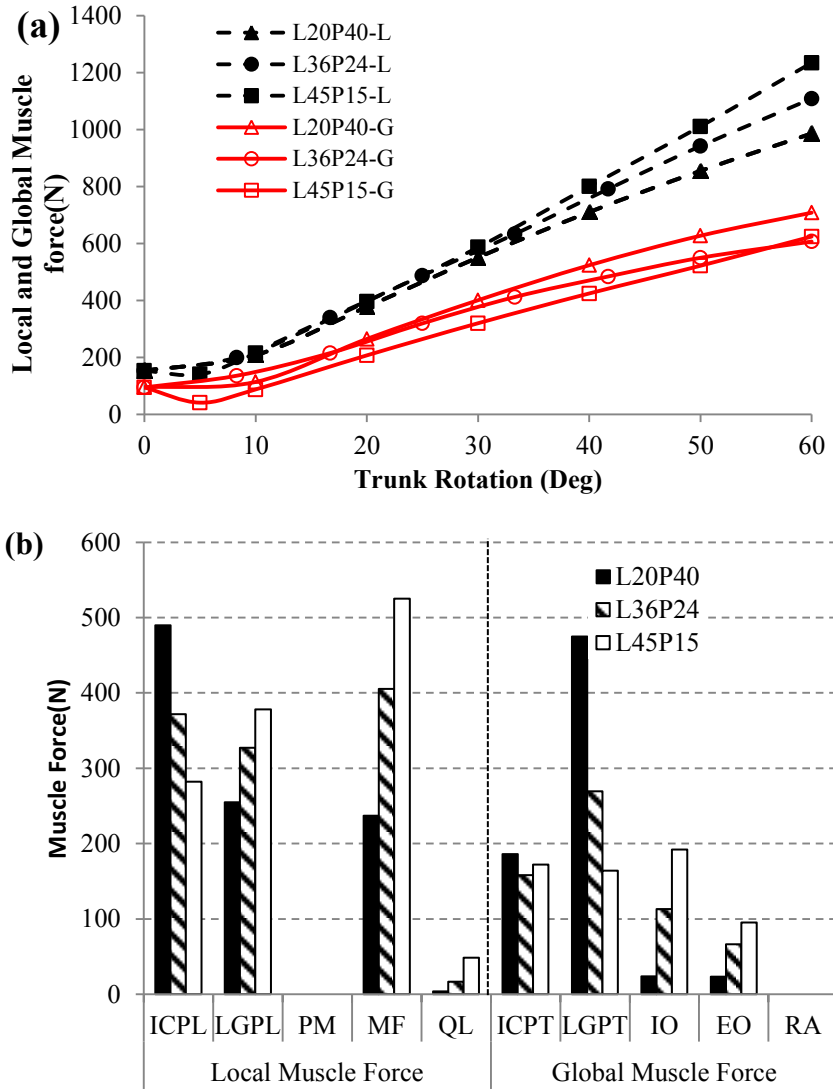


Fig. 4.4. (a) Variation of total local (L) and total global (G) muscle forces with lumbo-pelvic rhythms during 60° trunk forward flexion. (b) Variation of individual muscle group forces with lumbo-pelvic rhythms at 60° trunk forward flexion.

The total global and total local muscle forces were defined as the sum of all global and local muscle forces respectively (Fig. 4.4a). The total local muscle force increased almost linearly during the inclination of the upper body in all models. However, the total global muscle force fluctuated during the initial phrase of flexion and then increased during for the rest of the simulation. Both local and global muscle forces exhibited similar trends under the three different rhythms. The global muscle forces predicted by the L36P24 (moderate pelvic rotation) model exhibited the highest forces, followed by the L20P40 (high pelvic rotation) model, and finally by

the L45P15 (low pelvic rotation) model during the initial 20° of flexion. Higher global muscle forces were found using the L20P40 model, followed by the L36P24 model. The L45P15 model came third in terms of the magnitude of global muscle forces from 20° to 55°, and then second during the last 5° of flexion, as it predicted slightly higher forces than the L36P24 model. Minor differences between the three models were observed in terms of the local muscle forces during the first 30° of the flexion. Although these differences increased during the last 30° flexion, the trend followed the same order (L45P15>L36P24>L20P40).

The forces for each muscle group were also predicted (Fig. 4.4b). The results demonstrate that the RA muscle and PM muscle group were silent throughout flexion for all rhythms. The L36P24 model was second in terms of group muscle force predictions, except for the ICPT muscle group. The muscle forces presented an ascending order in particular muscle groups (LGPL, QL, MF, IO, EO), and a descending order in the ICPL, LGPT groups as the lumbo-pelvic ratios varied from 0.5 to 3. The ICPT muscle force predicted by the L20P40 model presented the highest force value, followed by the muscle forces predicted by L45P15 model, and finally by the L36P24 model.

4.3.3 Disc strain

All three models predicted high tensile strains in the innermost area of the collagen fibres at the L2-S1 levels, but small tensile strains at the L1-2 level. For the L20P40 model, high tensile strain first appeared at the anterior area of the innermost lamella at the L2-5 level and then extended to the whole area of the innermost lamella at the L5-S1 level (Fig. 4.5). For the L36P24 model, high tensile strain was first detected at the anterior area of the innermost lamella at the L2-3 level and then transferred to the posterior area of the innermost lamella from L3 to L5, finally extending to the entire innermost lamella at the L5-S1 level. In the L40P15 model, the same trend occurred at the L2-5 levels similar to the L36P24 model. It should also be noted that as the lumbo-pelvic ratio was varied from 0.5 to 3, the proportions of the high tensile strain increased at the L2-5 levels, but decreased at the L5-S1 and L1-2 levels.

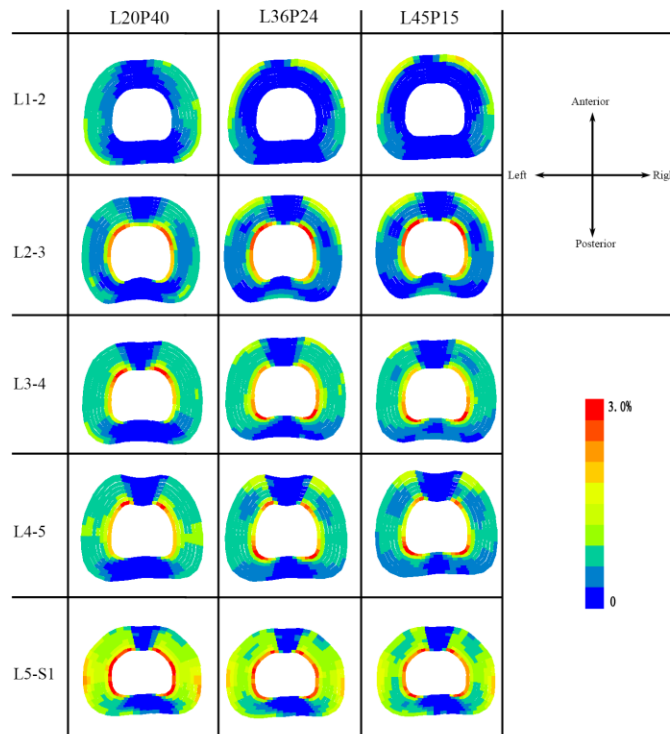


Fig. 4.5. Variation of annular fibers strain with lumbo-pelvic rhythms at 60° trunk forward flexion.

4.3.4 IDP

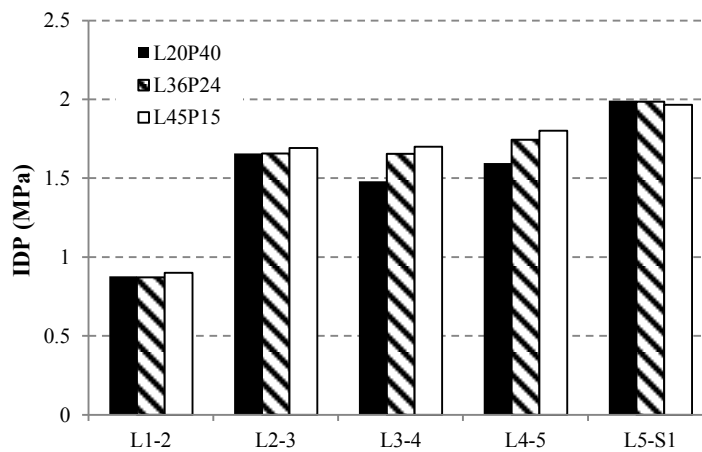


Fig. 4.6 Variation of IDP with lumbo-pelvic rhythms at 60° trunk forward flexion.

Overall, the L45P15 model predicted the highest IDP at all levels except the L5-S1. The maximum IDP difference was found between the L45P15 and the L20P40 models at the L4-5 level and reached ~15% (Fig. 4.6). The L20P40 and L36P24 models predicted almost the same

IDP at the L1-3 and L5-S1 levels while the L20P40 model predicted the lowest IDP at the L3-5 levels.

4.3.5 Disc force and moment

The compressive force increased from the L1 to S1 levels for both the L20P40 and L36P24 models. The same trend was observed for the L45P15 model, except at the L3-4 level. The compressive force predicted by the L20P40 model was higher in comparison to the value predicted by L36P24 and L45P15 models at the L1-4 levels.

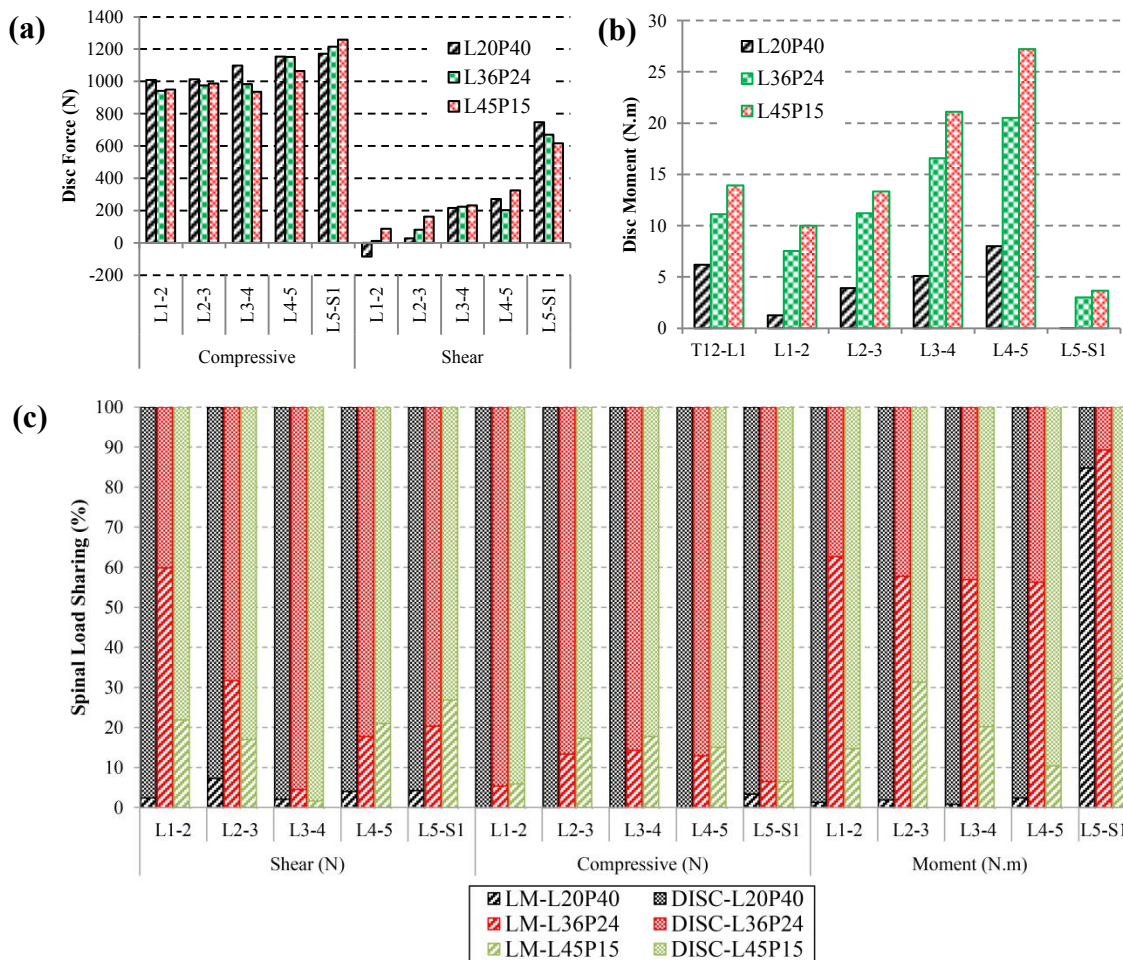


Fig. 4.7. Variation of disc internal forces (a) and moments (b) as well as load-sharing (c) with lumbo-pelvic rhythms at 60° trunk forward flexion (anterior shear force: +ve, sagittal moment: +ve in flexion, LM: ligament force, DISC: disc force, Facet joints have zero forces for three lumbo-pelvic rhythms).

The compressive force predicted by the L20P40 model was 115N greater than its counterpart from the L36P24 model, which was 47N greater than the compressive force predicted by the L45P15 model at the L3-4 level. However, the opposite pattern was observed at the L5-S1 level, where the maximum compression occurred in the L45P15 model and reached 1258N. The L20P40 and L36P24 models predicted similar compressive forces at the L4-5 levels, which were ~85N higher than the force predicted by the L45P15 model.

Shear forces demonstrated an increasing pattern from L1 to S1, where the maximum value was seen in the L20P40 model at 747N. The three models predicted anterior shear forces at all levels except the L20P40 model which predicted posterior shear force at the L1-2 level (Fig. 4.7a).

The L20P40 model with high pelvic rotation produced the smallest disc moment while the greatest moment magnitude resulted from the rhythm with low pelvic rotation (model L45P15) (Fig. 4.7b). The maximum difference between these magnitudes reached ~20Nm and occurred at the L4-5 level. The model with moderate pelvic rotation (L36P24) predicted disc moment values falling in between those predicted by the other models.

4.3.6 Load-sharing

Load sharing of a given spinal component is defined as a percentage of spinal load carried by that component (Liu et al., 2018). In the L20P40 model (high pelvic rotation), shear, compression and moment were almost entirely carried by the discs alone except at the L5-S1 level where the ligaments contribution to moment resistance reached 85%. In the L36P24 model (moderate pelvic rotation), the disc had noticeable contribution to compressive and shear forces resistance as well while the ligaments contributed more to moment resistance, where their maximum moment-sharing reached 90% at the L5-S1 level. The force- and moment-sharing of the discs were also significant, as compared to the ligaments in case of the rhythm with low pelvic rotation. No contribution was observed for the facet joints in any of the three rhythms (Fig. 4.7b).

4.4 Discussions

Quantitative assessment of the lumbo-pelvic rhythm impact on key spinal biomechanics parameters provides valuable insight towards LBP treatment and disc injury prevention. This study investigated the effects of the lumbo-pelvic rhythm during moderate forward flexion on

spinal response using a combined MSK and FE analysis approach. Three lumbo-pelvic rhythms with high, moderate, and low pelvic rotations were input into our previously validated MSK model in order to predict trunk muscle forces and joint reaction forces and moments for posture changing from upright to 60° forward flexion. The predicted forces and moments at 60° flexion were then applied to our previously validated FE model of a lumbosacral spine to predict the IDP, disc forces and moments, as well as load-sharing, and compare them in terms of the three lumbo-pelvic rhythms.

4.4.1 Muscle forces and disc loads

The observed influence of the lumbo-pelvic ratio on muscle forces was relatively small during initial flexion (<30°), but became increasingly larger when the flexion exceeded 30° particularly for the global muscles. The maximum difference in muscle forces predicted by the various lumbo-pelvic rhythms occurred at 60° flexion and reached ~248N for the local muscles and ~83N for the global muscles. This may be due to several factors including moment arms of the local muscles (Fig. 4.3) which are affected by the intervertebral rotation in the rhythm with high lumbar rotation and moment arms, or the global muscles which are influenced by the pelvic rotation in the rhythm with high pelvic rotation. The MF, LGPL, IO, EO, and QL muscles are attached to the vertebrae and pelvis (Fig. 4.1), and hence when the lumbar rotation increased (rhythm L45P15) the force in these muscles increased to ensure stability and balance the gravity forces. The ICPL, LGPT and ICPT muscles, attached to the thorax and sacrum (Fig. 4.1), generated greater forces when the rhythm involves high pelvic rotation. The optimization-based approach used in the current MSK model to estimate muscle forces predicted no force in the RA and PM muscles. Thus, the effects of the lumbo-pelvic rhythm on these muscles could not be quantified.

The lumbo-pelvic rhythm had less effect on the disc compressive and shear forces as compared to the moment. The variation in compression and shear is due to the variation in total (global + local) muscle force in the three rhythms, while the gravitational forces remained the same. However, the significant change in the disc moment is related to the lever arms of the gravity and muscle forces which changed with the lumbo-pelvic rhythm. Also, although the rhythms with moderate (L36P24) and high (L20P40) pelvic rotation have CoM with similar anterior location (i.e. similar lever arms for the gravitational forces), the former will have lower margin of

stability as it had higher CoM (El-Rich and Shirazi-Adl, 2005). The rhythm that involves moderate pelvic and lumbar rotation (L36P24) is considered as normal rhythm adopted by asymptomatic individuals (Tafazzol et al., 2014), hence it produces disc loads that fall within those produced by the other rhythms and a balanced synergy between local and global muscles forces.

Tafazzol et al. (2014) measured the lumbo-pelvic ratios on eight young healthy males performing full flexion using inertia tracking device. They predicted the spinal loads for ratios varying from 0.5 to 3 with an interval of 0.25 using a MSK model. Their results revealed that the compressive and shear forces showed a maximum reduction of 21% and 45% respectively, at any specific trunk flexion angle when lumbo-pelvic ratio increases. In addition, effects of the lumbo-pelvic ratio on spinal forces at L5-S1 level become pronounced and exhibit a nonlinear pattern due to passive components when the trunk rotation increases. The shear force predicted in the current research follows similar trend, while the compressive shows opposite pattern at the L5-S1 level. This disagreement might be due to the difference in spine geometry used in both studies including lordosis, discs height, muscle architecture (number of muscles, insertion and attachment points).

4.4.2 IDP and annular fiber strain

The IDP at the L1-3 and L5-S1 levels was not affected by the lumbo-pelvic rhythm (Fig. 4.6) as the disc resultant force (compression and shear) was almost similar (~970N at L1-2, ~1000N at L2-3, ~1390N at L5-S1) in all cases. The IDP magnitude at the L4-5 level in all rhythm cases ranged from 1.6 MPa to 1.8 MPa which is slightly higher than the value obtained by interpolation (Azari et al, 2017) using the *in-vivo* data reported by Wilke et al. (2001). This is due to the disc cross sectional area which is smaller in our FE model than the one reported by Wilke et al. (2001) in addition to the difference in the upper body mass distribution and musculature.

Overall, the lumbo-pelvic rhythm affected the IDP, mainly at the L3-5 levels, where 50% of the total lumbar rotation was applied. The rhythm with high lumbar rotation increased the IDP particularly at the L3-5 levels, and shifted a proportion of the high tensile strain from the L5-S1 to the L3-5 levels. These effects, however, were relatively small as compared to the muscle forces and disc moment. In alignment with literature, the current research also confirms that

using more pelvic motion relieves the IDP at L4-5 level (McClure et al., 1997). Our findings revealed that the lumbo-pelvic rhythm has little impact on IDP and annular fibers strain as compared to muscle forces and disc moment for moderate forward flexion ($\leq 60^\circ$). These effects may become more pronounced for greater flexion angles.

4.4.3 Disc and ligament load-sharing

Our results revealed that the contribution of the discs and ligaments in load-bearing during forward flexion depends on the coordination between the lumbar spine and the pelvis, and that the facet joints have no contribution at all. For the same flexion angle (60°), a lumbo-pelvic rhythm with high pelvic rotation and low lumbar rotation increases the role of disc in resisting spinal forces and moments to reach 100% at some levels. By contrast, a rhythm that involves more lumbar rotation engages the ligaments to resist spinal load, particularly moments. A normal rhythm such as L36P24 with balanced (almost equal) pelvic and lumbar rotations yields almost equal disc and ligament load-sharing, confirming the well-established major role of the discs in load-bearing during forward flexion.

4.4.4 Methodological issues and limitations

Similar to other computational studies, the current research has assumptions and limitations. The spinal rhythm measured *in-vivo* by Granata and Sanford (2000) and used by Arjmand and Shirazi (2006) was considered by the MSK model and kept constant during entire flexion for simplification. Future improvement requires continuous *in-vivo* measurement of the spinal rhythm and lumbo-pelvic rhythm during flexion. Once set, the lumbo-pelvic rhythms were also assumed constant during the simulation. The disc forces and moments were calculated based on equilibrium requirements at each level (Naserkhaki et al., 2016; Liu et al., 2018), where the FE model of the lumbosacral spine was subjected to the muscle, gravitational forces, and joint reaction forces and moments resulting from the upper body, as well as ligament forces at the T12-L1 level. The moments about points similar to the joint position in the MSK model (Liu et al., 2018) were calculated. Had the model considered different points such as the center of reaction (Ghezlbash et al., 2018), different magnitudes of disc moments would have been computed. The facet contact force in MSK was determined by detecting the distances between contact points located on adjacent facet surfaces. However, the surface-to-surface contact is employed in the FE model to simulate facet joint interactions. Other limitations of the

methodology are detailed elsewhere (Liu et al., 2018). In addition, although the influence of the lumbo-pelvic rhythm on muscle forces was quantified for posture changing from upright to 60° flexion, the disc loads, IDP, and load-sharing were determined at 60° flexion only as the effects of the lumbo-pelvic rhythm on muscle forces were maximum at this posture. This was also confirmed by the findings of Tafazzol et al. (2014). Thus, the predicted results are valid for moderate flexion only and may not be generalized for large flexion.

In conclusion, the lumbo-pelvic rhythm during forward flexion has important effects on muscle forces and disc loads, as well as on load-sharing. However, less influence on the IDP and annular fibers strain was observed. In general, a rhythm with high pelvic rotation involves more global muscles, while more local muscles were recruited in a rhythm with low pelvic rotation and high lumbar rotation. A normal rhythm yielded a more balanced synergy between global and local muscles and almost equal disc and ligament load-sharing. These findings improved knowledge on the spine biomechanics during forward flexion and are clinically relevant towards LBP treatment and disc injury prevention.

Conflicts of interest

The authors have no conflicts of interest concern.

Acknowledgment

This study is financially supported by the China Scholarship Council (201506080013) and NSERC Discovery Grant (402046-2013), Canada.

Reference

- Arjmand, N., Plamondon, A., Shirazi-Adl, A., Larivière, C., Parnianpour, M., 2011. Predictive equations to estimate spinal loads in symmetric lifting tasks. *J. Biomech.* 44, 84–91. <https://doi.org/10.1016/j.jbiomech.2010.08.028>
- Arjmand, N., Shirazi-Adl, A., 2006. Model and in vivo studies on human trunk load partitioning and stability in isometric forward flexions. *J. Biomech.* 39, 510–521. <https://doi.org/10.1016/j.jbiomech.2004.11.030>
- Arshad, R., Zander, T., Dreischarf, M., Schmidt, H., 2016. Influence of lumbar spine rhythms and intra-abdominal pressure on spinal loads and trunk muscle forces during upper body inclination. *Med. Eng. Phys.* 38, 333–338.
- Azari, F., Arjmand, N., Shirazi-Adl, A., Rahimi-Moghaddam, T., 2017. A combined passive and active musculoskeletal model study to estimate L4-L5 load sharing. *J. Biomech.* <https://doi.org/10.1016/j.jbiomech.2017.04.026>
- Cholewicki, J., McGill, S.M., 1996. Mechanical stability of the in vivo lumbar spine: implications for injury and chronic low back pain. *Clin. Biomech. Bristol Avon* 11, 1–15.
- Damsgaard, M., Rasmussen, J., Christensen, S.T., Surma, E., de Zee, M., 2006. Analysis of musculoskeletal systems in the AnyBody Modeling System. *Simul. Model. Pract. Theory, SIMS 2004* 14, 1100–1111. <https://doi.org/10.1016/j.simpat.2006.09.001>
- de Zee, M., Hansen, L., Wong, C., Rasmussen, J., Simonsen, E.B., 2007. A generic detailed rigid-body lumbar spine model. *J. Biomech.* 40, 1219–1227. <https://doi.org/10.1016/j.jbiomech.2006.05.030>
- Dreischarf, M., Zander, T., Shirazi-Adl, A., Puttlitz, C.M., Adam, C.J., Chen, C.S., Goel, V.K., Kiapour, A., Kim, Y.H., Labus, K.M., Little, J.P., Park, W.M., Wang, Y.H., Wilke, H.J., Rohlmann, A., Schmidt, H., 2014. Comparison of eight published static finite element models of the intact lumbar spine: predictive power of models improves when combined together. *J. Biomech.* 47, 1757–1766. <https://doi.org/10.1016/j.jbiomech.2014.04.002>
- El-Rich, M., Shirazi-Adl, A., 2005. Effect of load position on muscle forces, internal loads and stability of the human spine in upright postures. *Comput. Methods Biomech. Biomed. Engin.* 8, 359–368. <https://doi.org/10.1080/10255840500445630>

- El-Rich, M., Arnoux, P.-J., Wagnac, E., Brunet, C., Aubin, C.-E., 2009. Finite element investigation of the loading rate effect on the spinal load-sharing changes under impact conditions. *J. Biomech.* 42, 1252–1262. <https://doi.org/10.1016/j.jbiomech.2009.03.036>
- Esola, M.A., McClure, P.W., Fitzgerald, G.K., Siegler, S., 1996. Analysis of lumbar spine and hip motion during forward bending in subjects with and without a history of low back pain. *Spine* 21, 71–78.
- Fathallah, F.A., Marras, W.S., Parnianpour, M., 1999. Regression models for predicting peak and continuous three-dimensional spinal loads during symmetric and asymmetric lifting tasks. *Hum. Factors* 41, 373–388. <https://doi.org/10.1518/001872099779611094>
- Ghezelbash, F., Eskandari, A.H., Shirazi-Adl, A., Arjmand, N., El-Ouaaid, Z., Plamondon, A., 2018. Effects of motion segment simulation and joint positioning on spinal loads in trunk musculoskeletal models. *J. Biomech.* 70, 149–156.
- Granata, K.P., Sanford, A.H., 2000. Lumbar–pelvic coordination is influenced by lifting task parameters. *Spine* 25, 1413–1418.
- Kim, M., Yi, C., Kwon, O., Cho, S., Cynn, H., Kim, Y., Hwang, S., Choi, B., Hong, J., Jung, D., 2013. Comparison of lumbopelvic rhythm and flexion-relaxation response between 2 different low back pain subtypes. *Spine* 38, 1260–1267.
- Laird, R.A., Kent, P., Keating, J.L., 2016. How consistent are lordosis, range of movement and lumbo-pelvic rhythm in people with and without back pain? *BMC Musculoskelet. Disord.* 17. <https://doi.org/10.1186/s12891-016-1250-1>
- Liu, T., Khalaf, K., Naserkhaki, S., El-Rich, M., 2018. Load-sharing in the lumbosacral spine in neutral standing & flexed postures - A combined finite element and inverse static study. *J. Biomech.* <https://doi.org/10.1016/j.jbiomech.2017.10.033>
- McClure, P.W., Esola, M., Schreier, R., Siegler, S., 1997. Kinematic analysis of lumbar and hip motion while rising from a forward, flexed position in patients with and without a history of low back pain. *Spine* 22, 552–558.
- Naserkhaki, S., Jaremko, J.L., Adeeb, S., El-Rich, M., 2016. On the load-sharing along the ligamentous lumbosacral spine in flexed and extended postures: Finite element study. *J. Biomech.* 49, 974–982. <https://doi.org/10.1016/j.jbiomech.2015.09.050>

- Porter, J.L., Wilkinson, A., 1997. Lumbar-hip flexion motion. A comparative study between asymptomatic and chronic low back pain in 18- to 36-year-old men. *Spine* 22, 1508-1513; discussion 1513-1514.
- Rohlmann, A., Neller, S., Claes, L., Bergmann, G., Wilke, H.-J., 2001. Influence of a follower load on intradiscal pressure and intersegmental rotation of the lumbar spine. *Spine* 26, E557–E561.
- Rose, S.J., Sahrman, S.A., Norton, B.T., 1988 Quantitative assessment of lumbar-pelvic rhythm. *Phys. Ther.* 68.824
- Schmidt, H., Heuer, F., Simon, U., Kettler, A., Rohlmann, A., Claes, L., Wilke, H.-J., 2006. Application of a new calibration method for a three-dimensional finite element model of a human lumbar annulus fibrosus. *Clin. Biomech.* 21, 337–344. <https://doi.org/10.1016/j.clinbiomech.2005.12.001>
- Schmidt, H., Kettler, A., Heuer, F., Simon, U., Claes, L., Wilke, H.-J., 2007. Intradiscal pressure, shear strain, and fiber strain in the intervertebral disc under combined loading. *Spine* 32, 748–755.
- Tafazzol, A., Arjmand, N., Shirazi-Adl, A., Parnianpour, M., 2014. Lumbopelvic rhythm during forward and backward sagittal trunk rotations: Combined in vivo measurement with inertial tracking device and biomechanical modeling. *Clin. Biomech.* 29, 7–13. <https://doi.org/10.1016/j.clinbiomech.2013.10.021>
- Vazirian, M., Van Dillen, L.R., Bazrgari, B., 2016. Lumbopelvic rhythm in the sagittal plane: A review of the effects of participants and task characteristics. *Int. Musculoskelet. Med.* 38, 51–58. <https://doi.org/10.1080/17536146.2016.1241525>
- Wilke, H., Neef, P., Hinz, B., Seidel, H., Claes, L., 2001. Intradiscal pressure together with anthropometric data-a data set for the validation of models. *Clin. Biomech.* Bristol Avon 16 Suppl 1, S111-126.

Chapter 5

Numerical Investigation of Intra-Abdominal Pressure Effects on Spinal Loads and Load-Sharing in Flexion

This chapter has been submitted as Liu, T., Khalaf, K., Adeeb S., El-Rich, M., 2018, to Journal of Biomechanics.

Abstract

The intra-abdominal pressure (IAP) which generates extensor torque and unloads the spine is omitted in most of the numerical studies that use musculoskeletal (MSK) or finite element (FE) models of the spine. Hence, the spinal loads predicted by these models are not realistic. We quantified the effects of IAP variation in forward flexion on spinal loads and load-sharing using a novel computational tool that combines a MSK model of the trunk and a FE model of the ligamentous lumbosacral spine. The MSK model predicted the trunk muscle forces and reaction forces at the junction T12-L1 with or without IAP that will be input in the FE model to investigate the effects of IAP on spinal loads and load-sharing. The findings confirmed the unloading role of IAP, especially at large flexion angles. Inclusion of IAP reduced the global muscle forces, disc loads as well as intradiscal pressure (IDP). The drop in disc loads was compensated by increase in ligament forces. The annular fibers strain and IDP are more sensitive to the IAP at upper levels of spine. Considering the IAP also increased the ligaments load-sharing which alleviated the discs. These results are beneficial to clinical applications and disc implants design.

Keywords: Intra-abdominal pressure, finite element model, musculoskeletal model, spinal load, load-sharing

5.1 Introduction

Quantifying of the contribution of the active and passive components of the human trunk during various daily, occupational, or athletic activities is essential for the design of spinal fixation systems, and would most likely advance and accelerate biomechanical research on the lumbar spine and is invaluable for both spinal research and clinical communities alike. Intra-abdominal pressure (IAP), considered as the most probable factor to influence lumbar spinal mechanics, has been continuously investigated under static and dynamic lifting conditions for many decades now (Davis, 1956; Davis and Troup, 1964; Bartelink, 1957; Andersson et al., 1976; McGill et al., 1990; Marras and Mirka, 1996; Hagins et al., 2004; Arjmand and Shirazi-Adl, 2006). It is indeed universally accepted that the IAP produces extensor torque (Bartelink, 1957; Morris et al., 1961), which reduces the spinal loads and back muscle activity, hence influencing the overall loading scenarios and stability of the lumbar spine (Daggfeldt and Thorstensson, 1997, Daggfeldt and Thorstensson, 2003, Cholewicki and Reeves, 2004; Arjmand and Shirazi-Adl, 2006; Stokes et al., 2010).

Experimental studies have been employed to investigate the role of the IAP as related to spinal loading and stability. Tayashiki et al., (2018) explored the relationship between the IAP and the maximal voluntary isometric hip extension torque and revealed that a sufficient increase in IAP causes an enhancement of hip extension maximum voluntary contraction torque. The effects of human posture and respiratory activation of the diaphragm on the IAP have also been analyzed in conjunction with measured EMG data. The results showed that the diaphragm and Transversus Abdominis muscles continuously play a significant role in respiration and posture control (Hodges and Gandevia, 2000).

Due to the inherent complexity of the spine and its structural components both morphologically and mechanically, direct non-invasive measurement of the spinal loads and load-sharing among its various active (muscles) and passive (discs, ligaments, facets, etc.) components is not attainable. As a result, many MSK rigid body models, analytical and computational models, have emerged as effective tools for load-sharing assessment and prediction of joint reactions and muscle forces. In some of these models, the IAP was simulated to evaluate muscle and ligament forces more realistically. The computational studies conducted by Arjmand and Shirazi-Adl (2006), and Park et al., (2012) revealed that IAP reduced the spinal joint forces in weight bearing

standing position if no abdominal muscles co-activation is considered and that the unloading and stabilizing action of IAP is posture and task specific (Arjmand and Shirazi-Adl, 2006). Cholewicki et al. (1999) concluded that tasks such as lifting and jumping which involve more trunk extensor moment are beneficial to the IAP mechanism of stabilizing the lumbar spine. Stokes et al. (2011) revealed that the pressurization of abdomen increases the lumbar spine stability, but the degree of spine stability was not significantly affected by selective activation of either transversus abdominis or oblique muscles. The aforementioned studies either adopt many assumptions on physiological parameters or prescribed IAP.

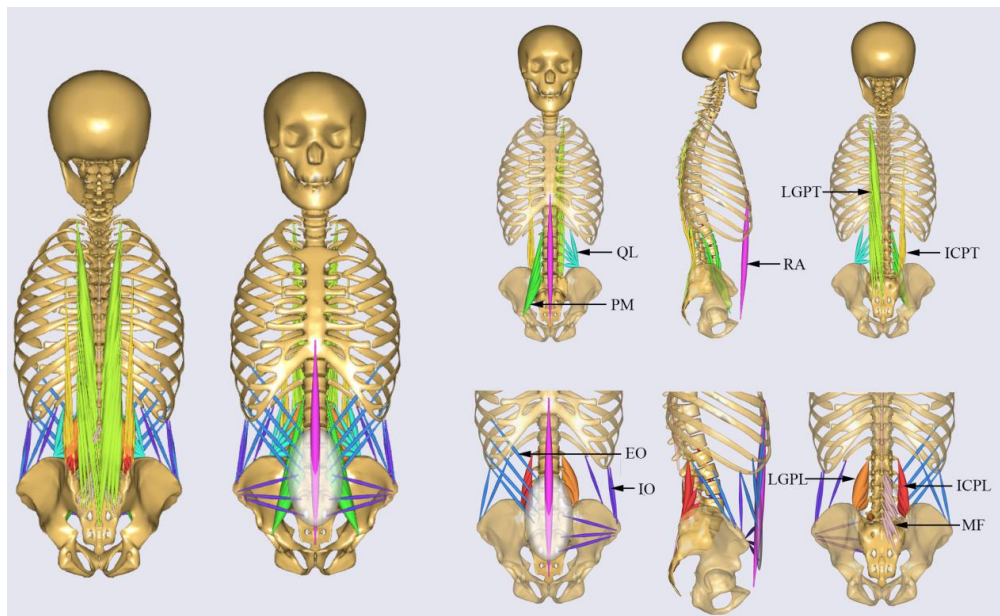


Fig. 5.1. Musculature of the MSK model; Global Muscles: RA-Rectus Abdominis, IO-Internal Oblique, EO-External Oblique, ICPT-Iliocostalis Lumborum Pars Thoracic, LGPT-Longissimus Thoracis Pars Thoracic; Local Muscles: ICPL-Iliocostalis Lumborum Pars Lumborum, LGPL-Longissimus Thoracis Pars Lumborum, PM-Psoas Major, MF-Multifidus, QL-Quadratus Lumborum.

Also, previous investigations of the IAP effects on muscle forces (Arshad et al., 2016; Hodges et al., 2001), spinal loads (Daggfeldt and Thorstensson, 2003; Arshad et al., 2015), as well as, stiffness of lumbar spine (Hodges et al., 2005) were attempted both experimentally and numerically to provide insight and shed further light on spinal biomechanics. However, the influence of the IAP on the IDP and spinal load-sharing remains unknown. Such investigations are critical for various clinical applications, including informing the design of disc implants, and

shedding more light on the elusive pathophysiology of low back pain and other spinal disorders. The current research, thus, aims at quantifying the effects of the IAP on muscle forces, IDP, as well as spinal load-sharing in the lumbosacral spine during forward flexion using our combined MSK and FE modeling methodology, previously validated and published (Liu et al., 2018).

5.2 Materials and methods

5.2.1 Musculoskeletal model

The AnyBody MSK model (Ver. 6.0, AnyBody Technology, Aalborg, Denmark, model version 1.63) was used to simulate the musculoskeletal biomechanics of a typical person of 70 kg weight and 168 cm height subjected to 60° forward flexion with and without IAP. The model is composed of the skull, cervical region, upper arms, thorax (T1-T12) and five rigid lumbar vertebrae (L1-L5) together with the pelvis and sacrum.

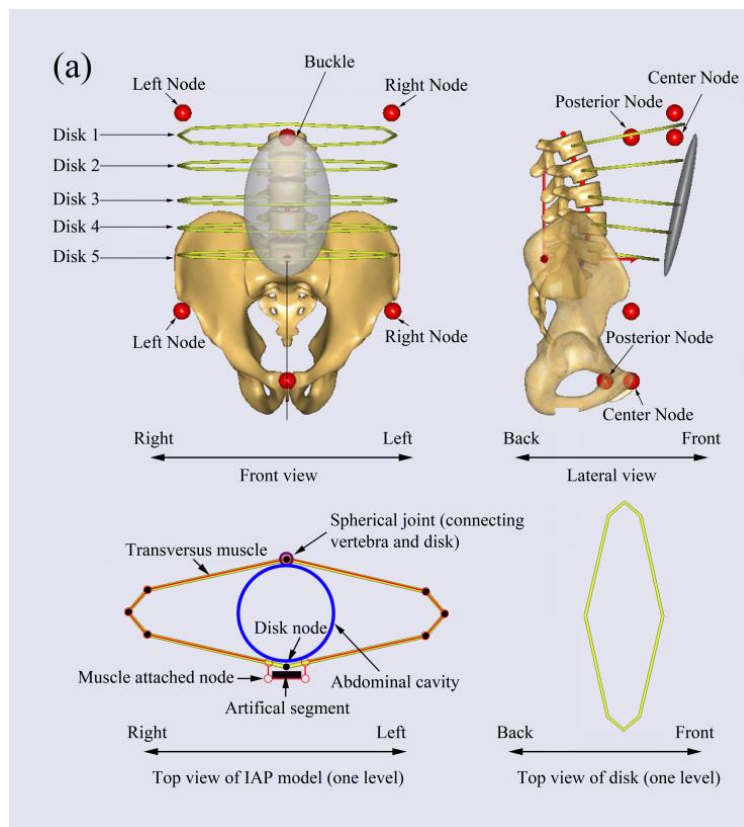
The Anterior Longitudinal Ligament (ALL), Posterior Longitudinal Ligament (PLL), Intertransverse Ligament (ITL), Ligamentum Flavum (LF), Supraspinous Ligament (SSL), and Interspinous Ligament (ISL) and Capsular Ligament (CL) were all incorporated in the model and modified to match the corresponding properties in our validated published FE model (Liu et al., 2018). The ligament forces were set to zero in the neutral standing position. The facet joint contacts were also activated during simulation.

All muscles in the MSK model were simulated by one dimension element (de Zee 2007), which can resist only tensile forces. The default tensile strength for individual muscles (Arshad et al., 2017; Ikai and Fukunaga, 1968) was adopted from literature. The trunk muscles were divided into two groups (El-Rich et al., 2004), specifically global muscles and local muscles. The global muscles included: 1 Rectus Abdominis (RA), 12 Internal Oblique (IO), 12 External Oblique (EO), 16 Iliocostalis Lumborum Pars Thoracic (ICPT), 24 Longissimus Thoracis Pars Thoracic (LGPT). The local muscles included: 8 Iliocostalis Lumborum Pars Lumborum (ICPL), 10 Longissimus Thoracis Pars Lumborum (LGPL), 22 Psoas Major (PM), 38 Multifidus (MF) and 10 Quadratus Lumborum muscle fascicles (QL) (Arshad et al., 2016) (Fig. 5.1). The corresponding cross section area and strength are shown in Table 5.1.

Table 5.1. Muscle physiological cross-sectional area (PCSA, cm²) for each side of the spine at different insertion level and the muscle stress for each individual muscle group (in parentheses, N/cm²)

| Local Muscles | ICPL(84.6) | LGPL(84.6) | PM(84.6) | MF(84.6) | QL(84.6) |
|----------------|------------|------------|----------|-----------|-----------|
| T12 | - | - | 2.11 | - | 1.28 |
| L1 | 1.08 | 0.79 | 2.72 | 2.16 | 0.88 |
| L2 | 1.54 | 0.91 | 2.62 | 3.14 | 0.8 |
| L3 | 1.82 | 1.03 | 3.64 | 2.49 | 0.75 |
| L4 | 1.89 | 1.1 | 2.39 | 4.1 | 0.7 |
| L5 | - | 1.16 | 1.15 | 2.18 | - |
| Global muscles | ICPT(84.6) | LGPT(84.6) | IO(84.6) | EO (84.6) | RA(253.9) |
| Thorax | 5.48 | 11.09 | 6.24 | 6.24 | 2.6 |

An optimization algorithm based on muscle recruitment criterion was employed to calculate the load distribution among the various muscle groups. The objective function used in the muscle recruitment optimization routine was to minimize the sum of the square of the ratios of muscle force to muscle strength (de Zee et al., 2007).



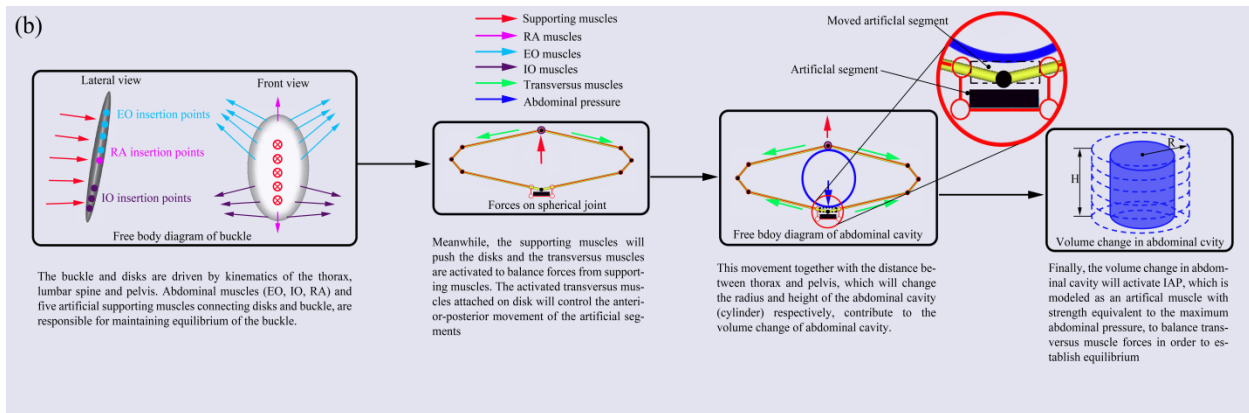


Fig. 5.2. Description of the IAP modelling (a) and mechanism of IAP generation (b) in AnyBody.

The abdominal cavity was simulated using a cylinder with maximum pressure equal to 26.6 kPa (Essendrop, 2003). The IAP model is mainly composed of one rigid buckle that provides attachments to the abdominal muscles (EO, IO, RA) and five rigid disks forming structure for the transversus muscles which are responsible for generating IAP (Fig. 5.2a). The buckle and disks are driven by kinematics of the thorax, lumbar spine and pelvis. The abdominal muscles (EO, IO, RA) and five artificial supporting muscles connecting disks and buckle, are responsible for maintaining equilibrium of the buckle (Fig. 5.2b) during flexion. Meanwhile, the supporting muscles will push the disks (Fig. 5.2b) and the transversus muscles will be activated to balance the forces generated by the supporting muscles. The activated transversus muscles attached to the disks will control the anterior-posterior movement of the artificial segments (Fig. 5.2b). This movement together with the distance between thorax and pelvis, which will change the radius and height of the abdominal cavity (cylinder) respectively, contribute to the volume change of abdominal cavity. Finally, the change in abdominal cavity will activate IAP, which is modeled as an artificial muscle with strength equivalent to the maximum abdominal pressure, to balance the transversus muscle forces and establish equilibrium (Fig. 5.2b). In other words, any change in these supporting muscles will affect the force in the transversus muscles which in turn will influence the IAP. This pressure will then act on the nodes defined on the thorax and pelvis in the form of concentrated forces (Fig. 5.2a). All muscles used in the model of IAP are governed by the optimization function used for the entire MSK model. The range of IAP values were approximated to vary between 2.2kPa and 4.4kPa from neutral standing to forward flexion (60°) based on literature (Schultz et al., 1982). The lumbar-pelvic ratio and lumbar rhythm were

selected based on published experimental data (Granata and Sanford, 2000). The muscle forces, and disc moment at the T12-L1 junction predicted by the MSK model together with the gravitational forces were input into our previously developed and validated FE model (Liu et al., 2018) to predict the IDP, disc forces and moments, and spinal load-sharing.

5.2.2 Finite Element model

Geometry of the lumbosacral vertebrae (L1-S1) in neutral standing posture was exported from the MSK model to create the FE model after detailed cleaning of spikes and sharp edges using the software Geomagic (Geomagic Studio 2014). Geometry meshing of the geometry was conducted using the software Hypermesh (Hyperworks 14.0). The detailed meshing process and material properties are elaborated in our previous work (Liu et al., 2018).

The disc moment, ligament forces, facet joint forces and muscle forces predicted at the junction T12-L1 together with muscle forces at all spinal levels of the MSK model were applied to the FE model. The flexural stiffness of joints in MSK model was modified to nonlinear stiffness curves that are predicted by FE models of corresponding functional spinal units devoid of ligaments and facet joints and subjected to a moment of 7.5Nm in flexion and extension. The resultant reaction force (shear and compression) at T12-L1 joint, however, was substituted by a sagittal translation applied in the direction of the reaction force to correct the small discrepancy between the deformed position predicted by the MSK model and the one resulted from FE model. This discrepancy is due to the difference in the approaches used to model the disc in both models (Liu et al., 2018), and this iteration process is performed until the reaction force generated by sagittal displacements in the FE model is almost equal (within predefined tolerance) to counterpart predefined in the MSK model under the same posture (Liu et al., 2018). The gravitational force of each vertebra was also applied to the FE model. The sacrum was rotated according to the lumbo-pelvic rhythm used in the MSK model and then it was fixed throughout simulation.

5.2.3 Simulated tasks

Forward flexion (60°) posture was selected to investigate the influence of the IAP on muscle forces, spinal loading and load sharing, The IAP was activated and deactivated by setting the artificial muscle activity to normal and zero, respectively (Arshad et al., 2016). During flexion, the arms were always kept parallel to the direction of gravity (Liu et al., 2018).

5.3 Results

5.3.1 Muscle force

The sum of the global and local muscle forces with and without IAP were predicted using the MSK model (Fig. 5.3) as the lumbar spine flexion varied from 0° to 60°. In the neutral standing posture, the total local muscle force was predicted at approximately 179N, which was 27N higher as compared with the results from the model without IAP. In contrast, the total global muscle force was 78N at the same posture, which was 17N lower as compared with the alternate model setting. Both global and local muscle forces increased substantially with the inclination of the trunk to reach 961N and 1185N, respectively when the IAP was excluded. Activation of this latter in the MSK model reduced the total global muscle substantially along with the inclination of the trunk. This reduction reaches 37% at 60° flexion. The total local muscle force reduced as well. However, the drop started at 40° and reached its maximum value of 6.5% at 60° flexion.

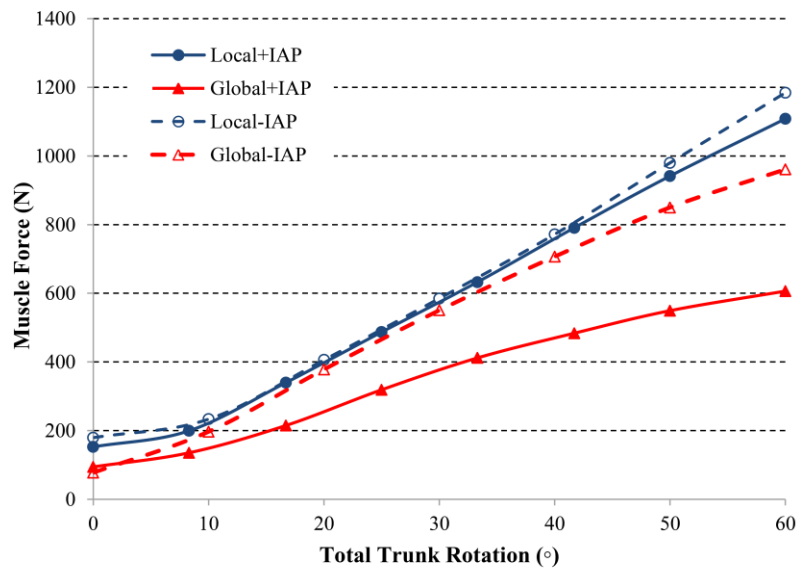


Fig. 5.3. Comparison of the predicted global and local muscle forces under activation or deactivation of the IAP during forward flexion.

The total force of each individual muscle group was predicted at the maximal trunk inclination (Fig. 5.4). The pronounced unloading effect of IAP was observed for almost all muscle groups except for the PM and RA muscle groups, which remained silent regardless of the IAP settings.

In the local muscle group, the MF muscle contributed the most at 60° forward flexion, reaching 423N, followed by the ICPL and LGPL, whose values were 379N and 349N, respectively. The

QL muscle produced the smallest force (34N). In the global muscle group, the LGPT produced the greatest force (504N) followed by the ICPT muscle (261N). The force in the abdominal muscles did not exceed 68N and 129N in the EO and IO muscles, respectively. These values correspond to the case of deactivated IAP. Including IAP in the model did not change the muscle forces pattern. However, it clearly reduced the force in all muscles particularly in the QL muscle and the global extensors LGPT and ICPT where the drop reached 52%, 46%, and 40%, respectively. The maximum decrease of the force in the remaining extensor and abdominal muscles did not exceed 12%.

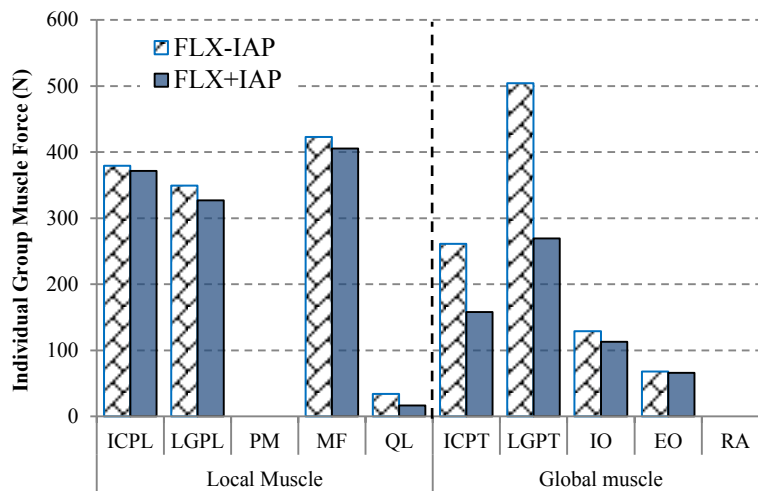


Fig. 5.4. Local and global muscle forces at 60° forward flexion for both activated IAP and deactivated IAP models.

5.3.2 Annular fibers strain

High tensile disc strain was produced at the innermost lamellae at either the posterior or anterior or both regions, except at the L1-2 level, regardless of the existence of IAP.

In the presence of the IAP, predicted high tensile strain in the collagen fibres was observed in the anterior region of the innermost lamella at L2-3 level. This high strain was then transferred to the posterior region of the innermost lamella at L3-4 level. High tensile stain in both anterior and posterior regions of the lamella was also observed at the L4-5 level. This trend became more pronounced at the L5-S1 level.

In contrast, the proportion of high tensile strain increased in the corresponding area of the lamellae for all discs, except at the L5-S1 level in the absence of IAP effects. A noticeable

reduced proportion of high tensile strain, however, was produced at the L5-S1 under the same IAP condition (Fig. 5.5).

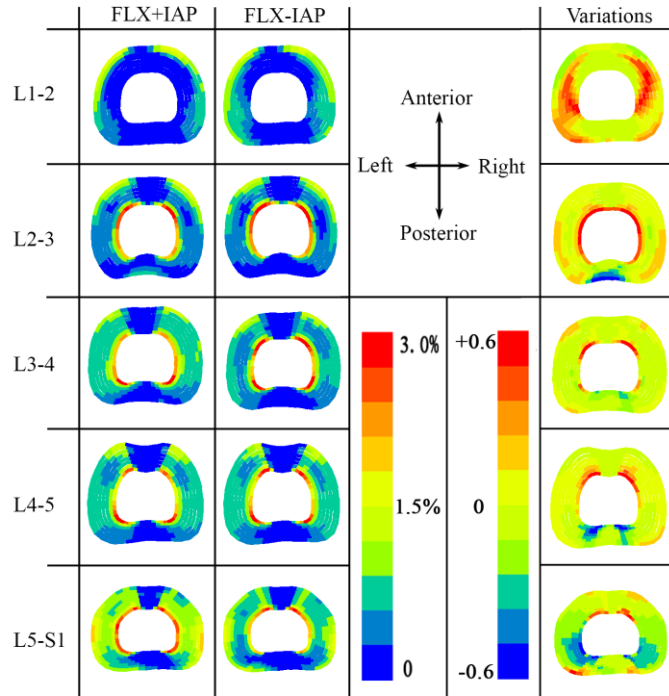


Fig. 5.5. Visualization variations (with respect to FLX+IAP model) of disc strain of all levels (L1-S1) from FE model at 60° forward flexion with (FLX+IAP) and without (FLX-IAP) IAP.

Variation of the annular tensile strain due to the inclusion or not of IAP (shown on the right end of Fig. 5) was calculated as the strain of the model with no IAP minus its counterpart of the model with IAP. The maximum positive variation occurred in the lateral left and right regions of the lamella of disc L1-2, and in the innermost region of the lamella for the remaining levels. The region of maximum variations decreased from upper to lower levels of the spine (Fig. 5). The minimum variation corresponding to the case where the model with IAP predicted higher tensile strains occurred in the posterior outermost region of the lamella at L2-3 level and in the posterior innermost region of the lamella at L3-S1 levels. The area of the minimum variations increased gradually from middle to lower levels of the spine.

5.3.3 IDP

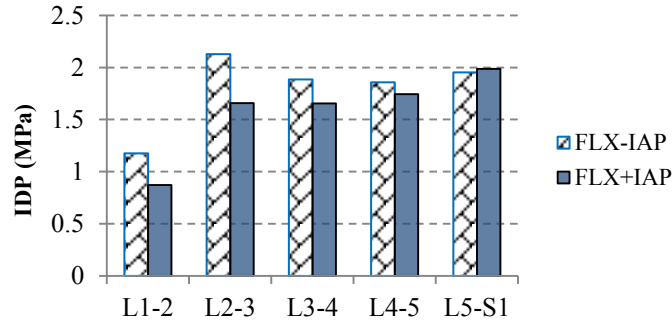


Fig. 5.6. IDP values at all spinal levels predicted at 60° forward flexion angle for both IAP settings.

The IDP exhibited the same pattern at all lumbar levels (L1-5) with or without accounting for the IAP (Fig. 5.6). On the other hand, a noticeable decrease in the IDP was observed in the presence of IAP at all levels except the L5-S1 level. The greatest drop occurred at the L1-2 level and reached 26% while the magnitude of IDP remained almost unchanged at the L5-S1 level.

5.3.4 Disc force and moment

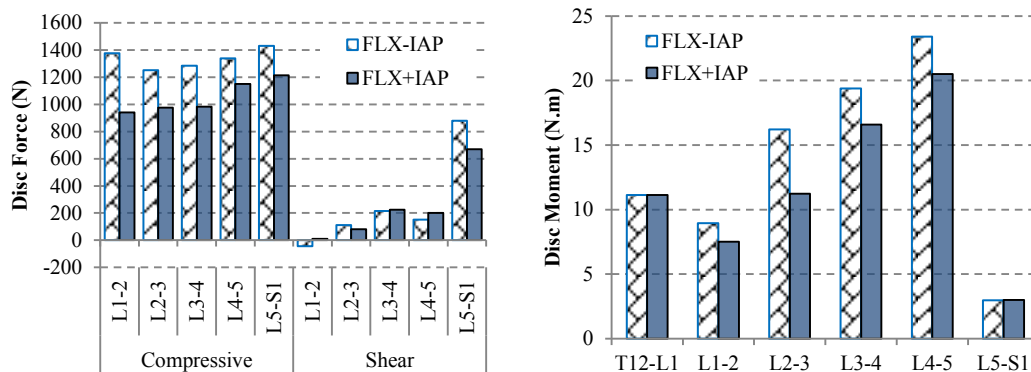


Fig. 5.7. Disc compressive and shear forces (+ve in anterior direction) and disc moments (+ve in flexion) at 60° forward flexion predicted by the FE model.

The disc compressive force followed the same pattern, a decrease from the L1-2 level to the L2-3 level followed by an increase along the lower levels, in both cases, with and without the IAP. Activating this latter reduced the compressive force at all levels. The decrease ranged from 15% to 32% at the levels L5-S1 and L1-2, respectively. When the IAP was active, the disc shear force reduced by 24% and 28% at the L5-S1 and L2-3 levels, respectively. However, the L3-4 and L4-5 levels experienced an increase of 5% and 33%, respectively and the shear force changed

direction from anterior to posterior at the L1-2 level (Fig. 5.7). The disc moment also dropped along the spinal levels except at the T12-L1 and L5-S1 levels when the IAP was included. The greatest change was 31% and occurred at the level L2-3.

5.3.5 Ligament forces

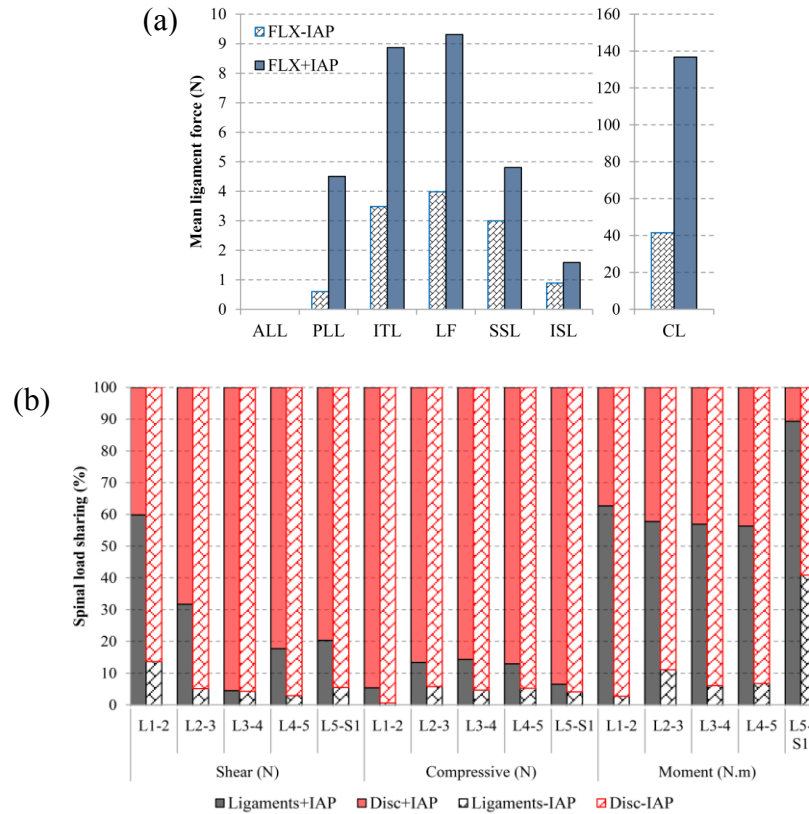


Fig. 5.8. Effects of IAP on ligaments (a) and spinal load sharing of the passive structures (disc, facet joints (FJF), ligaments) (b) evaluated at 60° forward flexion (FJF has zero forces).

Activating the IAP increased the force in all ligaments significantly. The highest increase was found in the PLL (from 0 to 5N) and CL (from 40N to 140N) ligaments (Fig. 5.8a). The ALL ligament experienced zero force in both IAP settings.

5.3.6 Spinal load-sharing

In the absence of IAP, the compressive force was resisted mostly by the disc while the ligament contribution did not exceed 5%. The ligaments had also minor contribution (less the 14%) to resist shear force and moment as compared to the discs except at the L5-S1 level where they carried about 41% of the moment. The facet joints had no contribution at all to load-sharing.

Activating the IAP, increased the role of the ligaments in carrying compressive and shear forces, as well as moments. The increase of the ligament contribution to moment resistance was substantial at all spinal levels. For instance, the ligament moment-sharing jumped from 14% to 60% and from 5% to 32% at the L1-2 and L2-3 levels, respectively. The facet joints remained silent in all cases.

5.4 Discussions

Despite the debate on which abdominal muscle is responsible to raise the IAP (Cholewicki and Reeves, 2004; Daggfeldt and Thorstensson, 2004), the role of this latter in unloading and stabilizing the lumbar spine has been established in the past few decades (Daggfeldt and Thorstensson, 1997, Daggfeldt and Thorstensson, 2003, Cholewicki and Reeves, 2004; Arjmand and Shirazi-Adl, 2006; Stokes et al., 2010, Park et al., 2012) and is well accepted within the spinal biomechanics community. The influence of IAP on spinal load-sharing, however, has not been studied yet. This work attempted to quantify these effects during forward flexion (60°), a posture associated with high abdominal muscle activity change (Creswell and Thorstensson, 1989), using our previously developed and validated method that combines MSK and FE models to predict muscle forces, ligaments forces, discs forces and moments, IDP, as well as spinal load-sharing (Liu et al., 2018).

Consistently with previous studies (Arjmand and Shirazi-Adl, 2006; Arshad et al., 2016), our results revealed that the inclusion of the IAP in the MSK model leads to a decrease in the muscle forces and it is more pronounced in the global muscle group at larger flexion angle (Figs. 5.3, 5.4). This is in alignment with Arshad et al. (2016). More specifically, two global muscle groups: the ICPT and the LGPT, decrease substantially in the presence of the IAP as compared to the case of its absence. This revealed that the IAP can produce an extensor moment which reduce the activity of the erector spinae muscles and, thus, alleviate the spinal loads (Daggfeldt and Thorstensson et al., 2003; Bartelink et al., 1957). In addition, such significant decrease confirms the hypothesized unloading role of the IAP and stresses the importance of its incorporation in simulation models of the lumbar spine, particularly when subjected to forward inclination (Cholewicki and Reeves, 2004). The unloading role of IAP in flexion can also be confirmed by the predicted disc force and moment. In the presence of the IAP, the compressive force decreases up to 434N (31%) at all levels, while a maximum reduction of 208N (24%) in the

shear force occurs. A maximum decrease up to 5N.m (32%) in disc moments at the L1-5 levels is also found, which is in agreement with previous work (Daggfeldt and Thorstensson, 2003). The drop in the disc loads due to activating the IAP is compensated by an increase in the ligaments forces to maintain the equilibrium at the same deformed posture i.e. under similar loading conditions. This confirms that neglecting the IAP in spine biomechanics studies will underestimate the ligaments role and yield unrealistic force and moment in the discs.

The variations among the annular fibers strain between the two cases (IAP on and IAP off) are little. A small increase in the proportion of the high tensile strains was observed at the L1-4 levels in the model with no IAP which is mainly due to the increase of IDP. The deformed posture of the spine is not affected by the IAP setting in this study. This assumption explains the slight effects of IAP on the annular fibers strain. We speculate that considering the change of posture due the IAP variation which in turn affects the centre of rotation (Park et al., 2012), would cause more noticeable effects on the annular fibers strain.

It is noteworthy that the IDP decreased at all levels except the L5-S1 level, which confirms again the previously mentioned hypothesized unloading role of the IAP. An increase up to 0.5MPa in the IDP is observed at the L2-3 level without consideration of the IAP effects. The drop of IDP was smaller at the lower levels L3-5 which agrees with the findings Hodges et al. (2005) who found that IAP has more effects on the L2 vertebra as compared to the L4 vertebra.

Load redistribution among the various passive components is markedly altered in the presence of the IAP. Our results confirmed the main contribution of the disc to resist external load in forward flexion which is more pronounced without the simulation of IAP. The disc force- and moment-sharing varied between 86% and 100% of the total spinal force and moment except at the L5-S1 level where the ligaments moment-sharing reached 40%. Including IAP alleviates the disc and increases the ligament load-sharing particularly the moment-sharing.

5.4.1 Model assumptions and limitations

The current MSK model predicted the IAP based on the change of the abdominal cavity volume during forward flexion rather than used prescribed experimental IAP values like other models (Arjmand et al., 2006, Stokes et al., 2011 and Cholewicki et al., 1999). The model also considered the interaction between abdominal muscles, physiological cross section area and

strength of these muscles. The transversus muscle, considered as significant contributor to raise the IAP (Cresswell et al., 1992; Cresswell, 1993) was also included in the IAP modelling. Setting the IAP (artificial muscle activity) to zero did not vanish the force in the abdominal muscles (EO and IO) as these muscles are attached to the buckle and disks and contribute to their equilibrium (Fig. 5.2b). Similar kinematics was considered in both IAP settings and no co-activity antagonism was simulated in this study. Also, the muscle forces and joint reaction loads were predicted by the MSK model using inverse static analysis that neglects inertia effects and time delays. Other limitations related to methodology are mentioned elsewhere (Liu et al., 2018).

5.4.2 Conclusions

In summary, the current research investigates the influence of the IAP on muscle forces, loads in the passive spinal structures and load-sharing during forward flexion using a previously validated tool that combines MSK of the upper body and FE model of the lumbosacral spine. In alignment with literature, this study confirms the unloading role of the IAP during upper body inclination. The IAP has significant influence on the global muscle forces, yet, negligible effects on the local muscle forces. The substantial increase in the IDP, internal disc force and load sharing triggered by absence of the IAP should be taken into consideration in future modeling efforts of the lumbar spine in flexion postures. This is the first study to the best knowledge of the investigators that attempts to quantitatively assess the role of the IAP on detailed spinal biomechanics. Such information is essential for the accurate modeling of the spine towards more effective therapeutic and rehabilitative modalities.

Conflict of interest

The authors have no conflicts of interest concern.

Acknowledgment

This study is financially supported by the China Scholarship Council (201506080013) and NSERC Discovery Grant (402046-2013), Canada.

References:

- Andersson, G.B.J., Örtengren, R., Nachemson, A., 1976. Quantitative Studies of Back Loads in Lifting. *Spine* 1, 178.
- Arjmand, N., Shirazi-Adl, A., 2006. Role of intra-abdominal pressure in the unloading and stabilization of the human spine during static lifting tasks. *Eur. Spine J.* 15, 1265–1275. <https://doi.org/10.1007/s00586-005-0012-9>
- Arshad, R., Zander, T., Dreischarf, M., Schmidt, H., 2016. Influence of lumbar spine rhythms and intra-abdominal pressure on spinal loads and trunk muscle forces during upper body inclination. *Med. Eng. Phys.* 38, 333–338. <https://doi.org/10.1016/j.medengphy.2016.01.013>
- Bartelink, D.L., 1957. The role of abdominal pressure in relieving the pressure on the lumbar intervertebral discs. *J. Bone Joint Surg. Br.* 39-B, 718–725.
- Cholewicki, J., Juluru, K., McGill, S.M., 1999. Intra-abdominal pressure mechanism for stabilizing the lumbar spine. *J. Biomech.* 32, 13–17.
- Cholewicki, J., Reeves, N.P., 2004. All abdominal muscles must be considered when evaluating the intra-abdominal pressure contribution to trunk extensor moment and spinal loading. *J. Biomech.* 37, 953–954. <https://doi.org/10.1016/j.jbiomech.2003.09.021>
- Cresswell, A.G., Thorstensson, A., 1989. The role of the abdominal musculature in the elevation of the intra-abdominal pressure during specified tasks. *Ergonomics* 32, 1237–1246. <https://doi.org/10.1080/00140138908966893>
- Cresswell, A.G., 1993. Responses of intra-abdominal pressure and abdominal muscle activity during dynamic trunk loading in man. *Eur. J. Appl. Physiol.* 66, 315–320.
- Cresswell, A.G., Grundström, H., Thorstensson, A., 1992. Observations on intra-abdominal pressure and patterns of abdominal intra-muscular activity in man. *Acta Physiol. Scand.* 144, 409–418. <https://doi.org/10.1111/j.1748-1716.1992.tb09314.x>
- Daggfeldt, K., Thorstensson, A., 2003. The mechanics of back-extensor torque production about the lumbar spine. *J. Biomech.* 36, 815–825.
- Daggfeldt, K., Thorstensson, A., 1997. The role of intra-abdominal pressure in spinal unloading. *J. Biomech.* 30, 1149–1155.
- Davis, P., 1956. Variations of the human intra-abdominal pressure during weight-lifting in different postures. *J Anat* 90, 601.

- Davis, P.R., Troup, J.D.G., 1964. Pressures in the trunk cavities when pulling, pushing and lifting. *ergonomics* 7, 465–474. <https://doi.org/10.1080/00140136408930764>
- de Zee, M., Hansen, L., Wong, C., Rasmussen, J., Simonsen, E.B., 2007. A generic detailed rigid-body lumbar spine model. *J. Biomech.* 40, 1219–1227. <https://doi.org/10.1016/j.jbiomech.2006.05.030>
- El-Rich, M., Shirazi-Adl, A., Arjmand, N., 2004. Muscle activity, internal loads, and stability of the human spine in standing postures: combined model and in vivo studies. *Spine* 29, 2633–2642.
- Essendrop, M., 2003. Significance of intra-abdominal pressure in work related trunk-loading. Ph. D. thesis, University of Copenhagen, Denmark.
- Granata, K.P., Sanford, A.H., 2000. Lumbar-pelvic coordination is influenced by lifting task parameters. *Spine* 25, 1413–1418.
- Hagins, M., Pietrek, M., Sheikzadeh, A., Nordin, M., Axen, K., 2004. The effects of breath control on intra-abdominal pressure during lifting tasks. *Spine* 29, 464–469.
- Hodges, P.W., Cresswell, A.G., Daggfeldt, K., Thorstensson, A., 2001. In vivo measurement of the effect of intra-abdominal pressure on the human spine. *J. Biomech.* 34, 347–353.
- Hodges, P.W., Eriksson, A.E.M., Shirley, D., Gandevia, S.C., 2005. Intra-abdominal pressure increases stiffness of the lumbar spine. *J. Biomech.* 38, 1873–1880. <https://doi.org/10.1016/j.jbiomech.2004.08.016>
- Hodges, P.W., Gandevia, S.C., 2000. Changes in intra-abdominal pressure during postural and respiratory activation of the human diaphragm. *J. Appl. Physiol. Bethesda Md* 1985 89, 967–976. <https://doi.org/10.1152/jappl.2000.89.3.967>
- Ikai, M., Fukunaga, T., 1968. Calculation of muscle strength per unit cross-sectional area of human muscle by means of ultrasonic measurement. *Int. Z. Für Angew. Physiol. Einschließlich Arbeitsphysiologie* 26, 26–32. <https://doi.org/10.1007/BF00696087>
- Liu, T., Khalaf, K., Naserkhaki, S., El-Rich, M., 2018. Load-sharing in the lumbosacral spine in neutral standing & flexed postures - A combined finite element and inverse static study. *J. Biomech.* 70, 43–50. <https://doi.org/10.1016/j.jbiomech.2017.10.033>
- Marras, W.S., Mirka, G.A., 1996. Intra-abdominal pressure during trunk extension motions. *Clin. Biomech. Bristol Avon* 11, 267–274.

- McGill, S.M., Norman, R.W., Sharratt, M.T., 1990. The effect of an abdominal belt on trunk muscle activity and intra-abdominal pressure during squat lifts. *Ergonomics* 33, 147–160. <https://doi.org/10.1080/00140139008927106>
- Morris, J.M., Lucas, D.B., Bresler, B., 1961. Role of the Trunk in Stability of the Spine. *JBJS* 43, 327.
- Park, W.M., Wang, S., Kim, Y.H., Wood, K.B., Sim, J.A., Li, G., 2012. Effect of the intra-abdominal pressure and the center of segmental body mass on the lumbar spine mechanics—a computational parametric study. *J. Biomech. Eng.* 134, 011009.
- Schultz, A., Andersson, G., Ortengren, R., Haderspeck, K., Nachemson, A., 1982. Loads on the lumbar spine. Validation of a biomechanical analysis by measurements of intradiscal pressures and myoelectric signals. *J. Bone Joint Surg. Am.* 64, 713–720.
- Stokes, I.A.F., Gardner-Morse, M.G., Henry, S.M., 2010. Intra-abdominal pressure and abdominal wall muscular function: Spinal unloading mechanism. *Clin. Biomech. Bristol Avon* 25, 859–866. <https://doi.org/10.1016/j.clinbiomech.2010.06.018>
- Stokes, I.A.F., Gardner-Morse, M.G., Henry, S.M., 2011. Abdominal muscle activation increases lumbar spinal stability: Analysis of contributions of different muscle groups. *Clin. Biomech.* 26, 797–803. <https://doi.org/10.1016/j.clinbiomech.2011.04.006>
- Tayashiki, K., Mizuno, F., Kanehisa, H., Miyamoto, N., 2018. Causal effect of intra-abdominal pressure on maximal voluntary isometric hip extension torque. *Eur. J. Appl. Physiol.* 118, 93–99. <https://doi.org/10.1007/s00421-017-3748-0>

Chapter 6

Summary and Conclusions

6.1 Summary

This research aims to develop a new computational tool that combines a musculoskeletal (MSK) model of the upper body and a Finite Element (FE) model of the ligamentous lumbosacral spine, thereby making it possible for researchers to predict spinal loads and load-sharing in *in-vivo* loading conditions. The muscle forces, intra-abdominal pressure (IAP), and disc moment at the thoracolumbar junction during forward flexion were predicted by the MSK model and then, fed into the FE model as external load to predict the ligaments forces, disc force and moment, intradiscal pressure (IDP) annular fibers strain, and load-sharing. This tool was validated using *in-vivo* data and its predictions were compared to the results of previous studies. This tool was used to investigate 1) spinal load and load-sharing of the ligamentous lumbosacral spine in neutral standing and flexed postures, 2) the effects of lumbo-pelvic rhythm on trunk muscle forces and disc loads, and 3) the impact of intra-abdominal pressure on spinal load-sharing. These findings improved knowledge of spine biomechanics in upright and forward flexion and they are clinically relevant and important to prosthetic disc design and spinal injury prevention.

6.2 Conclusions

6.2.1 Spinal load and load-sharing in standing and forward flexion postures using a new computational tool (Objective 1, Chapter 3)

The current study presents a novel methodology for combining MSK and FE modeling towards comprehensive quantitative analysis of spinal biomechanics. The results, in good overall agreement with the literature, showed that the disc forces and moments, as well as IDP, increased substantially from an upright to a flexed posture. Spinal forces and moments were mainly supported by discs in the upright posture, whereas the contribution of the ligaments in resisting shear and moment was more significant in the flexed position.

6.2.2 Effects of lumbo-pelvic rhythm on spinal load and load-sharing (Objective 2, Chapter 4)

A rhythm with high pelvic rotation and low lumbar flexion involves more global muscles and increases the role of the disc in resisting spinal loads, while its counterpart, with low pelvic rotation, recruits more local muscles and engages the ligaments to lower the disc loads. On the other hand, a normal rhythm that has relatively optimal pelvic and lumbar rotations yields almost equal disc and ligament load-sharing and results in more balanced synergy between global and local muscles. The lumbo-pelvic rhythm had minor effect on IDP and annular fibers strain. This work demonstrated that the spinal response during forward flexion is highly dependent on the lumbo-pelvic rhythm. It is therefore, essential to adapt this parameter in musculoskeletal modeling for accurate prediction of muscle forces, joint reaction forces and joint moments rather than using the default rhythms available in the MSK models. The findings provided by this work are expected to improve knowledge of spinal response during forward flexion, and are clinically relevant towards low back pain treatment and disc injury prevention.

6.2.3 Role of intra-abdominal pressure in flexed posture (Objective 3, Chapter 5)

The current research investigates the influence of IAP on muscle forces, loads in the passive spinal structures and load-sharing during forward flexion. In alignment with the literature, this study confirms the unloading role of IAP during upper body inclination. IAP has significant influences on the global muscle forces, yet, negligible effects on the local muscle forces. The substantial increase in IDP, internal disc force and load sharing triggered by the absence of IAP should be taken into consideration in future modeling efforts of the lumbosacral spine in flexion postures. This is the first study to the best knowledge of the investigators that attempts to quantitatively assess the role of IAP on detailed spinal biomechanics. Such information is essential for accurate modeling of flexed postures and more realistic spinal load-sharing.

6.3 Recommendations for the future research

The current MSK model chooses only one optimization function to predict muscle forces and did not consider muscle coactivity. Considering antagonist contraction will definitely improve predictions particularly in forward flexion.

Both the lumbo-pelvic and spine rhythms affect the spine behavior in forward flexion, thus, it is critical to use *in-vivo* values in the MSK models for accurate prediction of muscle forces and joint reaction forces and joint moments. These rhythms must be used with precaution when simulating low back pain (LBP) individuals.

The nonlinear behavior of intervertebral discs in FE model depends on the loads applied on it. The moment which is produced by discs, changes slightly when the compression force variation is relatively small. However, this effect should be taken into consideration when the lumbar spine is subjected to a relatively large compressive force.

Bibliography

- Abouhossein, A., Weisse, B., Ferguson, S.J., 2011. A multibody modelling approach to determine load sharing between passive elements of the lumbar spine. *Comput. Methods Biomech. Biomed. Engin.* 14, 527–537. <https://doi.org/10.1080/10255842.2010.485568>
- Adams, M.A., Dolan, P., Hutton, W.C., 1988. The lumbar spine in backward bending. *Spine* 13, 1019–1026.
- Adams, M.A., Hutton, W.C., 1981. The relevance of torsion to the mechanical derangement of the lumbar spine. *Spine* 6, 241–248.
- Adams, M.A., Hutton, W.C., Stott, J.R., 1980. The resistance to flexion of the lumbar intervertebral joint. *Spine* 5, 245–253.
- Althoff, I., Brinckmann, P., Frobin, W., Sandover, J., Burton, K., 1992. An improved method of stature measurement for quantitative determination of spinal loading. Application to sitting postures and whole body vibration. *Spine* 17, 682–693.
- Andersson, G.B.J., Örtengren, R., Nachemson, A., 1976. Quantitative Studies of Back Loads in Lifting. *Spine* 1, 178.
- Andersson, B.J., Örtengren, R., Nachemson, A., Elfström, G., 1974. Lumbar disc pressure and myoelectric back muscle activity during sitting. IV. Studies on a car driver's seat. *Scand. J. Rehabil. Med.* 6, 128–133.
- Arjmand, N., Gagnon, D., Plamondon, A., Shirazi-Adl, A., Larivière, C., 2010. A comparative study of two trunk biomechanical models under symmetric and asymmetric loadings. *J. Biomech.* 43, 485–491. doi:10.1016/j.jbiomech.2009.09.032
- Arjmand, N., Plamondon, A., Shirazi-Adl, A., Larivière, C., Parnianpour, M., 2011. Predictive equations to estimate spinal loads in symmetric lifting tasks. *J. Biomech.* 44, 84–91. <https://doi.org/10.1016/j.jbiomech.2010.08.028>
- Arjmand, N., Shirazi-Adl, A., 2006a. Model and in vivo studies on human trunk load partitioning and stability in isometric forward flexions. *J. Biomech.* 39, 510–521. doi:10.1016/j.jbiomech.2004.11.030
- Arjmand, N., Shirazi-Adl, A., 2006b. Sensitivity of kinematics-based model predictions to optimization criteria in static lifting tasks. *Med. Eng. Phys.* 28, 504–514. doi:10.1016/j.medengphy.2005.10.001

- Arjmand, N., Shirazi-Adl, A., 2006c. Role of intra-abdominal pressure in the unloading and stabilization of the human spine during static lifting tasks. *Eur. Spine J.* 15, 1265–1275. <https://doi.org/10.1007/s00586-005-0012-9>
- Arshad, R., Zander, T., Dreischarf, M., Schmidt, H., 2016. Influence of lumbar spine rhythms and intra-abdominal pressure on spinal loads and trunk muscle forces during upper body inclination. *Med. Eng. Phys.* 38, 333–338. doi:10.1016/j.medengphy.2016.01.013
- Azari, F., Arjmand, N., Shirazi-Adl, A., Rahimi-Moghaddam, T., 2017. A combined passive and active musculoskeletal model study to estimate L4-L5 load sharing. *J. Biomech.* <https://doi.org/10.1016/j.jbiomech.2017.04.026>
- Bartelink, D.L., 1957. The role of abdominal pressure in relieving the pressure on the lumbar intervertebral discs. *J. Bone Joint Surg. Br.* 39-B, 718–725.
- Boden, S.D., Davis, D.O., Dina, T.S., Patronas, N.J., Wiesel, S.W., 1990. Abnormal magnetic-resonance scans of the lumbar spine in asymptomatic subjects. A prospective investigation. *J. Bone Joint Surg. Am.* 72, 403–408.
- Breau, C., Shirazi-Adl, A., De Guise, J., 1991. Reconstruction of a human ligamentous lumbar spine using CT images—a three-dimensional finite element mesh generation. *Ann. Biomed. Eng.* 19, 291–302.
- Chaffin, D.B., 1969. A computerized biomechanical model—Development of and use in studying gross body actions. *J. Biomech.* 2, 429–441. [https://doi.org/10.1016/0021-9290\(69\)90018-9](https://doi.org/10.1016/0021-9290(69)90018-9)
- Cholewicki, J., McGill, S.M., 1996. Mechanical stability of the in vivo lumbar spine: implications for injury and chronic low back pain. *Clin. Biomech. Bristol Avon* 11, 1–15.
- Cholewicki, J., McGill, S.M., Norman, R.W., 1995. Comparison of muscle forces and joint load from an optimization and EMG assisted lumbar spine model: towards development of a hybrid approach. *J. Biomech.* 28, 321–331.
- Cholewicki, J., Juluru, K., McGill, S.M., 1999. Intra-abdominal pressure mechanism for stabilizing the lumbar spine. *J. Biomech.* 32, 13–17.
- Cholewicki, J., Reeves, N.P., 2004. All abdominal muscles must be considered when evaluating the intra-abdominal pressure contribution to trunk extensor moment and spinal loading. *J. Biomech.* 37, 953–954. <https://doi.org/10.1016/j.jbiomech.2003.09.021>

- Cresswell, A.G., 1993. Responses of intra-abdominal pressure and abdominal muscle activity during dynamic trunk loading in man. *Eur. J. Appl. Physiol.* 66, 315–320.
- Cresswell, A.G., Grundström, H., Thorstensson, A., 1992. Observations on intra-abdominal pressure and patterns of abdominal intra-muscular activity in man. *Acta Physiol. Scand.* 144, 409–418. <https://doi.org/10.1111/j.1748-1716.1992.tb09314.x>
- Cresswell, A.G., Thorstensson, A., 1989. The role of the abdominal musculature in the elevation of the intra-abdominal pressure during specified tasks. *Ergonomics* 32, 1237–1246. <https://doi.org/10.1080/00140138908966893>
- Daggfeldt, K., Thorstensson, A., 2003. The mechanics of back-extensor torque production about the lumbar spine. *J. Biomech.* 36, 815–825.
- Daggfeldt, K., Thorstensson, A., 1997. The role of intra-abdominal pressure in spinal unloading. *J. Biomech.* 30, 1149–1155.
- Damsgaard, M., Rasmussen, J., Christensen, S.T., Surma, E., de Zee, M., 2006. Analysis of musculoskeletal systems in the AnyBody Modeling System. *Simul. Model. Pract. Theory, SIMS 2004* 14, 1100–1111. <https://doi.org/10.1016/j.simpat.2006.09.001>
- Davis, P., 1956. Variations of the human intra-abdominal pressure during weight-lifting in different postures. *J Anat* 90, 601.
- Davis, P.R., 1959. Posture of the trunk during the lifting of weights. *Br. Med. J.* 1, 87–89.
- Davis, P.R., Troup, J.D.G., 1964. Pressures in the trunk cavities when pulling, pushing and lifting. *Ergonomics* 7, 465–474. <https://doi.org/10.1080/00140136408930764>
- de Zee, M., Hansen, L., Wong, C., Rasmussen, J., Simonsen, E.B., 2007. A generic detailed rigid-body lumbar spine model. *J. Biomech.* 40, 1219–1227. <https://doi.org/10.1016/j.jbiomech.2006.05.030>
- Dolan, P., Adams, M.A., 1993. The relationship between EMG activity and extensor moment generation in the erector spinae muscles during bending and lifting activities. *J. Biomech.* 26, 513–522.
- Dolan, P., Kingma, I., De Looze, M.P., van Dieen, J.H., Toussaint, H.M., Baten, C.T., Adams, M.A., 2001. An EMG technique for measuring spinal loading during asymmetric lifting. *Clin. Biomech. Bristol Avon* 16 Suppl 1, S17-24.

- Dreischarf, M., Rohlmann, A., Bergmann, G., Zander, T., 2012. Optimised in vitro applicable loads for the simulation of lateral bending in the lumbar spine. *Med. Eng. Phys.* 34, 777–780. <https://doi.org/10.1016/j.medengphy.2012.04.002>
- Dreischarf, M., Rohlmann, A., Bergmann, G., Zander, T., 2011. Optimised loads for the simulation of axial rotation in the lumbar spine. *J. Biomech.* 44, 2323–2327. <https://doi.org/10.1016/j.jbiomech.2011.05.040>
- Dreischarf, M., Shirazi-Adl, A., Arjmand, N., Rohlmann, A., Schmidt, H., 2016. Estimation of loads on human lumbar spine: A review of in vivo and computational model studies. *J. Biomech.* 49, 833–845. <https://doi.org/10.1016/j.jbiomech.2015.12.038>
- Dreischarf, M., Zander, T., Shirazi-Adl, A., Puttlitz, C.M., Adam, C.J., Chen, C.S., Goel, V.K., Kiapour, A., Kim, Y.H., Labus, K.M., Little, J.P., Park, W.M., Wang, Y.H., Wilke, H.J., Rohlmann, A., Schmidt, H., 2014. Comparison of eight published static finite element models of the intact lumbar spine: predictive power of models improves when combined together. *J. Biomech.* 47, 1757–1766. <https://doi.org/10.1016/j.jbiomech.2014.04.002>
- Dreischarf, M., Rohlmann, A., Zhu, R., Schmidt, H., Zander, T., 2013. Is it possible to estimate the compressive force in the lumbar spine from intradiscal pressure measurements? A finite element evaluation. *Med. Eng. Phys.* 35, 1385–1390. <https://doi.org/10.1016/j.medengphy.2013.03.007>
- Eklund, J.A., Corlett, E.N., 1984. Shrinkage as a measure of the effect of load on the spine. *Spine* 9, 189–194.
- El-Rich, M., Arnoux, P.-J., Wagnac, E., Brunet, C., Aubin, C.-E., 2009. Finite element investigation of the loading rate effect on the spinal load-sharing changes under impact conditions. *J. Biomech.* 42, 1252–1262. <https://doi.org/10.1016/j.jbiomech.2009.03.036>
- El-Rich, M., Shirazi-Adl, A., Arjmand, N., 2004. Muscle activity, internal loads, and stability of the human spine in standing postures: combined model and in vivo studies. *Spine* 29, 2633. <https://doi.org/10.1097/01.brs.0000146463.05288.0e>
- El-Rich, M., Shirazi-Adl, A., 2005. Effect of load position on muscle forces, internal loads and stability of the human spine in upright postures. *Comput. Methods Biomech. Biomed. Engin.* 8, 359–368. <https://doi.org/10.1080/10255840500445630>

- Esola, M.A., McClure, P.W., Fitzgerald, G.K., Siegler, S., 1996. Analysis of lumbar spine and hip motion during forward bending in subjects with and without a history of low back pain. *Spine* 21, 71–78.
- Essendrop, M., 2003. Significance of intra-abdominal pressure in work related trunk-loading. Ph. D. thesis, University of Copenhagen, Denmark.
- Fathallah, F.A., Marras, W.S., Parnianpour, M., 1999. Regression models for predicting peak and continuous three-dimensional spinal loads during symmetric and asymmetric lifting tasks. *Hum. Factors* 41, 373–388. <https://doi.org/10.1518/001872099779611094>
- Freivalds, A., Chaffin, D.B., Garg, A., Lee, K.S., 1984. A dynamic biomechanical evaluation of lifting maximum acceptable loads. *J. Biomech.* 17, 251–262.
- Funabashi, M., El-Rich, M., Prasad, N., Kawchuk, G.N., 2015. Quantification of loading in biomechanical testing: the influence of dissection sequence. *J. Biomech.* 48, 3522–3526. [doi:10.1016/j.jbiomech.2015.06.020](https://doi.org/10.1016/j.jbiomech.2015.06.020)
- Gagnon, D., Larivière, C., Loisel, P., 2001. Comparative ability of EMG, optimization, and hybrid modelling approaches to predict trunk muscle forces and lumbar spine loading during dynamic sagittal plane lifting. *Clin. Biomech.* 16, 359–372. [https://doi.org/10.1016/S0268-0033\(01\)00016-X](https://doi.org/10.1016/S0268-0033(01)00016-X)
- Garg, A., Waters, T., Kapellusch, J., Karwowski, W., 2014. Psychophysical basis for maximum pushing and pulling forces: A review and recommendations. *Int. J. Ind. Ergon.* 44, 281–291. <https://doi.org/10.1016/j.ergon.2012.09.005>
- Ghezelbash, F., Eskandari, A.H., Shirazi-Adl, A., Arjmand, N., El-Ouaaid, Z., Plamondon, A., 2018. Effects of motion segment simulation and joint positioning on spinal loads in trunk musculoskeletal models. *J. Biomech.* 70, 149–156.
- Granata, K.P., Sanford, A.H., 2000. Lumbar-pelvic coordination is influenced by lifting task parameters. *Spine* 25, 1413–1418.
- Granata, K.P., Marras, W.S., 1995. An EMG-assisted model of trunk loading during free-dynamic lifting. *J. Biomech.* 28, 1309–1317.
- Gudavalli, M.R., Triano, J.J., 1999. An analytical model of lumbar motion segment in flexion. *J. Manipulative Physiol. Ther.* 22, 201–208.
- Hagins, M., Pietrek, M., Sheikhzadeh, A., Nordin, M., Axen, K., 2004. The effects of breath control on intra-abdominal pressure during lifting tasks. *Spine* 29, 464–469.

- Han, K.-S., Zander, T., Taylor, W.R., Rohlmann, A., 2012. An enhanced and validated generic thoraco-lumbar spine model for prediction of muscle forces. *Med. Eng. Phys.* 34, 709–716. doi:10.1016/j.medengphy.2011.09.014
- Hemborg, B., Moritz, U., Hamberg, J., Löwing, H., Akesson, I., 1983. Intraabdominal pressure and trunk muscle activity during lifting-effect of abdominal muscle training in healthy subjects. *Scand. J. Rehabil. Med.* 15, 183–196.
- Heuer, F., Schmidt, H., Klezl, Z., Claes, L., Wilke, H.J., 2007. Stepwise reduction of functional spinal structures increase range of motion and change lordosis angle. *J. Biomech.* 40, 271–280. <https://doi.org/10.1016/j.jbiomech.2006.01.007>
- Heydari, A., Nargol, A.V.F., Jones, A.P.C., Humphrey, A.R., Greenough, C.G., 2010. EMG analysis of lumbar paraspinal muscles as a predictor of the risk of low-back pain. *Eur. Spine J. Off. Publ. Eur. Spine Soc. Eur. Spinal Deform. Soc. Eur. Sect. Cerv. Spine Res. Soc.* 19, 1145–1152. <https://doi.org/10.1007/s00586-010-1277-1>
- Hodges, P.W., Cresswell, A.G., Daggfeldt, K., Thorstensson, A., 2001. In vivo measurement of the effect of intra-abdominal pressure on the human spine. *J. Biomech.* 34, 347–353.
- Hodges, P.W., Eriksson, A.E.M., Shirley, D., Gandevia, S.C., 2005. Intra-abdominal pressure increases stiffness of the lumbar spine. *J. Biomech.* 38, 1873–1880. <https://doi.org/10.1016/j.jbiomech.2004.08.016>
- Hodges, P.W., Gandevia, S.C., 2000. Changes in intra-abdominal pressure during postural and respiratory activation of the human diaphragm. *J. Appl. Physiol. Bethesda Md* 1985 89, 967–976. <https://doi.org/10.1152/jappl.2000.89.3.967>
- Hoogendoorn, W.E., Bongers, P.M., de Vet, H.C., Douwes, M., Koes, B.W., Miedema, M.C., Ariëns, G.A., Bouter, L.M., 2000. Flexion and rotation of the trunk and lifting at work are risk factors for low back pain: results of a prospective cohort study. *Spine* 25, 3087–3092.
- Hoozemans, M.J., van der Beek, A.J., Frings-Dresen, M.H., van Dijk, F.J., van der Woude, L.H., 1998. Pushing and pulling in relation to musculoskeletal disorders: a review of risk factors. *Ergonomics* 41, 757–781. <https://doi.org/10.1080/001401398186621>
- Hoozemans, M.J.M., Kuijper, P.P.F.M., Kingma, I., van Dieën, J.H., de Vries, W.H.K., van der Woude, L.H.V., Veeger, D.J.H.E.J., van der Beek, A.J., Frings-Dresen, M.H.W., 2004.

- Mechanical loading of the low back and shoulders during pushing and pulling activities. *Ergonomics* 47, 1–18. <https://doi.org/10.1080/00140130310001593577>
- Hughes, R.E., Chaffin, D.B., Lavender, S.A., Andersson, G.B., 1994. Evaluation of muscle force prediction models of the lumbar trunk using surface electromyography. *J. Orthop. Res. Off. Publ. Orthop. Res. Soc.* 12, 689–698. <https://doi.org/10.1002/jor.1100120512>
- Ikai, M., Fukunaga, T., 1968. Calculation of muscle strength per unit cross-sectional area of human muscle by means of ultrasonic measurement. *Int. Z. Für Angew. Physiol. Einschließlich Arbeitsphysiologie* 26, 26–32. <https://doi.org/10.1007/BF00696087>
- Ivicsics, M.F., Bishop, N.E., Püschel, K., Morlock, M.M., Huber, G., 2014. Increase in facet joint loading after nucleotomy in the human lumbar spine. *J. Biomech.* 47, 1712–1717. <https://doi.org/10.1016/j.jbiomech.2014.02.021>
- Jäger, M., Sawatzki, K., Glitsch, U., Ellegast, R., Ottersbach, H.J., Schaub, K., Franz, G., Luttmann, A., 2007. Load on the lumbar spine of flight attendants during pushing and pulling trolleys aboard aircraft. *Int. J. Ind. Ergon., Musculoskeletal Load of Push–Pull Tasks* 37, 863–876. <https://doi.org/10.1016/j.ergon.2007.07.010>
- Kiefer, A., Shirazi-Adl, A., Parnianpour, M., 1997. Stability of the human spine in neutral postures. *Eur. Spine J. Off. Publ. Eur. Spine Soc. Eur. Spinal Deform. Soc. Eur. Sect. Cerv. Spine Res. Soc.* 6, 45–53.
- Knapik, G.G., Marras, W.S., 2009. Spine loading at different lumbar levels during pushing and pulling. *Ergonomics* 52, 60–70. <https://doi.org/10.1080/00140130802480828>
- Kim, M., Yi, C., Kwon, O., Cho, S., Cynn, H., Kim, Y., Hwang, S., Choi, B., Hong, J., Jung, D., 2013. Comparison of lumbopelvic rhythm and flexion-relaxation response between 2 different low back pain subtypes. *Spine* 38, 1260–1267.
- Laird, R.A., Kent, P., Keating, J.L., 2016. How consistent are lordosis, range of movement and lumbo-pelvic rhythm in people with and without back pain? *BMC Musculoskelet. Disord.* 17. <https://doi.org/10.1186/s12891-016-1250-1>
- Liu, T., Khalaf, K., Naserkhaki, S., El-Rich, M., 2018. Load-sharing in the lumbosacral spine in neutral standing & flexed postures - A combined finite element and inverse static study. *J. Biomech.* 70, 43–50. <https://doi.org/10.1016/j.jbiomech.2017.10.033>
- Manchikanti, L., 2000. Epidemiology of low back pain. *Pain Physician* 3, 167–192.

- Marras, W.S., Mirka, G.A., 1996. Intra-abdominal pressure during trunk extension motions. *Clin. Biomech. Bristol Avon* 11, 267–274.
- Marras, W.S., Granata, K.P., 1997. The development of an EMG-assisted model to assess spine loading during whole-body free-dynamic lifting. *J. Electromyogr. Kinesiol. Off. J. Int. Soc. Electrophysiol. Kinesiol.* 7, 259–268.
- McClure, P.W., Esola, M., Schreier, R., Siegler, S., 1997. Kinematic analysis of lumbar and hip motion while rising from a forward, flexed position in patients with and without a history of low back pain. *Spine* 22, 552–558.
- McGill, S.M., Norman, R.W., 1986. Partitioning of the L4-L5 dynamic moment into disc, ligamentous, and muscular components during lifting. *Spine* 11, 666–678.
- McGill, S.M., Norman, R.W., Cholewicki, J., 1996. A simple polynomial that predicts low-back compression during complex 3-D tasks. *Ergonomics* 39, 1107–1118. <https://doi.org/10.1080/00140139608964532>
- McGill, S.M., Norman, R.W., Sharratt, M.T., 1990. The effect of an abdominal belt on trunk muscle activity and intra-abdominal pressure during squat lifts. *Ergonomics* 33, 147–160. <https://doi.org/10.1080/00140139008927106>
- Morris, J.M., Lucas, D.B., Bresler, B., 1961. Role of the Trunk in Stability of the Spine. *JBJS* 43, 327.
- Mustafy, T., El-Rich, M., Mesfar, W., Moglo, K., 2014. Investigation of impact loading rate effects on the ligamentous cervical spinal load-partitioning using finite element model of functional spinal unit C2–C3. *J. Biomech.* 47, 2891–2903. <https://doi.org/10.1016/j.jbiomech.2014.07.016>
- Nachemson, A.L., 1981. Disc pressure measurements. *Spine* 6, 93–97.
- Naserkhaki, S., Jaremko, J.L., Adeeb, S., El-Rich, M., 2016a. On the load-sharing along the ligamentous lumbosacral spine in flexed and extended postures: Finite element study. *J. Biomech.* 49, 974–982. <https://doi.org/10.1016/j.jbiomech.2015.09.050>
- Naserkhaki, S., Jaremko, J.L., El-Rich, M., 2016b. Effects of inter-individual lumbar spine geometry variation on load-sharing: Geometrically personalized Finite Element study. *J. Biomech.* 49, 2909–2917. <https://doi.org/10.1016/j.jbiomech.2016.06.032>
- Naserkhaki, S., 2015. On the lumbosacral spine geometry variation and spinal load-sharing: personalized finite element modelling. Ph. D. thesis, University of Alberta. Canada.

- Naserkhaki, S., Arjmand, N., Shirazi-Adl, A., Farahmand, F., El-Rich, M., 2017. Effects of eight different ligament property datasets on biomechanics of a lumbar L4-L5 finite element model. *J. Biomech.* doi:10.1016/j.jbiomech.2017.05.003
- Nissan, M., Gilad, I., 1986. Dimensions of human lumbar vertebrae in the sagittal plane. *J. Biomech.* 19, 753757–755758.
- Noailly, J., Wilke, H.-J., Planell, J.A., Lacroix, D., 2007. How does the geometry affect the internal biomechanics of a lumbar spine bi-segment finite element model? Consequences on the validation process. *J. Biomech.* 40, 2414–2425. <https://doi.org/10.1016/j.jbiomech.2006.11.021>
- Okushima, H., 1970. [Study on hydrodynamic pressure of lumbar intervertebral disc]. *Nihon Geka Hokan Arch. Jpn. Chir.* 39, 45–57.
- Panjabi, M.M., 1992. The stabilizing system of the spine. Part I. Function, dysfunction, adaptation, and enhancement. *J. Spinal Disord.* 5, 383–389; discussion 397.
- Park, W.M., Wang, S., Kim, Y.H., Wood, K.B., Sim, J.A., Li, G., 2012. Effect of the intra-abdominal pressure and the center of segmental body mass on the lumbar spine mechanics—a computational parametric study. *J. Biomech. Eng.* 134, 011009.
- Pearcy, M.J., Bogduk, N., 1999. Instantaneous axes of rotation of the lumbar intervertebral joints. *Spine* 13, 1033-1041.
- Pintar, F.A., Yoganandan, N., Myers, T., Elhagediab, A., Sances, A., 1992. Biomechanical properties of human lumbar spine ligaments. *J. Biomech.* 25, 1351–1356.
- Pollintine, P., Dolan, P., Tobias, J.H., Adams, M.A., 2004. Intervertebral disc degeneration can lead to “stress-shielding” of the anterior vertebral body: a cause of osteoporotic vertebral fracture? *Spine* 29, 774–782.
- Pope, M.H., Novotny, J.E., 1993. Spinal biomechanics. *J. Biomech. Eng.* 115, 569–574.
- Porter, J.L., Wilkinson, A., 1997. Lumbar-hip flexion motion. A comparative study between asymptomatic and chronic low back pain in 18- to 36-year-old men. *Spine* 22, 1508-1513; discussion 1513-1514.
- Rabinowitz, D., Bridger, R.S., Lambert, M.I., 1998. Lifting technique and abdominal belt usage: a biomechanical, physiological and subjective investigation. *Saf. Sci.* 28, 155–164.

- Rohlmann, A., Bergmann, G., Graichen, F., 1999. Loads on internal spinal fixators measured in different body positions. *Eur. Spine J.* 8, 354–359. <https://doi.org/10.1007/s005860050187>
- Rohlmann, A., Dreischarf, M., Zander, T., Graichen, F., Strube, P., Schmidt, H., Bergmann, G., 2013. Monitoring the load on a telemeterised vertebral body replacement for a period of up to 65 months. *Eur. Spine J.* 22, 2575–2581. <https://doi.org/10.1007/s00586-013-3057-1>
- Rohlmann, A., Zander, T., Rao, M., Bergmann, G., 2009. Realistic loading conditions for upper body bending. *J. Biomech.* 42, 884–890. <https://doi.org/10.1016/j.jbiomech.2009.01.017>
- Rohlmann, A., Zander, T., Schmidt, H., Wilke, HJ., Bergmann, G., 2006a. Analysis of the influence of disc degeneration on the mechanical behaviour of a lumbar motion segment using the finite element method. *J. Biomech.* 39, 2484–2490. <https://doi.org/10.1016/j.jbiomech.2005.07.026>
- Rohlmann, A., Bauer, L., Zander, T., Bergmann, G., Wilke, HJ., 2006b. Determination of trunk muscle forces for flexion and extension by using a validated finite element model of the lumbar spine and measured in vivo data. *J. Biomech.* 39, 981–989. [doi:10.1016/j.jbiomech.2005.02.019](https://doi.org/10.1016/j.jbiomech.2005.02.019)
- Rohlmann, A., Neller, S., Claes, L., Bergmann, G., Wilke, H.-J., 2001. Influence of a follower load on intradiscal pressure and intersegmental rotation of the lumbar spine. *Spine* 26, E557–E561.
- Rose, S.J., Sahrman, S.A., Norton, B.T., 1988 Quantitative assessment of lumbar-pelvic rhythm. *Phys. Ther.* 68.824
- Sato, K., Kikuchi, S., Yonezawa, T., 1999. In vivo intradiscal pressure measurement in healthy individuals and in patients with ongoing back problems. *Spine* 24, 2468–2474.
- Schmidt, H., Heuer, F., Simon, U., Kettler, A., Rohlmann, A., Claes, L., Wilke, H.-J., 2006. Application of a new calibration method for a three-dimensional finite element model of a human lumbar annulus fibrosus. *Clin. Biomech.* 21, 337–344.
- Schmidt, H., Galbusera, F., Rohlmann, A., Shirazi-Adl, A., 2013. What have we learned from finite element model studies of lumbar intervertebral discs in the past four decades? *J. Biomech.* 46, 2342–2355. <https://doi.org/10.1016/j.jbiomech.2013.07.014>
- Schmidt, H., Kettler, A., Heuer, F., Simon, U., Claes, L., Wilke, H.-J., 2007. Intradiscal pressure,

- shear strain, and fiber strain in the intervertebral disc under combined loading. *Spine* 32, 748–55. doi:10.1097/01.brs.0000259059.90430.c2
- Schmidt, T.A., An, H.S., Lim, T.H., Nowicki, B.H., Haughton, V.M., 1998, The Stiffness of lumbar spinal motion segments with a high-intensity zone in the anulus fibrosus. *Spine* 23, 2167-2173.
- Schultz, A., Andersson, G., Ortengren, R., Haderspeck, K., Nachemson, A., 1982. Loads on the lumbar spine. Validation of a biomechanical analysis by measurements of intradiscal pressures and myoelectric signals. *J. Bone Joint Surg. Am.* 64, 713–720.
- Schultz, A.B., Warwick, D.N., Berkson, M.H., Nachemson, A.L., 1979. Mechanical properties of human lumbar spine motion segments. *J Biomech Eng* 101, 46–52.
- Sharma, M., Langrana, N.A., Rodriguez, J., 1995. Role of ligaments and facets in lumbar spinal stability. *Spine* 20, 887–900.
- Shirazi-Adl, A., Parnianpour, M., 2000. Load-bearing and stress analysis of the human spine under a novel wrapping compression loading. *Clin. Biomech. Bristol Avon* 15, 718–725.
- Shirazi-Adl, A., Sadouk, S., Parnianpour, M., Pop, D., El-Rich, M., 2002. Muscle force evaluation and the role of posture in human lumbar spine under compression. *Eur. Spine J. Off. Publ. Eur. Spine Soc. Eur. Spinal Deform. Soc. Eur. Sect. Cerv. Spine Res. Soc.* 11, 519–526. <https://doi.org/10.1007/s00586-002-0397-7>
- Shirazi-Adl, A., 2006. Analysis of large compression loads on lumbar spine in flexion and in torsion using a novel wrapping element. *J. Biomech.* 39, 267–275. <https://doi.org/10.1016/j.jbiomech.2004.11.022>
- Shirazi-Adl, A., Ahmed, A.M., Shrivastava, S.C., 1986. Mechanical response of a lumbar motion segment in axial torque alone and combined with compression. *Spine* 11, 914–927.
- Stokes, I.A.F., Gardner-Morse, M.G., Henry, S.M., 2010. Intra-abdominal pressure and abdominal wall muscular function: Spinal unloading mechanism. *Clin. Biomech. Bristol Avon* 25, 859–866. <https://doi.org/10.1016/j.clinbiomech.2010.06.018>
- Stokes, I.A.F., Gardner-Morse, M.G., Henry, S.M., 2011. Abdominal muscle activation increases lumbar spinal stability: Analysis of contributions of different muscle groups. *Clin. Biomech.* 26, 797–803. <https://doi.org/10.1016/j.clinbiomech.2011.04.006>
- Tafazzol, A., Arjmand, N., Shirazi-Adl, A., Parnianpour, M., 2014. Lumbopelvic rhythm during forward and backward sagittal trunk rotations: Combined in vivo measurement with

- inertial tracking device and biomechanical modeling. *Clin. Biomech.* 29, 7–13.
<https://doi.org/10.1016/j.clinbiomech.2013.10.021>
- Takahashi, I., Kikuchi, S., Sato, K., Sato, N., 2006. Mechanical load of the lumbar spine during forward bending motion of the trunk—a biomechanical study. *Spine* 31, 18–23.
- Andersson, G.B.J., Örtengren, R., Nachemson, A., 1976. Quantitative Studies of Back Loads in Lifting. *Spine* 1, 178.
- Arjmand, N., Shirazi-Adl, A., 2006. Role of intra-abdominal pressure in the unloading and stabilization of the human spine during static lifting tasks. *Eur. Spine J.* 15, 1265–1275.
<https://doi.org/10.1007/s00586-005-0012-9>
- Arshad, R., Zander, T., Dreischarf, M., Schmidt, H., 2016. Influence of lumbar spine rhythms and intra-abdominal pressure on spinal loads and trunk muscle forces during upper body inclination. *Med. Eng. Phys.* 38, 333–338.
<https://doi.org/10.1016/j.medengphy.2016.01.013>
- Bartelink, D.L., 1957. The role of abdominal pressure in relieving the pressure on the lumbar intervertebral discs. *J. Bone Joint Surg. Br.* 39-B, 718–725.
- Cholewicki, J., Juluru, K., McGill, S.M., 1999. Intra-abdominal pressure mechanism for stabilizing the lumbar spine. *J. Biomech.* 32, 13–17.
- Cholewicki, J., Reeves, N.P., 2004. All abdominal muscles must be considered when evaluating the intra-abdominal pressure contribution to trunk extensor moment and spinal loading. *J. Biomech.* 37, 953–954. <https://doi.org/10.1016/j.jbiomech.2003.09.021>
- Cresswell, A.G., Thorstensson, A., 1989. The role of the abdominal musculature in the elevation of the intra-abdominal pressure during specified tasks. *Ergonomics* 32, 1237–1246.
<https://doi.org/10.1080/00140138908966893>
- Cresswell, A.G., 1993. Responses of intra-abdominal pressure and abdominal muscle activity during dynamic trunk loading in man. *Eur. J. Appl. Physiol.* 66, 315–320.
- Cresswell, A.G., Grundström, H., Thorstensson, A., 1992. Observations on intra-abdominal pressure and patterns of abdominal intra-muscular activity in man. *Acta Physiol. Scand.* 144, 409–418. <https://doi.org/10.1111/j.1748-1716.1992.tb09314.x>
- Daggfeldt, K., Thorstensson, A., 2003. The mechanics of back-extensor torque production about the lumbar spine. *J. Biomech.* 36, 815–825.

- Daggfeldt, K., Thorstensson, A., 1997. The role of intra-abdominal pressure in spinal unloading. *J. Biomech.* 30, 1149–1155.
- Davis, P., 1956. Variations of the human intra-abdominal pressure during weight-lifting in different postures. *J Anat* 90, 601.
- Davis, P.R., Troup, J.D.G., 1964. Pressures in the trunk cavities when pulling, pushing and lifting. *ergonomics* 7, 465–474. <https://doi.org/10.1080/00140136408930764>
- de Zee, M., Hansen, L., Wong, C., Rasmussen, J., Simonsen, E.B., 2007. A generic detailed rigid-body lumbar spine model. *J. Biomech.* 40, 1219–1227. <https://doi.org/10.1016/j.jbiomech.2006.05.030>
- El-Rich, M., Shirazi-Adl, A., Arjmand, N., 2004. Muscle activity, internal loads, and stability of the human spine in standing postures: combined model and in vivo studies. *Spine* 29, 2633–2642.
- Essendrop, M., 2003. Significance of intra-abdominal pressure in work related trunk-loading. Ph. D. thesis, University of Copenhagen, Denmark.
- Granata, K.P., Sanford, A.H., 2000. Lumbar-pelvic coordination is influenced by lifting task parameters. *Spine* 25, 1413–1418.
- Hagins, M., Pietrek, M., Sheikhzadeh, A., Nordin, M., Axen, K., 2004. The effects of breath control on intra-abdominal pressure during lifting tasks. *Spine* 29, 464–469.
- Hodges, P.W., Cresswell, A.G., Daggfeldt, K., Thorstensson, A., 2001. In vivo measurement of the effect of intra-abdominal pressure on the human spine. *J. Biomech.* 34, 347–353.
- Hodges, P.W., Eriksson, A.E.M., Shirley, D., Gandevia, S.C., 2005. Intra-abdominal pressure increases stiffness of the lumbar spine. *J. Biomech.* 38, 1873–1880. <https://doi.org/10.1016/j.jbiomech.2004.08.016>
- Hodges, P.W., Gandevia, S.C., 2000. Changes in intra-abdominal pressure during postural and respiratory activation of the human diaphragm. *J. Appl. Physiol. Bethesda Md* 1985 89, 967–976. <https://doi.org/10.1152/jappl.2000.89.3.967>
- Ikai, M., Fukunaga, T., 1968. Calculation of muscle strength per unit cross-sectional area of human muscle by means of ultrasonic measurement. *Int. Z. Für Angew. Physiol. Einschließlich Arbeitsphysiologie* 26, 26–32. <https://doi.org/10.1007/BF00696087>

- Liu, T., Khalaf, K., Naserkhaki, S., El-Rich, M., 2018. Load-sharing in the lumbosacral spine in neutral standing & flexed postures - A combined finite element and inverse static study. *J. Biomech.* 70, 43–50. <https://doi.org/10.1016/j.jbiomech.2017.10.033>
- Marras, W.S., Mirka, G.A., 1996. Intra-abdominal pressure during trunk extension motions. *Clin. Biomech. Bristol Avon* 11, 267–274.
- McGill, S.M., Norman, R.W., Sharratt, M.T., 1990. The effect of an abdominal belt on trunk muscle activity and intra-abdominal pressure during squat lifts. *Ergonomics* 33, 147–160. <https://doi.org/10.1080/00140139008927106>
- Morris, J.M., Lucas, D.B., Bresler, B., 1961. Role of the Trunk in Stability of the Spine. *JBJS* 43, 327.
- Park, W.M., Wang, S., Kim, Y.H., Wood, K.B., Sim, J.A., Li, G., 2012. Effect of the intra-abdominal pressure and the center of segmental body mass on the lumbar spine mechanics—a computational parametric study. *J. Biomech. Eng.* 134, 011009.
- Schultz, A., Andersson, G., Ortengren, R., Haderspeck, K., Nachemson, A., 1982. Loads on the lumbar spine. Validation of a biomechanical analysis by measurements of intradiscal pressures and myoelectric signals. *J. Bone Joint Surg. Am.* 64, 713–720.
- Stokes, I.A.F., Gardner-Morse, M.G., Henry, S.M., 2010. Intra-abdominal pressure and abdominal wall muscular function: Spinal unloading mechanism. *Clin. Biomech. Bristol Avon* 25, 859–866. <https://doi.org/10.1016/j.clinbiomech.2010.06.018>
- Stokes, I.A.F., Gardner-Morse, M.G., Henry, S.M., 2011. Abdominal muscle activation increases lumbar spinal stability: Analysis of contributions of different muscle groups. *Clin. Biomech.* 26, 797–803. <https://doi.org/10.1016/j.clinbiomech.2011.04.006>
- Tayashiki, K., Mizuno, F., Kanehisa, H., Miyamoto, N., 2018. Causal effect of intra-abdominal pressure on maximal voluntary isometric hip extension torque. *Eur. J. Appl. Physiol.* 118, 93–99. <https://doi.org/10.1007/s00421-017-3748-0>
- Thiese, M.S., Hegmann, K.T., Wood, E.M., Garg, A., Moore, J.S., Kapellusch, J., Foster, J., Ott, U., 2014. Prevalence of low back pain by anatomic location and intensity in an occupational population. *BMC Musculoskelet. Disord.* 15, 283. <https://doi.org/10.1186/1471-2474-15-283>

- Toumanidou, T., Noailly, J., 2015. Musculoskeletal Modeling of the Lumbar Spine to Explore Functional Interactions between Back Muscle Loads and Intervertebral Disk Multiphysics. *Front. Bioeng. Biotechnol.* 3, 111.
- van Dieën, J.H., Creemers, M., Draisma, I., Toussaint, H.M., Kingma, I., 1994. Repetitive lifting and spinal shrinkage, effects of age and lifting technique. *Clin. Biomech.* 9, 367–374. <https://doi.org/10.1016/j.jbiomech.2013.03.003>
- Vazirian, M., Van Dillen, L.R., Bazrgari, B., 2016. Lumbopelvic rhythm in the sagittal plane: A review of the effects of participants and task characteristics. *Int. Musculoskelet. Med.* 38, 51–58. <https://doi.org/10.1080/17536146.2016.1241525>
- Wilke, H., Neef, P., Hinz, B., Seidel, H., Claes, L., 2001. Intradiscal pressure together with anthropometric data—a data set for the validation of models. *Clin. Biomech. Bristol Avon* 16 Suppl 1, S111-126.
- Zhu, R., Zander, T., Dreischarf, M., Duda, G.N., Rohlmann, A., Schmidt, H., 2013. Considerations when loading spinal finite element models with predicted muscle forces from inverse static analyses. *J. Biomech.* 46, 1376–1378. <https://doi.org/10.1016/j.jbiomech.2013.03.003>

Appendix A: The loading reference points and their influence radius for FE model

| Number | Load Name | Coordinate (mm) | | | Radius |
|--------|---|-----------------|----------|---------|--------|
| | | X | Y | Z | |
| 1 | MusclesSpineRight_Multifidi_MFdL1L3 | 45 | 1272.333 | 5.000 | 5 |
| 2 | MusclesSpineRight_Multifidi_MFmL1L4 | 41 | 1268.6 | 5.000 | 6 |
| 3 | MusclesSpineRight_Multifidi_MFtsL1L5 | 37 | 1263 | 0.000 | 6 |
| 4 | MusclesSpineRight_ErectorSpinae_ILpL1CI | 48 | 1296.6 | 34.000 | 5 |
| 5 | MusclesSpineRight_ErectorSpinae_LTpL1SIPS | 49 | 1296.6 | 27.000 | 5 |
| 6 | MusclesSpineRight_ErectorSpinae_ILptC5SIPS | 29 | 1268.6 | 31.314 | 26.3 |
| 7 | MusclesSpineRight_ErectorSpinae_ILptC6SIPS | 29 | 1268.6 | 34.654 | 30 |
| 8 | MusclesSpineRight_ErectorSpinae_ILptC7CI | 29 | 1268.6 | 37.871 | 33 |
| 9 | MusclesSpineRight_ErectorSpinae_ILptC8CI | 29 | 1268.6 | 41.479 | 34 |
| 10 | MusclesSpineRight_ErectorSpinae_ILptC9CI | 29 | 1268.6 | 45.265 | 36 |
| 11 | MusclesSpineRight_ErectorSpinae_ILptC10CI | 29 | 1268.6 | 48.778 | 39 |
| 12 | MusclesSpineRight_ErectorSpinae_ILptC11CI | 29 | 1268.6 | 52.219 | 39 |
| 13 | MusclesSpineRight_ErectorSpinae_ILptC12CI | 39 | 1268.6 | 55.676 | 39 |
| 14 | MusclesSpineRight_ErectorSpinae_LTptT1L1 | 29 | 1276.067 | 0.000 | 5 |
| 15 | MusclesSpineRight_ErectorSpinae_LTptT2L2 | 39 | 1268.6 | 2.667 | 5 |
| 16 | MusclesSpineRight_ErectorSpinae_LTptT3L3 | 41 | 1268.6 | 5.140 | 5 |
| 17 | MusclesSpineRight_ErectorSpinae_LTptT4L4 | 41 | 1268.6 | 7.727 | 5 |
| 18 | MusclesSpineRight_ErectorSpinae_LTptT5L5 | 39 | 1268.6 | 10.465 | 8 |
| 19 | MusclesSpineRight_ErectorSpinae_LTptT6S1 | 37 | 1268.6 | 12.410 | 10 |
| 20 | MusclesSpineRight_ErectorSpinae_LTptT7S2 | 37 | 1268.6 | 14.711 | 12 |
| 21 | MusclesSpineRight_ErectorSpinae_LTptT8S3 | 37 | 1268.6 | 17.692 | 13 |
| 22 | MusclesSpineRight_ErectorSpinae_LTptT9S4 | 37 | 1268.6 | 20.795 | 14 |
| 23 | MusclesSpineRight_ErectorSpinae_LTptT10Sacrum | 37 | 1268.6 | 30.185 | 21 |
| 24 | MusclesSpineRight_ErectorSpinae_LTptT11Sacrum | 37 | 1268.6 | 33.784 | 23 |
| 25 | MusclesSpineRight_ErectorSpinae_LTptT12Sacrum | 39 | 1268.6 | 36.683 | 26 |
| 26 | MusclesSpineRight_PsoasMajor_PML1I_TM | 100 | 1285.4 | 22.000 | 15 |
| 27 | MusclesSpineRight_PsoasMajor_PML1T_TM | 58 | 1297.533 | 25.000 | 5 |
| 28 | MusclesSpineRight_QuadratusLumborum_QLL1_CI | 54 | 1297.533 | 32.000 | 4 |
| 29 | MusclesSpineRight_SemispinalisRigth_SEL1T8 | 50 | 1307.053 | 15.300 | 5 |
| 30 | MusclesSpineRight_SemispinalisRigth_SEL1T10 | 47.7 | 1307.52 | 17.000 | 5 |
| 31 | MusclesSpineRight_SemispinalisRigth_SEL1T11 | 51 | 1306.493 | 9.500 | 5 |
| 32 | MusclesSpineRight_ThoracicMultifidiRigth_MFL1T8 | 48 | 1296.6 | 23.000 | 5 |
| 33 | MusclesSpineLeft_Multifidi_MFdL1L3 | 45 | 1272.333 | -5.000 | 8 |
| 34 | MusclesSpineLeft_Multifidi_MFmL1L4 | 41 | 1268.6 | -5.000 | 5 |
| 35 | MusclesSpineLeft_ErectorSpinae_ILpL1CI | 48 | 1296.6 | -34.000 | 5 |
| 36 | MusclesSpineLeft_ErectorSpinae_LTpL1SIPS | 49 | 1296.6 | -27.000 | 8 |
| 37 | MusclesSpineLeft_ErectorSpinae_ILptC5SIPS | 29 | 1268.6 | -31.314 | 27 |
| 38 | MusclesSpineLeft_ErectorSpinae_ILptC6SIPS | 29 | 1268.6 | -34.654 | 30 |

| | | | | | |
|----|---|------|----------|---------|------|
| 39 | MusclesSpineLeft_ErectorSpinae_ILptC7CI | 29 | 1268.6 | -37.871 | 32 |
| 40 | MusclesSpineLeft_ErectorSpinae_ILptC8CI | 29 | 1268.6 | -41.479 | 34 |
| 41 | MusclesSpineLeft_ErectorSpinae_ILptC9CI | 29 | 1268.6 | -45.265 | 36 |
| 42 | MusclesSpineLeft_ErectorSpinae_ILptC10CI | 29 | 1268.6 | -48.778 | 37 |
| 43 | MusclesSpineLeft_ErectorSpinae_ILptC11CI | 29 | 1268.6 | -52.219 | 39 |
| 44 | MusclesSpineLeft_ErectorSpinae_ILptC12CI | 39 | 1268.6 | -55.676 | 39 |
| 45 | MusclesSpineLeft_ErectorSpinae_LTptT2L2 | 39 | 1268.6 | -2.667 | 3 |
| 46 | MusclesSpineLeft_ErectorSpinae_LTptT3L3 | 41 | 1268.6 | -5.140 | 5 |
| 47 | MusclesSpineLeft_ErectorSpinae_LTptT4L4 | 41 | 1268.6 | -7.727 | 5 |
| 48 | MusclesSpineLeft_ErectorSpinae_LTptT5L5 | 39 | 1268.6 | -10.465 | 8 |
| 49 | MusclesSpineLeft_ErectorSpinae_LTptT6S1 | 37 | 1268.6 | -12.410 | 9 |
| 50 | MusclesSpineLeft_ErectorSpinae_LTptT7S2 | 37 | 1268.6 | -14.711 | 11 |
| 51 | MusclesSpineLeft_ErectorSpinae_LTptT8S3 | 37 | 1268.6 | -17.692 | 13 |
| 52 | MusclesSpineLeft_ErectorSpinae_LTptT9S4 | 37 | 1268.6 | -20.795 | 15 |
| 53 | MusclesSpineLeft_ErectorSpinae_LTptT10Sacrum | 37 | 1268.6 | -30.185 | 22 |
| 54 | MusclesSpineLeft_ErectorSpinae_LTptT11Sacrum | 37 | 1268.6 | -33.784 | 24 |
| 55 | MusclesSpineLeft_ErectorSpinae_LTptT12Sacrum | 39 | 1268.6 | -36.683 | 26 |
| 56 | MusclesSpineLeft_PsoasMajor_PMLII_TM | 100 | 1285.4 | -22.000 | 15 |
| 57 | MusclesSpineLeft_PsoasMajor_PMLIT_TM | 58 | 1297.533 | -25.000 | 5 |
| 58 | MusclesSpineLeft_QuadratusLumborum_QLL1_CI | 54 | 1297.533 | -32.000 | 5 |
| 59 | MusclesSpineLeft_SemispinalisLeft_SEL1T8 | 50 | 1307.053 | -15.300 | 5 |
| 60 | MusclesSpineLeft_SemispinalisLeft_SEL1T10 | 47.7 | 1307.52 | -17.000 | 5 |
| 61 | MusclesSpineLeft_SemispinalisLeft_SEL1T11 | 51 | 1306.493 | -9.500 | 5 |
| 62 | MusclesSpineLeft_ThoracicMultifidiLeft_MFL1T8 | 48 | 1296.6 | -23.000 | 5 |
| 63 | MusclesSpine_Spinalis_SPL1T3 | 28.5 | 1276.44 | 0.000 | 5 |
| 64 | MusclesSpine_Spinalis_SPL1T4 | 28.3 | 1275.507 | 0.000 | 5 |
| 65 | MusclesSpine_Spinalis_SPL1T5 | 28.2 | 1274.573 | 0.000 | 5 |
| 66 | MusclesSpine_Transversus_TransversusL1 | 74 | 1298.933 | 0.000 | 15 |
| 67 | Right_ShoulderArm_Mus_latissimus_dorsi_3 | 26 | 1298.933 | 0.000 | 19.7 |
| 68 | JointsLumbar_T12L1Jnt_Constraints_Reaction | 68 | 1313.4 | 0.000 | 5 |
| 69 | MusclesSpineRight_Multifidi_MFdL2L4 | 57 | 1243.4 | 5.000 | 6 |
| 70 | MusclesSpineRight_Multifidi_MFmL2L5 | 53 | 1239.667 | 5.000 | 6 |
| 71 | MusclesSpineRight_Multifidi_MFtsL2L5 | 50 | 1233.133 | 0.000 | 5 |
| 72 | MusclesSpineRight_ErectorSpinae_ILpL1CI_1 | 47 | 1238.733 | 27.271 | 20 |
| 73 | MusclesSpineRight_ErectorSpinae_ILpL2CI | 59 | 1266.733 | 34.000 | 5 |
| 74 | MusclesSpineRight_ErectorSpinae_LTpL1SIPS_1 | 47 | 1238.733 | 30.235 | 24 |
| 75 | MusclesSpineRight_ErectorSpinae_LTpL2SIPS | 61 | 1267.667 | 27.000 | 5 |
| 76 | MusclesSpineRight_ErectorSpinae_ILptC5SIPS_1 | 37 | 1238.733 | 27.657 | 26 |
| 77 | MusclesSpineRight_ErectorSpinae_ILptC6SIPS_1 | 37 | 1238.733 | 31.065 | 28.6 |
| 78 | MusclesSpineRight_ErectorSpinae_ILptC7CI_1 | 37 | 1238.733 | 34.400 | 31 |
| 79 | MusclesSpineRight_ErectorSpinae_ILptC8CI_1 | 37 | 1238.733 | 37.992 | 34 |

| | | | | | |
|-----|--|------|----------|---------|------|
| 80 | MusclesSpineRight_ErectorSpinae_ILptC9CI_1 | 37 | 1238.733 | 41.693 | 35.3 |
| 81 | MusclesSpineRight_ErectorSpinae_ILptC10CI_1 | 37 | 1238.733 | 45.222 | 38.5 |
| 82 | MusclesSpineRight_ErectorSpinae_ILptC11CI_1 | 37 | 1238.733 | 48.712 | 39 |
| 83 | MusclesSpineRight_ErectorSpinae_ILptC12CI_1 | 43 | 1238.733 | 52.216 | 39 |
| 84 | MusclesSpineRight_ErectorSpinae_LTptT2L2_1 | 41 | 1246.2 | 0.000 | 10 |
| 85 | MusclesSpineRight_ErectorSpinae_LTptT3L3_1 | 47 | 1238.733 | 1.564 | 5 |
| 86 | MusclesSpineRight_ErectorSpinae_LTptT4L4_1 | 44 | 1238.733 | 4.091 | 5 |
| 87 | MusclesSpineRight_ErectorSpinae_LTptT5L5_1 | 46 | 1238.733 | 6.744 | 8 |
| 88 | MusclesSpineRight_ErectorSpinae_LTptT6S1_1 | 44 | 1238.733 | 8.554 | 9 |
| 89 | MusclesSpineRight_ErectorSpinae_LTptT7S2_1 | 42 | 1238.733 | 10.821 | 10 |
| 90 | MusclesSpineRight_ErectorSpinae_LTptT8S3_1 | 42 | 1238.733 | 13.590 | 13 |
| 91 | MusclesSpineRight_ErectorSpinae_LTptT9S4_1 | 42 | 1238.733 | 16.556 | 14 |
| 92 | MusclesSpineRight_ErectorSpinae_LTptT10Sacrum_1 | 42 | 1238.733 | 27.477 | 23 |
| 93 | MusclesSpineRight_ErectorSpinae_LTptT11Sacrum_1 | 42 | 1238.733 | 31.388 | 25.5 |
| 94 | MusclesSpineRight_ErectorSpinae_LTptT12Sacrum_1 | 42 | 1238.733 | 34.754 | 28 |
| 95 | MusclesSpineRight_PsoasMajor_PMT12I_TM | 99 | 1272.333 | 27.834 | 13 |
| 96 | MusclesSpineRight_PsoasMajor_PML1T_TM_1 | 77 | 1267.667 | 31.208 | 10 |
| 97 | MusclesSpineRight_PsoasMajor_PML2I_TM | 106 | 1257.4 | 22.000 | 10 |
| 98 | MusclesSpineRight_PsoasMajor_PML2T_TM | 69 | 1268.6 | 25.000 | 5 |
| 99 | MusclesSpineRight_QuadratusLumborum_QLL2_CI | 65 | 1267.667 | 32.000 | 3 |
| 100 | MusclesSpineRight_SemispinalisRighth_SEL2T9 | 57 | 1275.787 | 19.000 | 5 |
| 101 | MusclesSpineRight_SemispinalisRighth_SEL2T10 | 58.9 | 1278.213 | 17.000 | 8 |
| 102 | MusclesSpineRight_SemispinalisRighth_SEL2T11 | 61 | 1278.493 | 13.000 | 5 |
| 103 | MusclesSpineRight_SemispinalisRighth_SEL2T12 | 61.5 | 1277.467 | 10.000 | 10 |
| 104 | MusclesSpineRight_ThoracicMultifidiRighth_MFL2T9 | 59 | 1267.667 | 23.000 | 3 |
| 105 | MusclesSpineLeft_Multifidi_MFdL2L4 | 57 | 1243.4 | -5.000 | 5 |
| 106 | MusclesSpineLeft_Multifidi_MFmL2L5 | 53 | 1239.667 | -5.000 | 5 |
| 107 | MusclesSpineLeft_ErectorSpinae_ILplL1CI_1 | 47 | 1238.733 | -27.271 | 20 |
| 108 | MusclesSpineLeft_ErectorSpinae_ILplL2CI | 59 | 1266.733 | -34.000 | 5 |
| 109 | MusclesSpineLeft_ErectorSpinae_LTplL1SIPS_1 | 47 | 1238.733 | -30.235 | 23 |
| 110 | MusclesSpineLeft_ErectorSpinae_LTplL2SIPS | 61 | 1267.667 | -27.000 | 5 |
| 111 | MusclesSpineLeft_ErectorSpinae_ILptC5SIPS_1 | 37 | 1238.733 | -27.657 | 26.5 |
| 112 | MusclesSpineLeft_ErectorSpinae_ILptC6SIPS_1 | 37 | 1238.733 | -31.065 | 29 |
| 113 | MusclesSpineLeft_ErectorSpinae_ILptC7CI_1 | 37 | 1238.733 | -34.400 | 32 |
| 114 | MusclesSpineLeft_ErectorSpinae_ILptC8CI_1 | 37 | 1238.733 | -37.992 | 34 |
| 115 | MusclesSpineLeft_ErectorSpinae_ILptC9CI_1 | 37 | 1238.733 | -41.693 | 36 |
| 116 | MusclesSpineLeft_ErectorSpinae_ILptC10CI_1 | 37 | 1238.733 | -45.222 | 38 |
| 117 | MusclesSpineLeft_ErectorSpinae_ILptC11CI_1 | 37 | 1238.733 | -48.712 | 39 |
| 118 | MusclesSpineLeft_ErectorSpinae_ILptC12CI_1 | 43 | 1238.733 | -52.216 | 39 |
| 119 | MusclesSpineLeft_ErectorSpinae_LTptT3L3_1 | 47 | 1238.733 | -1.564 | 3 |
| 120 | MusclesSpineLeft_ErectorSpinae_LTptT4L4_1 | 44 | 1238.733 | -4.091 | 5 |

| | | | | | |
|-----|--|------|----------|---------|------|
| 121 | MusclesSpineLeft_ErectorSpinae_LTptT5L5_1 | 46 | 1238.733 | -6.744 | 5 |
| 122 | MusclesSpineLeft_ErectorSpinae_LTptT6S1_1 | 44 | 1238.733 | -8.554 | 8 |
| 123 | MusclesSpineLeft_ErectorSpinae_LTptT7S2_1 | 42 | 1238.733 | -10.821 | 10 |
| 124 | MusclesSpineLeft_ErectorSpinae_LTptT8S3_1 | 42 | 1238.733 | -13.590 | 13 |
| 125 | MusclesSpineLeft_ErectorSpinae_LTptT9S4_1 | 42 | 1238.733 | -16.556 | 14 |
| 126 | MusclesSpineLeft_ErectorSpinae_LTptT10Sacrum_1 | 42 | 1238.733 | -27.477 | 23.5 |
| 127 | MusclesSpineLeft_ErectorSpinae_LTptT11Sacrum_1 | 42 | 1238.733 | -31.388 | 26 |
| 128 | MusclesSpineLeft_ErectorSpinae_LTptT12Sacrum_1 | 42 | 1238.733 | -34.754 | 28 |
| 129 | MusclesSpineLeft_PsoasMajor_PMT12I_TM | 99 | 1272.333 | -27.834 | 15 |
| 130 | MusclesSpineLeft_PsoasMajor_PML1T_TM_1 | 77 | 1267.667 | -31.208 | 10 |
| 131 | MusclesSpineLeft_PsoasMajor_PML2I_TM | 106 | 1257.4 | -22.000 | 10 |
| 132 | MusclesSpineLeft_PsoasMajor_PML2T_TM | 69 | 1268.6 | -25.000 | 5 |
| 133 | MusclesSpineLeft_QuadratusLumborum_QLL2_CI | 65 | 1267.667 | -32.000 | 5 |
| 134 | MusclesSpineLeft_SemispinalisLeft_SEL2T9 | 57 | 1275.787 | -19.000 | 5 |
| 135 | MusclesSpineLeft_SemispinalisLeft_SEL2T10 | 58.9 | 1278.213 | -17.000 | 5 |
| 136 | MusclesSpineLeft_SemispinalisLeft_SEL2T11 | 61 | 1278.493 | -13.000 | 10 |
| 137 | MusclesSpineLeft_SemispinalisLeft_SEL2T12 | 61.5 | 1277.467 | -10.000 | 5 |
| 138 | MusclesSpineLeft_ThoracicMultifidiLeft_MFL2T9 | 59 | 1267.667 | -23.000 | 5 |
| 139 | MusclesSpine_Transversus_TransversusL2 | 85 | 1270.933 | 0.000 | 15 |
| 140 | MusclesSpineRight_Multifidi_MFdL1L3_1 | 65 | 1247.133 | 22.000 | 5 |
| 141 | MusclesSpineRight_Multifidi_MFdL3L5 | 60 | 1219.133 | 5.000 | 6 |
| 142 | MusclesSpineRight_Multifidi_MFmL3S1 | 55 | 1215.4 | 5.000 | 6 |
| 143 | MusclesSpineRight_Multifidi_MFmL3Ligament | 50 | 1210.733 | 0.000 | 6 |
| 144 | MusclesSpineRight_ErectorSpinae_ILpL1CI_2 | 43 | 1217.267 | 24.775 | 22 |
| 145 | MusclesSpineRight_ErectorSpinae_ILpL2CI_1 | 43 | 1217.267 | 27.522 | 24 |
| 146 | MusclesSpineRight_ErectorSpinae_ILpL3CI | 65 | 1242.467 | 35.000 | 5 |
| 147 | MusclesSpineRight_ErectorSpinae_LTpL1SIPS_2 | 43 | 1217.267 | 31.435 | 28 |
| 148 | MusclesSpineRight_ErectorSpinae_LTpL2SIPS_1 | 43 | 1217.267 | 28.884 | 25 |
| 149 | MusclesSpineRight_ErectorSpinae_LTpL3SIPS | 68 | 1243.4 | 28.000 | 5 |
| 150 | MusclesSpineRight_ErectorSpinae_ILptC5SIPS_2 | 38 | 1217.267 | 25.029 | 24 |
| 151 | MusclesSpineRight_ErectorSpinae_ILptC6SIPS_2 | 38 | 1217.267 | 28.486 | 28 |
| 152 | MusclesSpineRight_ErectorSpinae_ILptC7CI_2 | 38 | 1217.267 | 31.905 | 30 |
| 153 | MusclesSpineRight_ErectorSpinae_ILptC8CI_2 | 38 | 1217.267 | 35.486 | 33 |
| 154 | MusclesSpineRight_ErectorSpinae_ILptC9CI_2 | 38 | 1217.267 | 39.126 | 35 |
| 155 | MusclesSpineRight_ErectorSpinae_ILptC10CI_2 | 40 | 1217.267 | 42.667 | 35.5 |
| 156 | MusclesSpineRight_ErectorSpinae_ILptC11CI_2 | 42 | 1217.267 | 46.192 | 36 |
| 157 | MusclesSpineRight_ErectorSpinae_ILptC12CI_2 | 46 | 1217.267 | 49.730 | 37 |
| 158 | MusclesSpineRight_ErectorSpinae_LTptT3L3_2 | 43 | 1225.667 | 0.000 | 10 |
| 159 | MusclesSpineRight_ErectorSpinae_LTptT4L4_2 | 45 | 1217.267 | 1.477 | 5 |
| 160 | MusclesSpineRight_ErectorSpinae_LTptT5L5_2 | 47 | 1217.267 | 4.070 | 5 |
| 161 | MusclesSpineRight_ErectorSpinae_LTptT6S1_2 | 47 | 1217.267 | 5.783 | 5 |

| | | | | | |
|-----|---|------|----------|---------|------|
| 162 | MusclesSpineRight_ErectorSpinae_LTptT7S2_2 | 43 | 1217.267 | 8.024 | 10 |
| 163 | MusclesSpineRight_ErectorSpinae_LTptT8S3_2 | 43 | 1217.267 | 10.641 | 10 |
| 164 | MusclesSpineRight_ErectorSpinae_LTptT9S4_2 | 43 | 1217.267 | 13.510 | 13 |
| 165 | MusclesSpineRight_ErectorSpinae_LTptT10Sacrum_2 | 43 | 1217.267 | 25.531 | 22.6 |
| 166 | MusclesSpineRight_ErectorSpinae_LTptT11Sacrum_2 | 43 | 1217.267 | 29.665 | 25 |
| 167 | MusclesSpineRight_ErectorSpinae_LTptT12Sacrum_2 | 43 | 1217.267 | 33.367 | 28 |
| 168 | MusclesSpineRight_PsoasMajor_PMT12I_TM_1 | 107 | 1243.4 | 34.203 | 16 |
| 169 | MusclesSpineRight_PsoasMajor_PML1I_TM_1 | 107 | 1243.4 | 31.839 | 15 |
| 170 | MusclesSpineRight_PsoasMajor_PML1T_TM_2 | 86 | 1243.4 | 36.253 | 14.5 |
| 171 | MusclesSpineRight_PsoasMajor_PML2T_TM_1 | 83 | 1243.4 | 31.026 | 10 |
| 172 | MusclesSpineRight_PsoasMajor_PML3I_TM | 112 | 1226.6 | 22.000 | 10 |
| 173 | MusclesSpineRight_PsoasMajor_PML3T_TM | 76 | 1243.4 | 28.000 | 5 |
| 174 | MusclesSpineRight_QuadratusLumborum_QLL3_CI | 72 | 1243.4 | 33.000 | 5 |
| 175 | MusclesSpineRight_SemispinalisRighth_SEL3T11 | 64 | 1252.36 | 19.700 | 5 |
| 176 | MusclesSpineRight_SemispinalisRighth_SEL3T12 | 67.5 | 1253.853 | 18.000 | 10 |
| 177 | MusclesSpineRight_ThoracicMultifidiRighth_MFL3T10 | 66 | 1243.4 | 24.000 | 4 |
| 178 | MusclesSpineLeft_Multifidi_MFdL1L3_1 | 65 | 1247.133 | -22.000 | 5 |
| 179 | MusclesSpineLeft_Multifidi_MFdL3L5 | 60 | 1219.133 | -5.000 | 5 |
| 180 | MusclesSpineLeft_Multifidi_MFmL3S1 | 55 | 1215.4 | -5.000 | 5 |
| 181 | MusclesSpineLeft_ErectorSpinae_ILpL1CI_2 | 43 | 1217.267 | -24.775 | 22 |
| 182 | MusclesSpineLeft_ErectorSpinae_ILpL2CI_1 | 43 | 1217.267 | -27.522 | 24 |
| 183 | MusclesSpineLeft_ErectorSpinae_ILpL3CI | 65 | 1242.467 | -35.000 | 8 |
| 184 | MusclesSpineLeft_ErectorSpinae_LTpL1SIPS_2 | 43 | 1217.267 | -31.435 | 26 |
| 185 | MusclesSpineLeft_ErectorSpinae_LTpL2SIPS_1 | 43 | 1217.267 | -28.884 | 25 |
| 186 | MusclesSpineLeft_ErectorSpinae_LTpL3SIPS | 68 | 1243.4 | -28.000 | 5 |
| 187 | MusclesSpineLeft_ErectorSpinae_ILptC5SIPS_2 | 38 | 1217.267 | -25.029 | 25 |
| 188 | MusclesSpineLeft_ErectorSpinae_ILptC6SIPS_2 | 38 | 1217.267 | -28.486 | 27 |
| 189 | MusclesSpineLeft_ErectorSpinae_ILptC7CI_2 | 38 | 1217.267 | -31.905 | 30 |
| 190 | MusclesSpineLeft_ErectorSpinae_ILptC8CI_2 | 38 | 1217.267 | -35.486 | 33 |
| 191 | MusclesSpineLeft_ErectorSpinae_ILptC9CI_2 | 38 | 1217.267 | -39.126 | 35 |
| 192 | MusclesSpineLeft_ErectorSpinae_ILptC10CI_2 | 40 | 1217.267 | -42.667 | 35.5 |
| 193 | MusclesSpineLeft_ErectorSpinae_ILptC11CI_2 | 42 | 1217.267 | -46.192 | 37 |
| 194 | MusclesSpineLeft_ErectorSpinae_ILptC12CI_2 | 46 | 1217.267 | -49.730 | 37 |
| 195 | MusclesSpineLeft_ErectorSpinae_LTptT4L4_2 | 45 | 1217.267 | -1.477 | 5 |
| 196 | MusclesSpineLeft_ErectorSpinae_LTptT5L5_2 | 47 | 1217.267 | -4.070 | 5 |
| 197 | MusclesSpineLeft_ErectorSpinae_LTptT6S1_2 | 47 | 1217.267 | -5.783 | 5 |
| 198 | MusclesSpineLeft_ErectorSpinae_LTptT7S2_2 | 43 | 1217.267 | -8.024 | 8 |
| 199 | MusclesSpineLeft_ErectorSpinae_LTptT8S3_2 | 43 | 1217.267 | -10.641 | 10 |
| 200 | MusclesSpineLeft_ErectorSpinae_LTptT9S4_2 | 43 | 1217.267 | -13.510 | 13.5 |
| 201 | MusclesSpineLeft_ErectorSpinae_LTptT10Sacrum_2 | 43 | 1217.267 | -25.531 | 22.7 |
| 202 | MusclesSpineLeft_ErectorSpinae_LTptT11Sacrum_2 | 43 | 1217.267 | -29.665 | 26 |

| | | | | | |
|-----|---|------|----------|---------|------|
| 203 | MusclesSpineLeft_ErectorSpinae_LTptT12Sacrum_2 | 43 | 1217.267 | -33.367 | 28 |
| 204 | MusclesSpineLeft_PsoasMajor_PMT12I_TM_1 | 107 | 1243.4 | -34.203 | 16 |
| 205 | MusclesSpineLeft_PsoasMajor_PML1I_TM_1 | 107 | 1243.4 | -31.839 | 15 |
| 206 | MusclesSpineLeft_PsoasMajor_PML1T_TM_2 | 86 | 1243.4 | -36.253 | 14 |
| 207 | MusclesSpineLeft_PsoasMajor_PML2T_TM_1 | 83 | 1243.4 | -31.026 | 10 |
| 208 | MusclesSpineLeft_PsoasMajor_PML3I_TM | 112 | 1226.6 | -22.000 | 10 |
| 209 | MusclesSpineLeft_PsoasMajor_PML3T_TM | 76 | 1243.4 | -28.000 | 5 |
| 210 | MusclesSpineLeft_QuadratusLumborum_QLL3_CI | 72 | 1243.4 | -33.000 | 5 |
| 211 | MusclesSpineLeft_SemispinalisLeft_SEL3T11 | 64 | 1252.36 | -19.700 | 5 |
| 212 | MusclesSpineLeft_SemispinalisLeft_SEL3T12 | 67.5 | 1253.853 | -18.000 | 5 |
| 213 | MusclesSpineLeft_ThoracicMultifidiLeft_MFL3T10 | 66 | 1243.4 | -24.000 | 5 |
| 214 | MusclesSpine_Transversus_TransversusL3 | 93 | 1242 | 0.000 | 15 |
| 215 | Right_ShoulderArm_Mus_latissimus_dorsi_4 | 63 | 1242 | 0.000 | 8 |
| 216 | MusclesSpineRight_Multifidi_MFdL2L4_1 | 72 | 1221 | 22.000 | 5 |
| 217 | MusclesSpineRight_Multifidi_MFdL4S1 | 60 | 1195.8 | 5.000 | 6 |
| 218 | MusclesSpineRight_Multifidi_MFmL4Sacrum | 55 | 1193 | 5.000 | 6 |
| 219 | MusclesSpineRight_Multifidi_MFtsL4Sacrum | 49 | 1189.267 | 0.000 | 5 |
| 220 | MusclesSpineRight_ErectorSpinae_ILpL1CI_3 | 38 | 1196.733 | 22.388 | 23 |
| 221 | MusclesSpineRight_ErectorSpinae_ILpL2CI_2 | 38 | 1196.733 | 24.833 | 25 |
| 222 | MusclesSpineRight_ErectorSpinae_ILpL4CI | 71 | 1216.333 | 35.000 | 5 |
| 223 | MusclesSpineRight_ErectorSpinae_LTpL4SIPS | 74 | 1217.267 | 28.000 | 5 |
| 224 | MusclesSpineRight_ErectorSpinae_LTptT4L4_3 | 45 | 1205.133 | 0.000 | 10 |
| 225 | MusclesSpineRight_ErectorSpinae_LTptT5L5_3 | 47 | 1196.733 | 1.512 | 5 |
| 226 | MusclesSpineRight_ErectorSpinae_LTptT6S1_3 | 47 | 1196.733 | 3.133 | 5 |
| 227 | MusclesSpineRight_ErectorSpinae_LTptT7S2_3 | 45 | 1196.733 | 5.350 | 8 |
| 228 | MusclesSpineRight_ErectorSpinae_LTptT8S3_3 | 43 | 1196.733 | 7.821 | 10 |
| 229 | MusclesSpineRight_ErectorSpinae_LTptT9S4_3 | 43 | 1196.733 | 10.596 | 12 |
| 230 | MusclesSpineRight_ErectorSpinae_LTptT10Sacrum_3 | 43 | 1196.733 | 23.669 | 22 |
| 231 | MusclesSpineRight_ErectorSpinae_LTptT11Sacrum_3 | 43 | 1196.733 | 28.018 | 25.5 |
| 232 | MusclesSpineRight_ErectorSpinae_LTptT12Sacrum_3 | 43 | 1196.733 | 32.040 | 28 |
| 233 | MusclesSpineRight_PsoasMajor_PMT12I_TM_2 | 111 | 1209.8 | 41.600 | 21 |
| 234 | MusclesSpineRight_PsoasMajor_PML1I_TM_2 | 111 | 1209.8 | 39.711 | 20 |
| 235 | MusclesSpineRight_PsoasMajor_PML1T_TM_3 | 96 | 1209.8 | 43.237 | 22 |
| 236 | MusclesSpineRight_PsoasMajor_PML2I_TM_1 | 116 | 1209.8 | 34.875 | 18 |
| 237 | MusclesSpineRight_PsoasMajor_PML2T_TM_2 | 96 | 1209.8 | 39.061 | 17 |
| 238 | MusclesSpineRight_PsoasMajor_PML3T_TM_1 | 91 | 1209.8 | 36.643 | 15 |
| 239 | MusclesSpineRight_PsoasMajor_PML4I_TM | 113 | 1191.133 | 22.000 | 5 |
| 240 | MusclesSpineRight_PsoasMajor_PML4T_TM | 80 | 1216.333 | 28.000 | 6 |
| 241 | MusclesSpineRight_QuadratusLumborum_QLL4_CI | 77 | 1216.333 | 33.000 | 5 |
| 242 | MusclesSpineRight_ThoracicMultifidiRighth_MFL4T11 | 71 | 1217.267 | 24.000 | 5 |
| 243 | MusclesSpineLeft_Multifidi_MFdL2L4_1 | 72 | 1221 | -22.000 | 5 |

| | | | | | |
|-----|---|-----|----------|---------|------|
| 244 | MusclesSpineLeft_Multifidi_MFdl4S1 | 60 | 1195.8 | -5.000 | 5 |
| 245 | MusclesSpineLeft_Multifidi_MFmL4Sacrum | 55 | 1193 | -5.000 | 5 |
| 246 | MusclesSpineLeft_ErectorSpinae_ILplL1CI_3 | 38 | 1196.733 | -22.388 | 22 |
| 247 | MusclesSpineLeft_ErectorSpinae_ILplL2CI_2 | 38 | 1196.733 | -24.833 | 25 |
| 248 | MusclesSpineLeft_ErectorSpinae_ILplL4CI | 71 | 1216.333 | -35.000 | 8 |
| 249 | MusclesSpineLeft_ErectorSpinae_LTplL4SIPS | 74 | 1217.267 | -28.000 | 5 |
| 250 | MusclesSpineLeft_ErectorSpinae_LTptT5L5_3 | 47 | 1196.733 | -1.512 | 5 |
| 251 | MusclesSpineLeft_ErectorSpinae_LTptT6S1_3 | 47 | 1196.733 | -3.133 | 5 |
| 252 | MusclesSpineLeft_ErectorSpinae_LTptT7S2_3 | 45 | 1196.733 | -5.350 | 6 |
| 253 | MusclesSpineLeft_ErectorSpinae_LTptT8S3_3 | 43 | 1196.733 | -7.821 | 9 |
| 254 | MusclesSpineLeft_ErectorSpinae_LTptT9S4_3 | 43 | 1196.733 | -10.596 | 12.5 |
| 255 | MusclesSpineLeft_ErectorSpinae_LTptT10Sacrum_3 | 43 | 1196.733 | -23.669 | 22 |
| 256 | MusclesSpineLeft_ErectorSpinae_LTptT11Sacrum_3 | 43 | 1196.733 | -28.018 | 26 |
| 257 | MusclesSpineLeft_ErectorSpinae_LTptT12Sacrum_3 | 43 | 1196.733 | -32.040 | 28 |
| 258 | MusclesSpineLeft_PsoasMajor_PMT12I_TM_2 | 111 | 1209.8 | -41.600 | 24 |
| 259 | MusclesSpineLeft_PsoasMajor_PML1I_TM_2 | 111 | 1209.8 | -39.711 | 23 |
| 260 | MusclesSpineLeft_PsoasMajor_PML1T_TM_3 | 96 | 1209.8 | -43.237 | 21 |
| 261 | MusclesSpineLeft_PsoasMajor_PML2I_TM_1 | 116 | 1209.8 | -34.875 | 18 |
| 262 | MusclesSpineLeft_PsoasMajor_PML2T_TM_2 | 96 | 1209.8 | -39.061 | 18 |
| 263 | MusclesSpineLeft_PsoasMajor_PML3T_TM_1 | 91 | 1209.8 | -36.643 | 15 |
| 264 | MusclesSpineLeft_PsoasMajor_PML4I_TM | 113 | 1191.133 | -22.000 | 10 |
| 265 | MusclesSpineLeft_PsoasMajor_PML4T_TM | 80 | 1216.333 | -28.000 | 5 |
| 266 | MusclesSpineLeft_QuadratusLumborum_QLL4_CI | 77 | 1216.333 | -33.000 | 5 |
| 267 | MusclesSpineLeft_ThoracicMultifidiLeft_MFL4T11 | 71 | 1217.267 | -24.000 | 5 |
| 268 | MusclesSpine_Transversus_TransversusL4 | 96 | 1210.733 | 0.000 | 13 |
| 269 | MusclesSpineRight_Multifidi_MFdl3L5_1 | 73 | 1193 | 22.000 | 6 |
| 270 | MusclesSpineRight_Multifidi_MFdl5S1 | 54 | 1178.067 | 5.000 | 10 |
| 271 | MusclesSpineRight_Multifidi_MFmL5Sacrum | 50 | 1179 | 5.000 | 6 |
| 272 | MusclesSpineRight_Multifidi_MFtsL5Sacrum | 47 | 1176.2 | 0.000 | 5 |
| 273 | MusclesSpineRight_ErectorSpinae_LTplL5Ilium | 74 | 1190.2 | 28.000 | 5 |
| 274 | MusclesSpineRight_ErectorSpinae_LTptT5L5_4 | 47 | 1184.6 | 0.000 | 10 |
| 275 | MusclesSpineRight_ErectorSpinae_LTptT6S1_4 | 48 | 1179.933 | 0.964 | 8 |
| 276 | MusclesSpineRight_ErectorSpinae_LTptT7S2_4 | 44 | 1179.933 | 3.161 | 10 |
| 277 | MusclesSpineRight_ErectorSpinae_LTptT8S3_4 | 42 | 1179.933 | 5.513 | 10 |
| 278 | MusclesSpineRight_ErectorSpinae_LTptT9S4_4 | 42 | 1179.933 | 8.212 | 12 |
| 279 | MusclesSpineRight_ErectorSpinae_LTptT10Sacrum_4 | 42 | 1179.933 | 22.146 | 21 |
| 280 | MusclesSpineRight_ErectorSpinae_LTptT11Sacrum_4 | 42 | 1179.933 | 26.670 | 24 |
| 281 | MusclesSpineRight_ErectorSpinae_LTptT12Sacrum_4 | 42 | 1179.933 | 30.955 | 26 |
| 282 | MusclesSpineRight_PsoasMajor_PMT12I_TM_3 | 110 | 1177.133 | 48.791 | 29 |
| 283 | MusclesSpineRight_PsoasMajor_PML1I_TM_3 | 110 | 1177.133 | 47.364 | 28 |
| 284 | MusclesSpineRight_PsoasMajor_PML1T_TM_4 | 100 | 1177.133 | 50.027 | 28 |

| | | | | | |
|-----|--|--------|----------|---------|----|
| 285 | MusclesSpineRight_PsoasMajor_PML2I_TM_2 | 115 | 1177.133 | 43.710 | 26 |
| 286 | MusclesSpineRight_PsoasMajor_PML2T_TM_3 | 100 | 1177.133 | 46.873 | 25 |
| 287 | MusclesSpineRight_PsoasMajor_PML3I_TM_1 | 115 | 1177.133 | 38.120 | 20 |
| 288 | MusclesSpineRight_PsoasMajor_PML3T_TM_2 | 100 | 1177.133 | 45.046 | 23 |
| 289 | MusclesSpineRight_PsoasMajor_PML4T_TM_1 | 94 | 1177.133 | 40.032 | 18 |
| 290 | MusclesSpineRight_PsoasMajor_PML5_TM | 110 | 1179.933 | 21.000 | 10 |
| 291 | MusclesSpineRight_PsoasMajor_PML5T_TM | 80 | 1188.333 | 28.000 | 5 |
| 292 | MusclesSpineRight_ThoracicMultifidiRigth_MFL5T12 | 71 | 1190.2 | 24.000 | 5 |
| 293 | MusclesSpineLeft_Multifidi_MFdL3L5_1 | 73 | 1193 | -22.000 | 5 |
| 294 | MusclesSpineLeft_Multifidi_MFdL5S1 | 54 | 1178.067 | -5.000 | 5 |
| 295 | MusclesSpineLeft_Multifidi_MFmL5Sacrum | 50 | 1179 | -5.000 | 8 |
| 296 | MusclesSpineLeft_ErectorSpinae_LTpL5Ilium | 74 | 1190.2 | -28.000 | 5 |
| 297 | MusclesSpineLeft_ErectorSpinae_LTptT6S1_4 | 48 | 1179.933 | -0.964 | 5 |
| 298 | MusclesSpineLeft_ErectorSpinae_LTptT7S2_4 | 44 | 1179.933 | -3.161 | 8 |
| 299 | MusclesSpineLeft_ErectorSpinae_LTptT8S3_4 | 42 | 1179.933 | -5.513 | 10 |
| 300 | MusclesSpineLeft_ErectorSpinae_LTptT9S4_4 | 42 | 1179.933 | -8.212 | 13 |
| 301 | MusclesSpineLeft_ErectorSpinae_LTptT10Sacrum_4 | 42 | 1179.933 | -22.146 | 22 |
| 302 | MusclesSpineLeft_ErectorSpinae_LTptT11Sacrum_4 | 42 | 1179.933 | -26.670 | 24 |
| 303 | MusclesSpineLeft_ErectorSpinae_LTptT12Sacrum_4 | 42 | 1179.933 | -30.955 | 26 |
| 304 | MusclesSpineLeft_PsoasMajor_PMT12I_TM_3 | 110 | 1177.133 | -48.791 | 29 |
| 305 | MusclesSpineLeft_PsoasMajor_PML1I_TM_3 | 110 | 1177.133 | -47.364 | 30 |
| 306 | MusclesSpineLeft_PsoasMajor_PML1T_TM_4 | 100 | 1177.133 | -50.027 | 28 |
| 307 | MusclesSpineLeft_PsoasMajor_PML2I_TM_2 | 115 | 1177.133 | -43.710 | 25 |
| 308 | MusclesSpineLeft_PsoasMajor_PML2T_TM_3 | 100 | 1177.133 | -46.873 | 25 |
| 309 | MusclesSpineLeft_PsoasMajor_PML3I_TM_1 | 115 | 1177.133 | -38.120 | 20 |
| 310 | MusclesSpineLeft_PsoasMajor_PML3T_TM_2 | 100 | 1177.133 | -45.046 | 25 |
| 311 | MusclesSpineLeft_PsoasMajor_PML4T_TM_1 | 94 | 1177.133 | -40.032 | 18 |
| 312 | MusclesSpineLeft_PsoasMajor_PML5_TM | 110 | 1179.933 | -21.000 | 10 |
| 313 | MusclesSpineLeft_PsoasMajor_PML5T_TM | 80 | 1188.333 | -28.000 | 5 |
| 314 | MusclesSpineLeft_ThoracicMultifidiLeft_MFL5T12 | 71 | 1190.2 | -24.000 | 5 |
| 315 | T12L1Lig_IALLofT12L1 | 88.000 | 1319.000 | 0.000 | 5 |
| 316 | T12L1Lig_ICR1ofT12L1 | 42.000 | 1306.000 | 17.500 | 5 |
| 317 | T12L1Lig_ICL1ofT12L1 | 42.000 | 1306.000 | -17.500 | 5 |
| 318 | T12L1Lig_ICR2ofT12L1 | 41.000 | 1295.000 | 13.500 | 5 |
| 319 | T12L1Lig_ICL2ofT12L1 | 41.000 | 1295.000 | -13.500 | 5 |
| 320 | T12L1Lig_ICR3ofT12L1 | 35.000 | 1300.000 | 17.000 | 5 |
| 321 | T12L1Lig_ICL3ofT12L1 | 35.000 | 1300.000 | -17.000 | 5 |
| 322 | T12L1Lig_ICR4ofT12L1 | 48.000 | 1298.000 | 8.000 | 5 |
| 323 | T12L1Lig_ICL4ofT12L1 | 48.000 | 1298.000 | -8.000 | 5 |
| 324 | T12L1Lig_IPLLoft12L1 | 58.094 | 1307.806 | 0.000 | 5 |
| 325 | T12L1Lig_IISofT12L11 | 38.500 | 1278.000 | 0.000 | 5 |

| | | | | | |
|------------|--------------------------------------|---------|----------|---------|----|
| 326 | T12L1Lig_ISSofT12L11 | 30.000 | 1275.000 | 0.000 | 5 |
| 327 | T12L1Lig_IFlavumofT12L1R | 51.000 | 1295.000 | 5.000 | 5 |
| 328 | T12L1Lig_IFlavumofT12L1L | 51.000 | 1295.000 | -5.000 | 5 |
| 329 | T12L1Lig_IInterTransverseofT12L1R | 47.681 | 1295.423 | 34.286 | 5 |
| 330 | T12L1Lig_IInterTransverseofT12L1L | 47.681 | 1295.423 | -34.286 | 5 |
| 331 | T12L1Lig_IInterTransverseofT12L1Rmid | 52.659 | 1293.480 | 24.530 | 5 |
| 332 | T12L1Lig_IInterTransverseofT12L1Lmid | 52.659 | 1293.480 | -24.530 | 5 |
| 333 | L1_Gravity | 77.000 | 1299.400 | 0.000 | 15 |
| 334 | L2_Gravity | 89.000 | 1272.300 | 0.000 | 15 |
| 335 | L3_Gravity | 97.000 | 1243.400 | 0.000 | 15 |
| 336 | L4_Gravity | 102.000 | 1210.730 | 0.000 | 15 |
| 337 | L5_Gravity | 97.000 | 1179.000 | 0.000 | 15 |

Note: The coordinate of reference point together with its influence radius used in the FE model are specified in Appendix A. Each reference point represents a unique point that the external load will be acting on. The muscle forces acting on the same point are combined and then applied to the reference point. The reference points are connected to the closest deformable vertebrae surface through continuum distribution coupling constraints with minimum influence radius for the purpose of reducing computational cost. All external loads are acting on the reference points in the form of concentrated load. Loads 1 through 68 are attached to the L1 vertebra. Loads 69 to 139 are applied to the L2 vertebra. Loads 140 to 215 are fed to L3 vertebra. Loads 216 through 268 are attached to L4 vertebra. Loads 269 to 314 are applied to the L5 vertebra. As the sacrum is fixed during the simulation, the muscle forces are not applied to it. Ligament forces (315-332) are applied to L1 vertebra. Gradational forces (333-337) are fed to each vertebra.